Influence of spectral and spatial inhomogeneities of the active medium on spectral dynamics of multi-mode solid-state lasers

Dissertation
zur Erlangung des Doktorgrades
des Fachbereichs Physik
der Universität Hamburg

vorgelegt von

Evgeny Ovchinnikov

aus Nizhny Novgorod

Hamburg
2003

Gutachter der Dissertation:	Priv.-Doz. Dr. V. M. Baev Prof. Dr. W. Neuhauser
Gutachter der Disputation :	Priv.-Doz. Dr. V. M. Baev Prof. Dr. K. Sengstock
Datum der Disputation:	08.12.2003
Vorsitzender des Prüfungsausschusses:	Dr. K. Petermann
Vorsitzender des Promotionsausschusses	Prof. Dr. R. Wiesendanger
Dekan des Fachbereichs Physik	Prof. Dr. G. Huber

Zusammenfassung

Die Emissionsspektren von Vielmodenlasern reagieren sehr empfindlich auf die Absorption und die Modenkopplung im Laserresonator. Die Absorptionsspektroskopie im Laserresonator (Intra-Cavity Absorption Spectroscopy, ICAS) ist eine der empfindlichsten Methoden zur Untersuchung der optischen Absorption. Die Empfindlichkeit von ICAS entspricht derjenigen herkömmlicher Absorptionsexperimente mit der effektiven optischen Absorptionsweglänge des Lichts von einigen bis zu mehreren tausend Kilometern. Die Modenkopplung verändert die Emissionsdynamik der Laser und verringert die Empfindlichkeit auf die Absorption im Resonator.

Diodengepumpte Vielmoden-Festkörperlaser und insbesondere Faserlaser sind sehr wichtig für die Herstellung von kompakten und empfindlichen ICAS-Spektometern. Die vorliegende Arbeit beschäftigt sich mit der Untersuchung der Emissionsdynamik verschiedener Festkörperlaser, mit der Bestimmung dominierender Modenkopplung in diesen Lasern und mit der Bestimmung der Begrenzung der Empfindlichkeit auf die Absorption im Laserresonator.

Als die wichtigste Modenkopplung in Festkörperlasern wurde die räumliche Inhomogenität des Verstärkungsprofils des Lasers in den longitudinalen und azimutalen Richtungen festgestellt. Diese Kopplung führt zu niederfrequenten Schwankungen der Lichtemission in individuellen longitudinalen Lasermoden bzw. in verschiedenen Polarisationsmoden und zur Veränderung des Emissionsspektrums. Experimentell wurde diese Kopplung mit den Lasern untersucht, bei denen nur wenige Moden angeregt sind und die Veränderungen sehr hervorgehoben sind. Es wurde festgestellt, dass der Modenkopplungsgrad und die Absorptionsempfindlichkeit der Laseremission durch die Anzahl der oszillierenden Moden und die Pumpleistung gesteuert werden kann. Mit einem 8 Meter langen Nd-dotierten Faserlaser wurde die Anzahl der oszillierenden Moden auf 50000 gesteigert und auf diese Weise die Absorptionsempfindlichkeit auf mehr als 100 km erhöht.

Die Spontanemission kann auch die spektrale Absorptionsempfindlichkeit von Vielmodenlasern begrenzen, insbesondere wenn die Resonatorverluste groß sind und der Laser nicht weit über der Schwelle betrieben wird. Der Einfluss der Spontanemission auf ICAS wurde durch die Messung von starken Absorptionslinien des Wasserdampfes im Resonator von Nd- und Yb-dotierten Faserlasern beobachtet. Der Einfluss der Spontanemission in diesen Lasern ist besonders in der Anwesenheit der starken Oszillationsschwingungen ausgeprägt.

Laser mit dem inhomogen verbreiterten spektralen Verstärkungsprofil, z.B. Faserlaser, zeigen zusätzlich die Abhängigkeit der Absorptionsempfindlichkeit von der Linienbreite des Absorbers. Das Emissionsspektrum des Lasers ist sehr empfindlich auf die Absorption im Resonator, wenn die Absorptionslinienbreite die homogene Linienbreite des Verstärkungsprofils nicht übersteigt. Wenn jedoch die Absorptionslinienbreite größer als die homogene Linienbreite der Verstärkungsprofils ist, sinkt die Empfindlichkeit erheblich. Dieses Phänomen wurde mit einem Nd-dotierten und einem Yb-dotierten Faserlaser gemessen.

Abhängig von den Laserparametern kann eines oder mehrere der oben genannten Merkmale die dominierende Ursache für die Begrenzung der Absorptionsempfindlichkeit sein. Die in der vorliegenden Arbeit erhaltenen Ergebnisse zeigen, dass die Empfindlichkeit der Absorptionsmessungen im Laserresonator durch Verwendung des aktiven Mediums mit dem breiten spektralen Verstärkungsprofil, Auswahl nur einer Polarisationsmode, Anwendung kleiner Pumpraten, Verringerung der Resonatorverluste, Vergrößerung der Resonatorlänge und Verkleinerung der Länge des aktiven Mediums erhöht werden kann.

Abstract

Emission spectra of multimode lasers are very sensitive to intracavity absorption and to mode coupling in the cavity. Intracavity absorption spectroscopy (ICAS) is one of the most sensitive techniques for the detection of optical absorption. Sensitivity of ICAS corresponds to conventional absorption measurements with an effective absorption path length from a few kilometers to several thousands kilometers. Mode coupling in the laser modifies the emission dynamics and reduces sensitivity of the laser to intracavity absorption.

Diode pumped multimode solid-state lasers and especially fibre lasers are very useful for the construction of compact and sensitive ICAS-spectrometers. The present work deals with the investigation of the emission dynamics of various solid-state lasers, with the identification of the dominant mode coupling in these lasers and with the determination of the sensitivity limitation to intracavity absorption.

The most important mode coupling in solid-state lasers is found to be spatial inhomogeneity of the laser gain in longitudinal and azimuthal directions. This coupling results in low frequency fluctuations of the laser emission in individual longitudinal and polarization modes and in the modification of the emission spectrum. Experimentally this coupling has been studied with lasers, where only few laser modes are excited and the modifications are the most pronounced. It was found that the strength of mode coupling and the sensitivity of the laser emission to intracavity absorption can be controlled by the number of oscillating laser modes and by the pump power. With an 8-meter long Nd-doped fiber laser the number of oscillating modes has been increased to 50,000 and in this way the sensitivity of ICAS has been increased to more than 100 km.

Spontaneous emission becomes the main factor limiting the spectral sensitivity of the multimode lasers to intracavity absorption if the cavity loss is large and if the laser operates not far above the threshold. The influence of spontaneous emission on ICAS has been observed by measuring strong absorption lines of water vapour in the cavity of Nd- and Yb-doped fibre lasers. The influence of spontaneous emission in these lasers is especially pronounced due to the presence of strong relaxation oscillations.

Lasers with inhomogeneously broadened spectral gain, such as fibre lasers, additionally show the dependence of the sensitivity of ICAS on the absorber linewidth. The emission spectrum of the laser is very sensitive to intracavity absorption, if the absorptive linewidth does not exceed the homogeneous linewidth of the gain. If, however, the absorptive linewidth is larger than the homogeneous linewidth of the gain, the sensitivity drops significantly. This phenomenon has been measured with Nd- and Yb-doped fibre lasers.

Depending on laser parameters one or several of the above mentioned features can be dominating factors limiting the spectral sensitivity of ICAS. The results obtained in the present work show that the sensitivity of intracavity absorption measurements can be increased by using the active media with broad spectral gain, selecting one polarization mode only, applying smaller pump rates, reducing cavity losses, increasing the cavity length and reducing the length of the active media.

Contents

1. Introduction

The investigation of the spectral dynamics of solid-state and fibre lasers is very important for many practical applications, e.g. for high-sensitive intracavity absorption spectroscopy (ICAS) [1] and for the determination of the conditions for a stable laser operation. ICAS allows the investigation of absorption spectra of atoms and molecules localised in the cavity at very small concentrations. That makes possible the detection of pollutions in the atmospheric air with very high sensitivity.

The most important phenomena limiting the sensitivity of intracavity absorption measurements are nonlinear mode coupling, spontaneous emission, Rayleigh scattering and inhomogeneous spectral broadening of the laser gain. One of the most important mode coupling in solid state lasers is the result of spatial inhomogeneity of the laser gain in longitudinal [2-5] and azimuthal [6] directions. It results in antiphase cross-saturation dynamics of the transient modal emission featuring low-frequency relaxation oscillations.

Mode coupling by spatial inhomogeneity in longitudinal direction has been studied with a Nd:doped thin disc glass laser [4]. Numerical simulations show that the saturation of the inversion by standing waves causes spatial inhomogeneity of the laser gain, couples the modes and results in low frequency oscillations of the light flux in the individual laser modes. With the frequencies in the range of 10-500 kHz these oscillations are steadily driven by quantum noise and appear as 15% fluctuations of the power in each mode. In-phase fluctuations in the laser modes appear at the frequency of the main relaxation oscillation of the total laser power. Antiphase fluctuations appear at other frequencies and in individual longitudinal laser modes only. The dominant frequency of these fluctuations is determined by the light power in the mode.

The strength of mode coupling by longitudinal ingomogeneity of the gain increases when the number of oscillating mode decreases. Investigations of a Nd:YAG laser emitting a small number of longitudinal modes [2,3], show strong modification of the laser emission even without intracavity absorption. The important factor responsible for the sensitivity of intracavity absorption measurements is the filling factor of the cavity with the gain medium. Large filling factor leads to the strong mode coupling, as it is the case with fibre lasers, and may provide strong sensitivity limitation. It is expected that mode coupling can be reduced by varying the different laser parameters such as the linewidth of the gain, the pump rate, the

cavity loss, the cavity length and the length of the active medium. These features have been studied in detail in the present work.

Mode coupling by spatial inhomogeneity in azimuthal direction has been studied with a bipolarized Nd:YAG lasers [6]. It results in instabilities of polarization modes. The instability of laser emission by interactions of two orthogonally polarized modes is especially pronounced in lasers with intracavity second harmonic generation. The polarization dynamics of the lasers depends strongly on the phase anisotropy (birefringence of the medium). Two factors acting on the polarization selection of the laser are the gain anisotropy due to the linearly polarized pump and the anisotropy of the saturation in the passive medium.

Lasers with inhomogeneously broadened spectral gain, e.g. fibre lasers, show another specific feature that should be taken into account with intracavity absorption measurements [7]: the dependence of the sensitivity of ICAS on the absorber linewidth. If the linewidth of intracavity absorption is larger than the homogeneous linewidth of the gain, the sensitivity drops. This phenomenon has been investigated in this work by introducing the absorber with a variable linewidth into the laser cavity. Therefore it became possible the determination of the homogeneous broadening of the gain.

The emission power of fibre lasers is rather weak, and their spectrum usually comprises many thousands of laser modes. Therefore, spontaneous emission may become the dominating factor limiting spectral sensitivity of ICA measurements, especially, if the laser operates not far above the threshold and if it shows strong relaxation oscillations [8]. This phenomena has been studied in the present work with fibre lasers.

Depending on laser parameters one or several of the above features can dominate the sensitivity limit to intracavity absorption. The results obtained in this work show some of the ways how the sensitivity of ICAS measurements can be enhanced.

2. Sensitive measurements of absorption spectra

2.1. Conventional absorption measurements

In conventional absorption spectroscopy the light passes through the absorbing sample that modifies the spectrum of the transmitted light (Fig. 2.1).

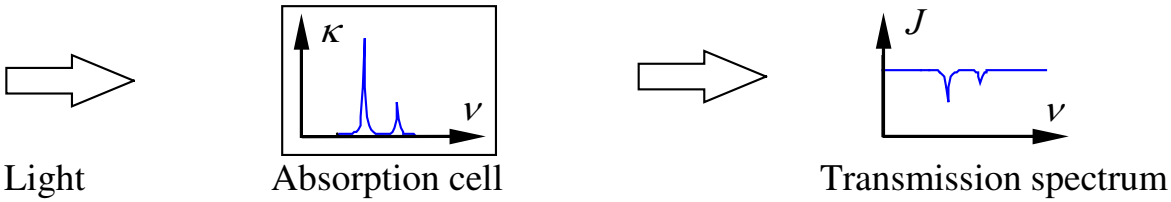

Fig. 2.1: Conventional absorption measurements

The transmitted light experiences the extinction in the spectral regions of the absorption lines of the sample. The extinction is governed by the Lambert-Beers law [1]:

$$J_\nu = J_\nu^0 \exp(-\kappa_\nu L_{\text{opt}}) \tag{2.1}$$

where J_ν^0, J_ν are incident and transmitted spectral light fluxes, L_{opt} is the optical path length of the absorber, κ_ν is the absorption coefficient of the absorber in the cell.

Absorption signal is defined as [1]:

$$K = \ln\left(\frac{J_\nu^0}{J_\nu(\kappa)}\right) = \kappa_\nu L_{\text{opt}} \tag{2.2}$$

With Eqs. (2.1) and (2.2) absorption signal in conventional measurement is:

$$K = \kappa_\nu L_{\text{opt}} \tag{2.3}$$

The spectral sensitivity S of absorption measurements can be defined as the absorption signal divided by the corresponding absorption coefficient:

$$S = K / \kappa_\nu \tag{2.4}$$

From Eqs. (2.1-2.4) follows that the spectral sensitivity of conventional measurements is:

$$S = L_{\text{opt}} \tag{2.5}$$

2.2. Intracavity absorption spectroscopy (ICAS)

Extremely high spectral sensitivity is achievable by the laser intracavity absorption spectroscopy, when the absorber is placed inside the cavity of a multimode laser as it is shown in Fig. 2.2. The laser light passes many times through the absorber, and intracavity absorption is accumulated in its spectrum as in a multipass cell. The necessary condition for high sensitivity to absorption is: the linewidth of the absorber must be smaller than the homogeneous linewidth of the gain of the active medium.

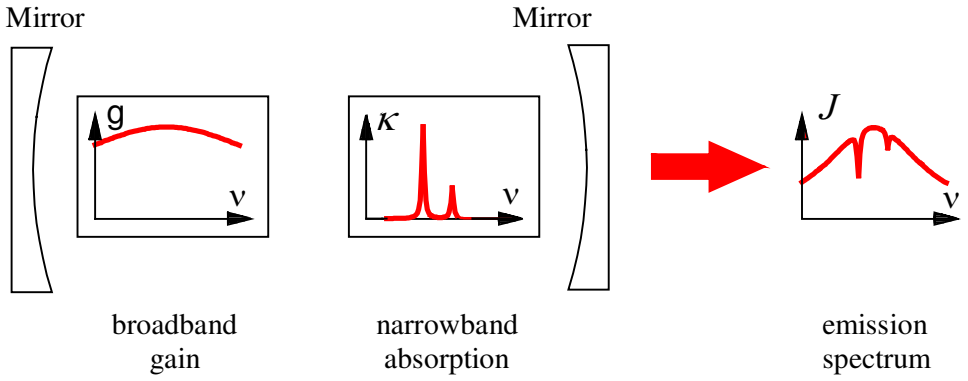

Fig. 2.2: Measurements of intracavity absorption.

The spectral sensitivity in this case is defined similar to Eqs. (2.4) and (2.5) as an effective absorption pathlength:

$$S = K / \kappa_\nu = L_{\text{eff}} \tag{2.6}$$

It may be expressed also through the spectral saturation time t_s:

$$L_{\text{eff}} = c\, t_s \tag{2.7}$$

Spectral saturation time is the time required for reaching the stationary laser emission or pulse duration, if it is shorter than the spectral saturation time.

The simplified theoretical model of ICAS is described by the rate equations for the mean values of photon numbers M_q in the laser mode q, and for the laser inversion N in the approach of the ideal 4-level laser [1]:

$$\dot{M}_q = -\gamma M_q + B_q N\left(M_q + 1\right) - \kappa_q \mathrm{c} M_q \tag{2.8}$$

$$\dot{N} = P - AN - N\sum_q B_q M_q \tag{2.9}$$

where γ is the broadband cavity loss, B_q is the gain coefficient for mode q, κ_q is the intracavity absorption coefficient at the frequency of mode q, P is the pump rate, A is the rate of spontaneous decay of the upper laser level.

A homogeneously broadened laser gain, expressed as a rate B_q of induced emission per one inverted active particle and per one photon in mode q, is approximated by the Lorentzian profile

$$B_q = \frac{B_{\mathrm{o}}}{1 + \left(\dfrac{q - q_{\mathrm{o}}}{Q}\right)^2}, \tag{2.10}$$

with the frequency variable scaled in units of the mode numbers, $q = 2L/\lambda_q$. Here, L is the length of the cavity, and λ_q is the wavelength of the light in mode q. The maximum gain at

the central mode q_0 is B_0, and the spectral width of the gain is Q (HWHM). The laser gain B_0 is the product of the Einstein coefficient for stimulated emission, and a factor that depends upon the particular geometry of the laser beam in the cavity.

Narrow-band intracavity absorption κ_q causes additional loss in the corresponding laser modes and, as a consequence, exponential decay of the photon numbers as compared with the undisturbed laser mode. The solution of rate equations (2.8) and (2.9) with intracavity absorption (ICA) is [1]:

$$M_{q,\kappa}(t) = M_q(t)\exp(-\kappa_q c t), \tag{2.11}$$

which is equivalent to the Lambert-Beer law, Eq. (2.1), where the absorption path length is substituted by the effective absorption path length $L_{\text{eff}} = c\,t$.

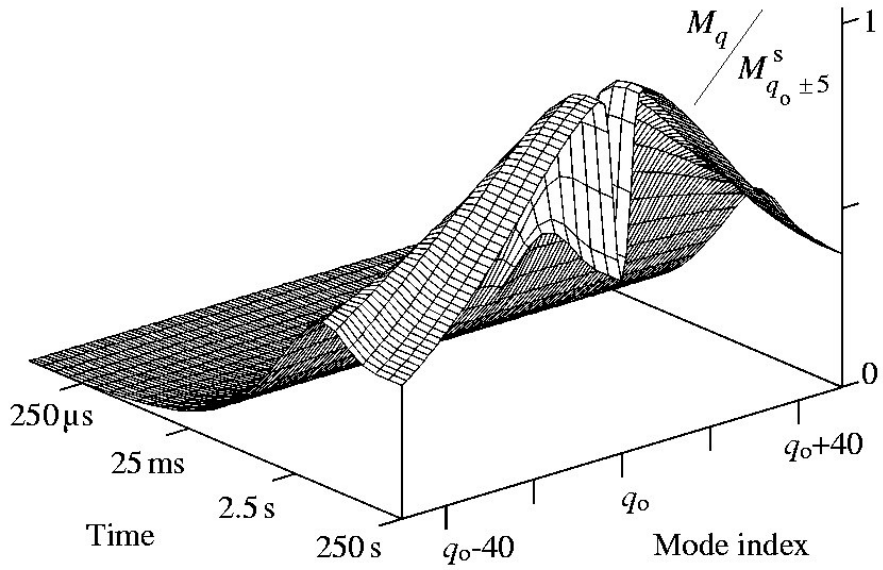

Fig. 2.3: Transient dynamics of the emission spectrum calculated for the ideal laser. Photon numbers M_q are normalized by the stationary photon number in the strongest modes, $q_0 \pm 5$.

Fig. 2.3 demonstrates the spectral dynamics of the absorption signal calculated for the ideal laser. In the case of the ideal laser one neglects all nonlinear phenomena that can limit spectral sensitivity of ICA measurements, e.g. spatial and spectral inhomogeneities of the gain. It means that the population inversion is independent of the position in the cavity and the

gain is homogeneously broadened. In Fig. 2.3 the central mode q_0 is the mode with the maximum gain. The intracavity absorption line with the coefficient $\kappa = 1.2 \cdot 10^{-12}$ cm^{-1} is in the middle of the gain spectrum and has the linewidth $\Delta q = 2$. Fig 2.3 shows the absorption signal in the centre of the emission spectrum. This signal initially increases with the duration of laser emission, and finally saturates to its stationary spectral shape. According to (2.2) the value of the absorption signal K_q in mode q is:

$$K_q = \ln \frac{M_q}{M_{q,\kappa}}, \tag{2.12}$$

where $M_{q,\kappa}$ and M_q are the number of photons in mode q in the presence of ICA, and without ICA respectively. The value M_q may be estimated by determining the number of photons in one of the neighbouring modes that is not modified by the absorption. As a result, the difference of the net loss in the cavity at the wavelengths of the corresponding laser modes can be derived.

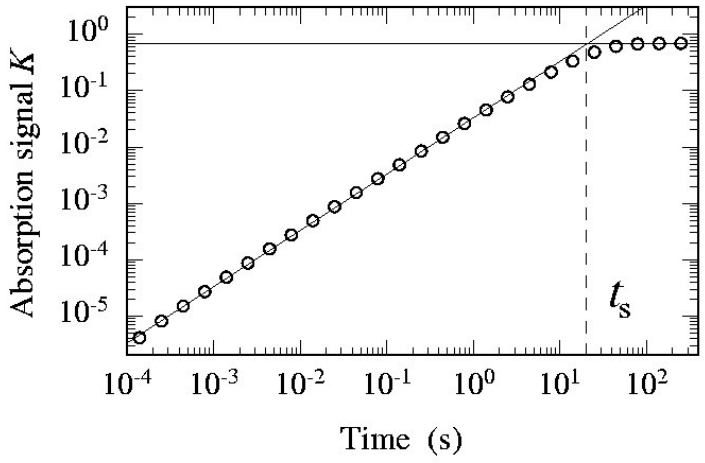

Fig. 2.4: Absorption signal K in the mode q_0, vs. duration of laser emission calculated from the spectrum in Fig. 2.3; t_s is the spectral saturation time of absorption signal.

Figure 2.4 shows the absorption signal K_q of the mode q_0, due to ICA, corresponding to Fig.2.3. The absorption signal grows linearly, with the duration of laser emission during the initial stage of laser operation, as expected from Eqs. (2.11) and (2.12),

$$K_q = \kappa_q \, c \, t \, . \tag{2.13}$$

The absorption signal is estimated by taking the photon numbers in the mode q_0 for $M_{q,\kappa}$, and in mode $(q_0 + 5)$ for M_q. The solid line in Fig. 2.4, an extrapolation of the linear fit of K_q in the initial stage, shows the temporal evolution of this absorption signal, expected with the linear dependence of (2.12), which holds up to 20 s. Afterwards, the absorption signal saturates to its stationary value.

2.3. Sensitivity limits of ICAS

The most important phenomena limiting the sensitivity of intracavity absorption measurements are nonlinear mode coupling, spontaneous emission and Rayleigh scattering. The most important nonlinearity in solid state lasers is spatial inhomogeneity of the laser gain in longitudinal [2-5] and azimuthal [6] directions.

Spontaneous emission

The perturbation by spontaneous emission, $X_q = B_q N$, is fundamental and present in all lasers. It is included even in the simplified model (Eqs. (2.8) and (2.9)). Under stationary laser operation $B_q N^s \cong \gamma$, and the sensitivity to ICA grows with the pump rate, which complies well with diode lasers [1]. In contrast to diode lasers, solid state lasers, such as Ti:sapphire [9, 10] and doped fibre lasers [11, 12], show only weak dependence of their sensitivity upon the pump rate. Moreover, the sensitivity to ICA achieved with dye lasers decreases with the pump rate [13, 14].

Rayleigh scattering

Rayleigh scattering of the laser light by local fluctuations of density and temperature in a dense-gain material shifts the frequency and the phase of a fraction of the light in the cavity modes. Since the frequency shift is small, the scattered light remains in the same mode and disturbs the phase coherence of the light [15]. The rate of perturbation of the laser is expressed by the fractional rate of scattered light $X_q = RM_q^s$, with R being the rate of scattering into the laser mode. In this case the spectral sensitivity $L_{\text{eff}} = c/R$ [1] is independent of the pump power. Whenever Rayleigh scattering is supposed to be the dominant perturbation, the sensitivity to ICA is not expected to vary upon the pump rate and photon numbers in laser modes. Such a performance has been observed with some solid state lasers.

Mode coupling

Particularly harmful to the attainment of good spectral sensitivity is any interaction that efficiently couples the laser modes. Major contributions to mode coupling in a solid-state or liquid laser arise from the nonlinearities of the active medium and the saturated gain. An incident pair of light waves of different frequencies generates a material excitation at its beat frequency; in turn, the material excitation interacts with each of the incident waves and induces dielectric polarizations whose frequencies are shifted away from that of the incident waves by the beat frequency. This coupling generates four-wave mixing of the light. If only two light modes are involved, the four-wave mixing is degenerate and gives rise to spatial hole burning. In a multimode laser, however, there are many light waves of different frequencies corresponding to the longitudinal cavity modes. Each pair of these light waves reads out material excitations, created by all other pairs of light waves with the same beat frequency. Hence, stimulated scattering in a multimode laser entails degenerate and nondegenerate four-wave mixing.

The highest sensitivity to ICA has been obtained so far with a cw dye laser [16, 17]. The width of the dye jet takes such a small portion of the cavity that the effect of Rayleigh scattering is almost absent. The sensitivity is limited by one of various third-order nonlinearities. This perturbation may be expressed by $X_q = D\left(M_q^s\right)^2$, where D is a field-independent function of the relevant nonlinear susceptibility [18], if the mode amplitudes are considered

uncorrelated. The spectral sensitivity decreases with increasing light power in the mode [1]: $L_{\text{eff}} = c \Big/ DM_q^{\text{s}}$. In this case the spectral saturation time decreases with the pump rate.

The identification of particular factors that limit the sensitivity in each type of laser allows the optimization of laser parameters for the most precise, sensitive, and reliable detection of ultra-weak or extremely rarefied absorbers. The most important nonlinearities governing the dynamics of multimode fiber lasers and reducing their sensitivity to ICA are mode coupling by spatial and spectral inhomogeneities of the gain.

Following features of the solid-state lasers which may limit the spectral sensitivity of ICA measurements will be considered in the present work: spontaneous emission, spatial inhomogeneities of the gain, and spectral inhomogeneities of the gain.

3. Sensitivity limitation of ICAS by spontaneous emission

3.1. Relaxation oscillations in solid state lasers

In solid-state lasers the transient dynamics is superimposed by relaxation oscillations [19] that can significantly modify the evolution of the signals of intracavity absorption. The influence is especially strong in the fibre lasers. The emission power of the fibre lasers is rather weak, and their spectrum usually comprises many thousands of laser modes. Therefore, spontaneous emission may become the dominating factor limiting spectral sensitivity of intracavity absorption measurements, especially if the laser shows strong relaxation oscillations.

Relaxation oscillations can be derived from the rate equations (2.8), (2.9). In the case of a single mode laser, without taking spontaneous emission into account in Eq. (2.8) (the term $BN = 0$) and without intracavity absorption Eqs. (2.8) and (2.9) transform to:

$$\dot{M} = -\gamma M + BNM \tag{3.1}$$

$$\dot{N} = P - AN - BNM \tag{3.2}$$

Slow variations of inversion lead in solid-state lasers to relaxation oscillations of photon numbers in the laser cavity. In other words, the relaxation oscillations take place when the decay time of the laser field in the cavity is much smaller than the live time of the upper laser level ($\gamma >> A$).

In steady state Eqs. (3.1) and (3.2) transform to:

$$0 = -\gamma M^s + BN^s M^s \tag{3.3}$$

$$0 = P - AN^s - BN^s M^s, \tag{3.4}$$

where M^s and N^s are stationary values of the photon number and of the population inversion, respectively.

The stationary value for the population inversion can be estimated from Eq. (3.3):

$$N^s = \frac{\gamma}{B} \tag{3.5}$$

The stationary inversion does not depend on the pump rate at $P > P_{thr}$, where P_{thr} is the threshold pump rate :

$$P_{thr} = AN^s = \frac{A\gamma}{B} \tag{3.6}$$

It follows from Eqs. (3.4) - (3.6) that the stationary value of the photon number is:

$$M^s = \frac{P}{\gamma} - \frac{A}{B} = \frac{A(\eta - 1)}{B}, \tag{3.7}$$

where

$$\eta = \frac{P}{P_{thr}} \tag{3.8}$$

is the pump rate.

As long as η < 1 the pump rate is consumed to the increase of the population inversion for the compensation of the cavity loss. At η = 1 the pump rate compensates the broadband cavity loss and lasing starts. At η > 1 the pump power transforms into the laser radiation.

Let us find the transient solutions of the rate equations (3.1) and (3.2). For that one should linearize Eqs. (3.1) and (3.2) and find the solutions in the presence of small perturbations of the system. We can represent the population inversion N and the photon number M as:

$$M(t) = M^s + m(t), \tag{3.9}$$

$$N(t) = N^s + n(t), \tag{3.10}$$

where $m(t) << M^s$ and $n(t) << N^s$.

Substitution of $M(t)$ and $N(t)$ into Eqs. (3.1), (3.2) and using of Eqs. (3.5) - (3.8) result in following equations:

$$\dot{m} = \eta \frac{A\gamma}{B} - A(\frac{\gamma}{B} + n) - B(\frac{\gamma}{B} + n)(\frac{A}{B}(\eta - 1) + m) \tag{3.11}$$

$$\dot{n} = -\gamma(\frac{A}{B}(\eta - 1) + m) + B(\frac{\gamma}{B} + n)(\frac{\gamma}{B} + n)(\frac{A}{B}(\eta - 1) + m) \tag{3.12}$$

From Eqs. (3.11) and (3.12) follows:

$$\dot{m} = nA(\eta - 1) \tag{3.13}$$

$$\dot{n} = -A\eta n - \gamma m \tag{3.14}$$

Here the second order terms $\sim n(t) \cdot m(t)$ have been neglected.

The solutions of Eqs. (3.13) and (3.14) can be found as:

$$m(t) = \hat{m} e^{pt} \tag{3.15}$$

$$n(t) = \hat{n} e^{pt} \tag{3.16}$$

Substitution of Eqs. (3.15) and (3.16) into Eqs. (3.13) and (3.14) gives the following equations:

$$\hat{n}A(\eta - 1) - p\hat{m} = 0 \tag{3.17}$$

$$\hat{n}(p + A\eta) + \gamma \hat{m} = 0 \tag{3.18}$$

The solution of Eqs. (3.17) and (3.18) exists, if the determinant equals zero:

$$\begin{vmatrix} A(\eta - 1) & -p \\ p + A\eta & \gamma \end{vmatrix} = 0 \tag{3.19}$$

From Eq. (3.19) follows:

$$\gamma A(\eta - 1) + p(p + A\eta) = 0 \tag{3.20}$$

Eq. (3.20) is the quadratic equation for p:

$$p^2 + pA\eta + A\gamma(\eta - 1) = 0\,, \tag{3.21}$$

Eq. (3.21) has the solutions:

$$p_{1,2} = -\Gamma \pm \sqrt{\Gamma^2 - \omega^2}\,, \tag{3.22}$$

where

$$\Gamma = \frac{A\eta}{2} \tag{3.23}$$

$$\omega = \sqrt{A\gamma(\eta - 1)} \tag{3.24}$$

One can identify Γ as the rate of damping, and ω as the frequency of relaxation oscillations in radians. The damping rate depends only on the livetime of the upper laser level and the pump rate. The frequency of relaxation oscillations in Hz is:

$$f = \frac{\omega}{2\pi} = \frac{\sqrt{A\gamma(\eta - 1)}}{2\pi} \tag{3.25}$$

The square root in Eq. (3.22) is imaginary $p_{1,2} = -\Gamma \pm i\omega'$ at the values of $|\Gamma| < |\omega|$ with $\omega' = \sqrt{\omega^2 - \Gamma^2}$. In this case the general solution of Eq. (3.13) is the damped harmonic oscillations [59]:

$$m(t) = Ce^{-\Gamma t}\sin(\omega' t + \varphi))\,, \tag{3.26}$$

where C and φ are established by the initial conditions.

Substitution of Eq. (3.26) into Eq. (3.13) and assumption $\Gamma << \omega'$ give the solution for $n(t)$:

$$n(t) \cong \frac{\omega' C}{A(\eta - 1)} e^{-\Gamma t} \cos(\omega' t + \varphi)), \tag{3.27}$$

One can see from Eqs. (3.26) and (3.27) that the photon number and the population inversion oscillate with the phase shift of π/2. Note that the oscillations of $n(t)$ precedes that of $m(t)$ by about half an oscillation period, since we must first have a growth of inversion $n(t)$ before we can have a corresponding growth of $m(t)$.

There are two real negative values of p at $|\Gamma| > |\omega|$. It corresponds to the solution for Eqs. (3.13) and (3.14) in the form of exponential decay without the relaxation oscillations.

Lasers are described by three relevant variables: field, population inversion and polarization. These variables usually decay on very different time scales, which are given by the relaxation rates γ, A, and $A_\perp$ correspondingly [19, 60]. The dipole moment polarization relaxation rate $A_\perp$ is the halfwidth of the spectral line: $A_\perp = \Delta\omega_0 / 2$. If one of these variables is large compared with the others, the corresponding variable relaxes fast and consequently adiabatically adjusts to the other variables. The number of equations describing the laser is then reduced. Those lasers for which the population and the polarization decay fast in comparison with the field A, $A_\perp >> \gamma$ have been named class A lasers. They reveal no relaxation oscillations because the active medium follows without delay all the field variations. Both the inversion and the polarization can be eliminated from the set of laser equations. The lasers for which only the polarization relaxes fast $A_\perp >> \gamma >> A$ belong to class B lasers with well pronounced relaxation oscillations. Only the polarization follows the field without delay and it is the only variable eliminated. Those lasers for which all three relaxation rates are of the same magnitude belong to class C lasers. In this case all the variables have to be equally considered.

It should be noted that all the lasers investigated in this work are class B lasers.

3.2. Modification of dynamics of intracavity absorption by spontaneous emission in the presence of relaxation oscillations

Modification of dynamics of intracavity absorption in the presence of relaxation oscillations can be estimated from numerical integration of Eqs. (2.8) and (2.9). These equations have been integrated for Nd- and Yb-doped fibre lasers with up to 20000 oscillating modes.

In the case of Nd-doped fibre following parameters have been used:

Cavity loss	$\gamma = 5.7 \cdot 10^6$ s^{-1}
Decay rate of the upper laser level	$A = 2174$ s^{-1}
Gain	$B = 1.3 \cdot 10^{-5}$ s^{-1}
Pump rate	$P = 5.34 \cdot 10^{17}$ s^{-1}
Relative pump rate	$\eta = 5.6$
Linewidth (FWHM)	$Q = 8 \cdot 10^4$
Time intervals of numerical solution	$\Delta t = 10^{-8}$ s

Fig. 3.1 shows the time evolution of the population inversion in the cavity of a Nd-doped laser after onset of the pump. Intracavity absorption was absent in this case. In the beginning the inversion grows linearly up to the onset of laser emission. After that the inversion oscillates around its stationary value N^s in accordance with Eq. (3.5).

Fig. 3.2 shows the time evolution of the total photon number corresponding to the Fig. 3.1. The photon number shows the relaxation oscillations after the threshold value of the population inversion is reached. It comes to its stationary value M^s according to Eq. (3.7).

Fig. 3.3 shows the time evolution of the photon numbers in individual laser modes, M_q, in the cavity of a Nd-doped laser. 20000 modes start to oscillate after the threshold is reached. This corresponds to the build up of first maximum of the relaxation oscillations when the gain compensates the cavity loss. Both the total photon number in the cavity and the photon number in every mode oscillate during the transition to the stationary state. The amplitude of the central mode grows whereas the amplitudes of the side modes drop, because the gain broadening is taken to be homogeneous. In this case the spectrum of laser emission condenses.

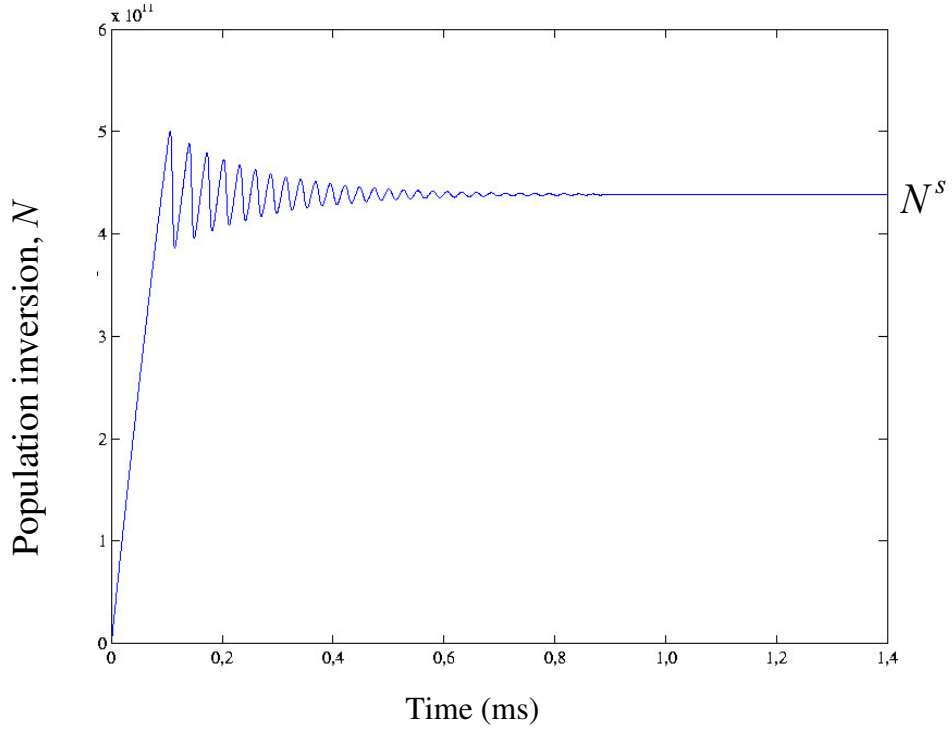

Fig. 3.1: Time dependence of the population inversion in a Nd-doped fibre laser at the pump rate $\eta = 5.6$. $t = 0$ is the beginning of the pump.

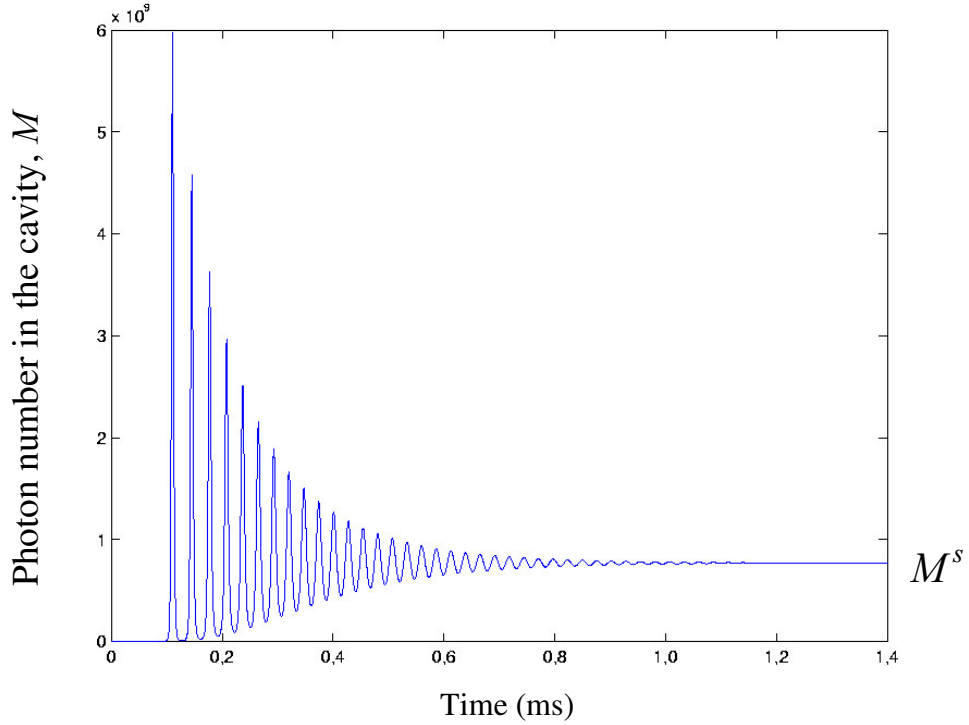

Fig. 3.2: Numerically solved total photon number M in the cavity of a Nd-doped fibre laser at the pump rate $\eta = 5.6$.

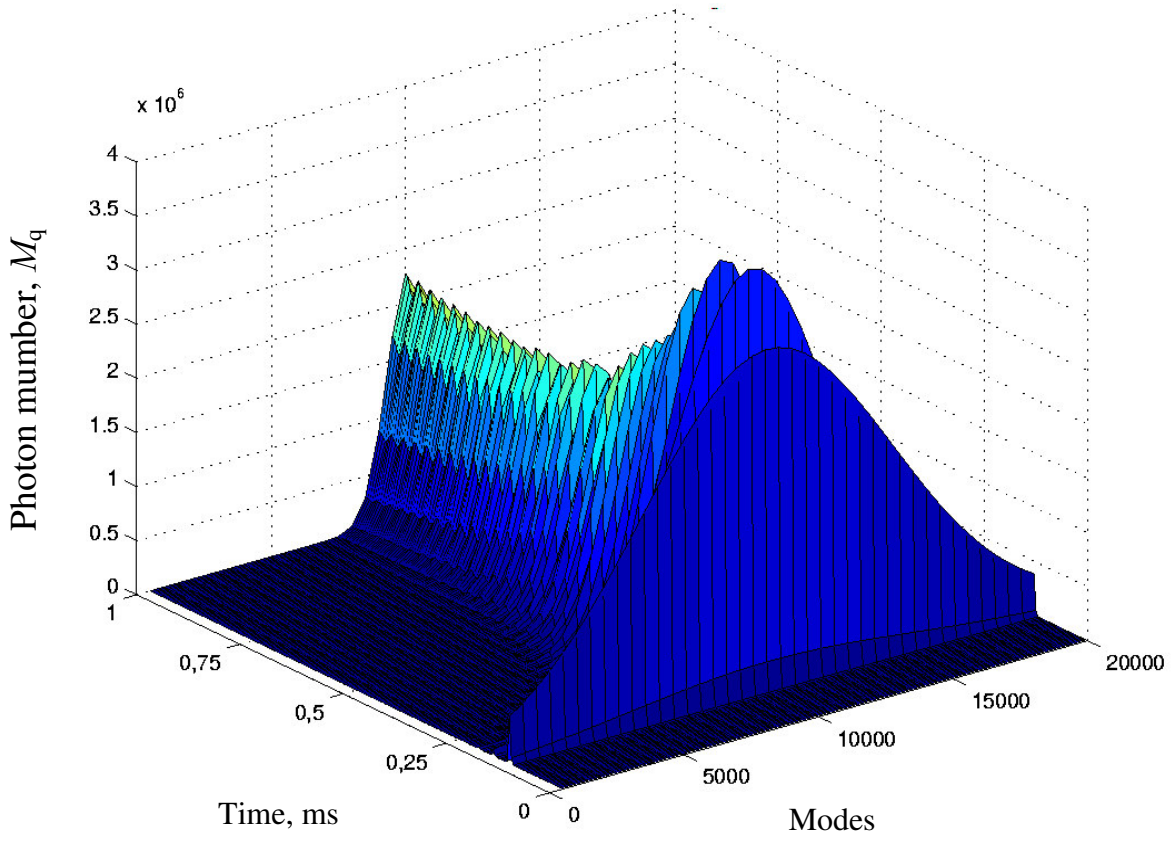

Fig. 3.3: Time evolution of the photon numbers, M_q, in the cavity of Nd-doped fibre laser at the pump rate $\eta = 5.6$.

In order to investigate the modification of dynamics of intracavity absorption in the presence of relaxation oscillation the rate equations (2.8) and (2.9) have been integrated with presence of intracavity absorption in the centre of the emission spectrum. Following absorption lines have been included:

Table 3.1. Absorption lines

Nr	Wave length (nm)	κ (cm^{-1})
1	1.085.31	$0.55 \cdot 10^{-6}$
2	1.084.31	$0.73 \cdot 10^{-6}$
3	1.088.54	$1.1 \cdot 10^{-6}$

The absorption signal is determined from Eq. (2.6) and Eq. (2.12):

$$K_q = \ln\left(\frac{M_q}{M_{q,\kappa}}\right) = \kappa_q L_{\text{eff}} \tag{3.28}$$

Fig. 3.4 demonstrates the evolution of the effective path length $L_{\text{eff}} = K/\kappa(\nu)$ for three absorption lines shown in the Table 3.1. The effective path length of all the absorption lines develops slower than theoretical limit $L_{\text{eff}} = ct$. The curve for the largest absorption coefficient κ =1.1·10^{-6} cm^{-1} shows the pronounced wave form caused by relaxation oscillations of the photon number. The following parameters of the laser were used: empty cavity length L_{ext}=1.9 m, length of the fibre L_{fibre}= 0.78 m, optical path length L_{opt}= 3.07 m, gain B = 1.94·10^{-6} s^{-1}, pump rate η = 5.6, loss γ= 5.7·10^{6} s^{-1}, refraction index n_κ= 1.5, A = 1852 s^{-1}, Q = 8·10^{4}, Δt = 10^{-8} s.

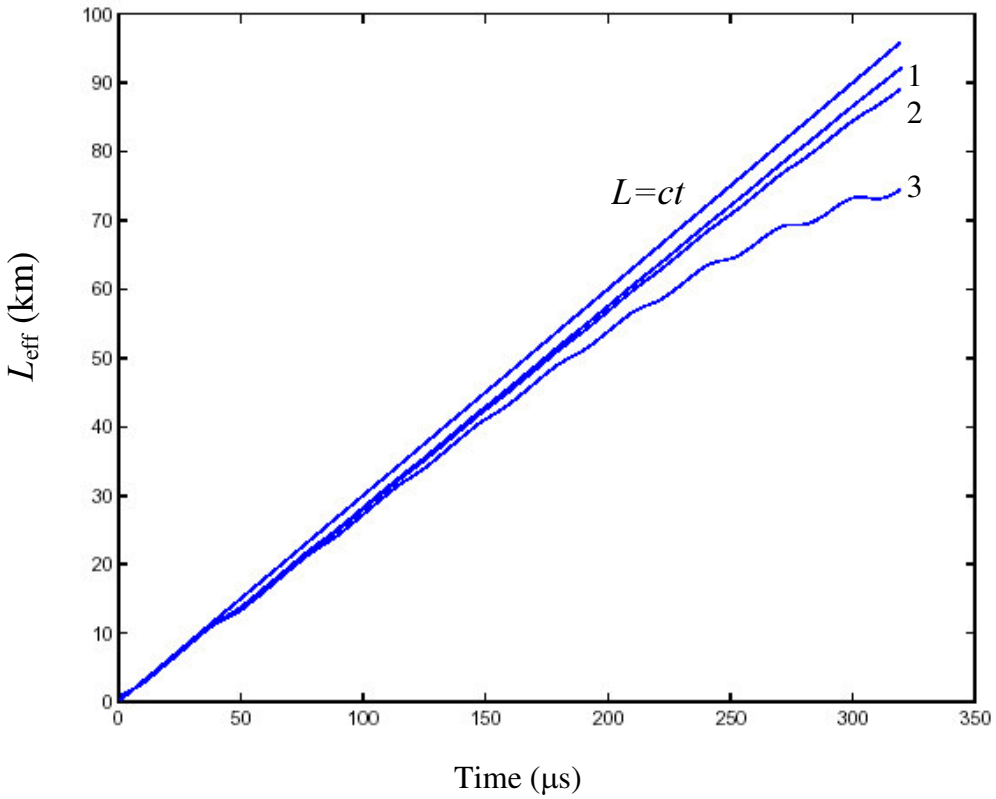

Fig. 3.4: Time evolution of the effective path length obtained with 3 absorption lines from Table 3.1.

Fig. 3.5 shows the time evolution of the absorption signal K for the absorption coefficient $\kappa = 1.1 \cdot 10^{-6}$ cm^{-1} at the pump rate $\eta = 1.9$ and the cavity loss $\gamma = 2.85 \cdot 10^{7}$ s^{-1}. One can see that in this case the influence of the relaxation oscillations is larger. The absorption signal grows slower or even drops during the time when the relaxation oscillations have minima (denoted in Fig. 3.5 by the circles). It caused by the increased influence of the spontaneous emission. In 10-th maximum the absorption signal has the value K=5.27 that is only 49% from the theoretical limit.

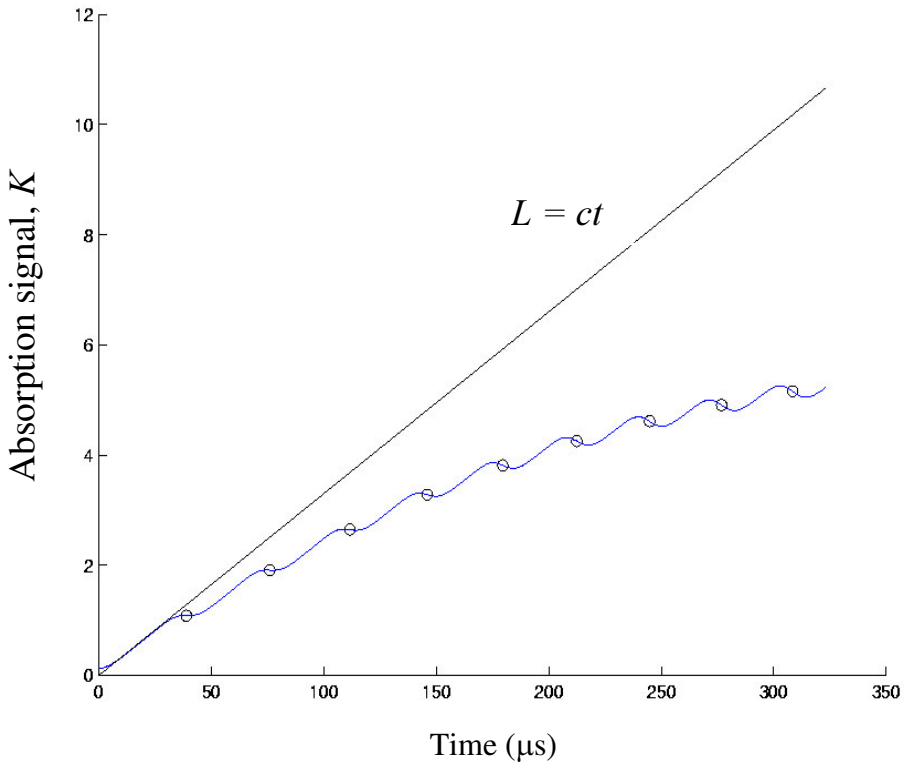

Fig. 3.5: Evolution of the absorption signal K in the region of the first 10 maximums of relaxation oscillations with intracavity absorption $\kappa = 1.1 \cdot 10^{-6}$ cm^{-1}, pump rate $\eta = 1.9$, cavity loss $\gamma = 2.85 \cdot 10^{7}$ s^{-1}. The circles show the positions of the relaxation minima.

These results show that spontaneous emission may limit the sensitivity of the laser to intracavity absorption if strong relaxation oscillations are present. This limitation depends on the parameters of the laser used in the experiment.

Figs. 3.6 and 3.7 show the dependence of the absorption signal divided by the laser duration K/t on the pump rate excess η-1 and the cavity loss γ for Nd- and Yb-doped fibre la-

sers obtained from numerical calculation for weak absorption lines. The pump rate varies in the range of 1.1-11, the cavity loss from 10^6 up to 10^8. If the sensitivity grows linearly with time that according to Eqs. (2.6-2.7), $K/t = \kappa c$. Any deviation from this value means the presence of sensitivity limitation.

Figs. 3.6 and 3.7 show that the sensitivity deviation is bellow 1% only if the cavity loss $\gamma < 3 \cdot 10^6$ s^{-1} and the pump rate $\eta \geq 2$ for the Nd-doped fibre laser and $\eta \geq 4$ for the Yb-doped fibre laser. In general, the deviation grows with larger cavity loss and with smaller pump rate.

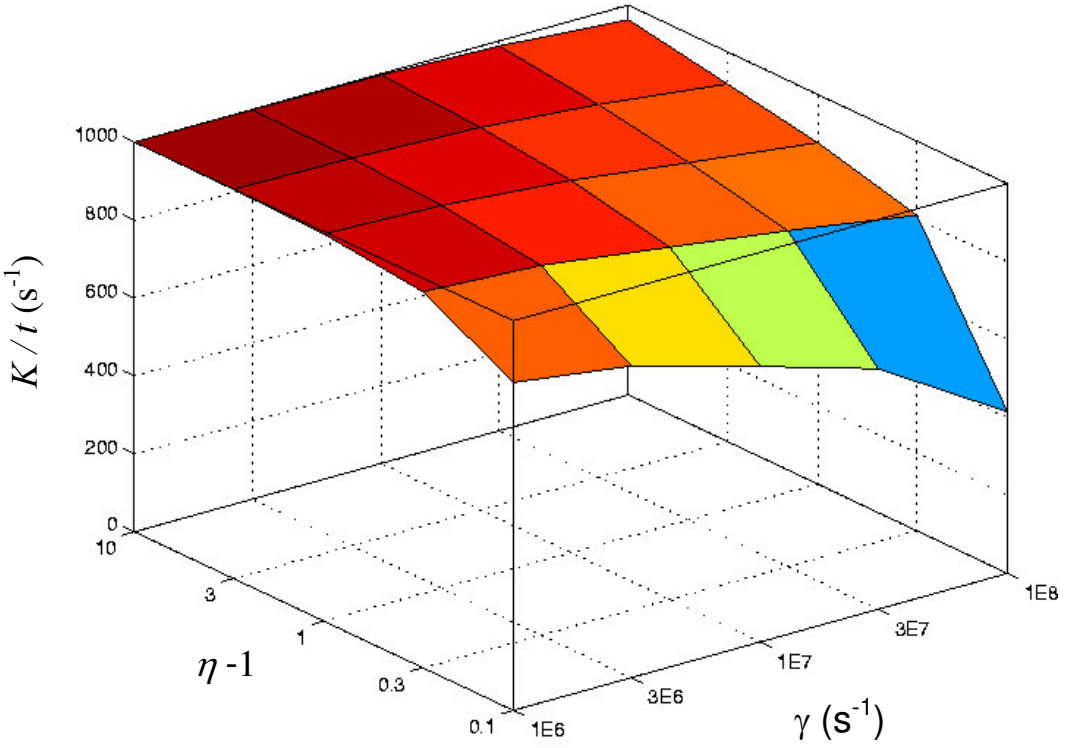

Fig. 3.6: Simulated absorption signal K/t in the cavity of Nd-doped fibre laser vs. pump rate excess η-1 and cavity loss γ at decay rate of the upper laser level A=2000 s^{-1}, gain B=1.3·10^{-6} s^{-1} and absorption coefficient κc=1000 s^{-1}.

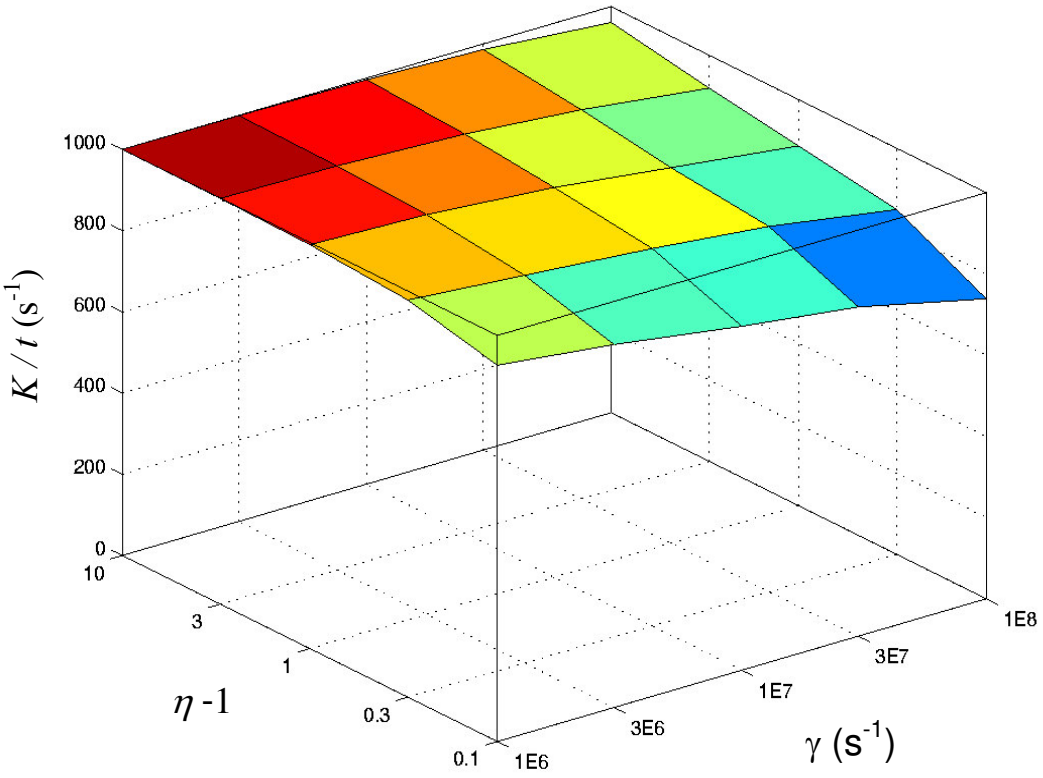

Fig. 3.7: Simulated absorption signal K/t in the cavity of Yb-doped fibre laser vs. pump rate excess η-1 and cavity loss γ at decay rate of the upper level A=1180 s^{-1}, gain B=1.94·10^{-6} s^{-1} and absorption coefficient κc=1000 s^{-1}.

3.3. Dynamics of intracavity absorption in a Nd- and Yb-doped fibre lasers

The experimental set-up is shown in Fig. 3.8. Both Nd^{3+} - and Yb^{3+} -doped fibres are silicate fibres with their cores containing GeO_2 that admit a single transversal mode. The fibre ends are cleaved perpendicular to the optical axis. One end of the fibres is directly coated with a set of dielectric layers, providing high reflectivity at the laser wavelength 1.1 μm, and 90 % transmission at the pump wavelength. It serves as the cavity end mirror M1.

The fibre laser is optically pumped by a diode laser at 820 nm in the case of Nd^{3+} doping, and at 905 nm in the case of Yb^{3+}. The threshold pump power is about 2 mW of the diode laser emission launched into the fibre, with the launching efficiency being about 50%.

The aspheric lenses L1, L2 and L3 are used for collimating the pump laser beam (L1), for focusing the pump light into the fibre (L2), and for collimating the fibre laser beam exiting from the open end of the fibre (L3, AR coated at 1.1 μm). The efficiency of coupling the laser light from the external mirror M2 back into the fibre exceeds 90 %. The lenses L2 and L3 are mounted on X-Y-Z translation stages with 50 nm accuracy of positioning. Lens L3 may be shifted in addition by a piezoelectric transducer. The laser emission is tuned by moving lens L3 along the optical axis, using the effect of chromatic aberration. An external plane dielectric mirror M2 with 1% transmission is used as the output coupler.

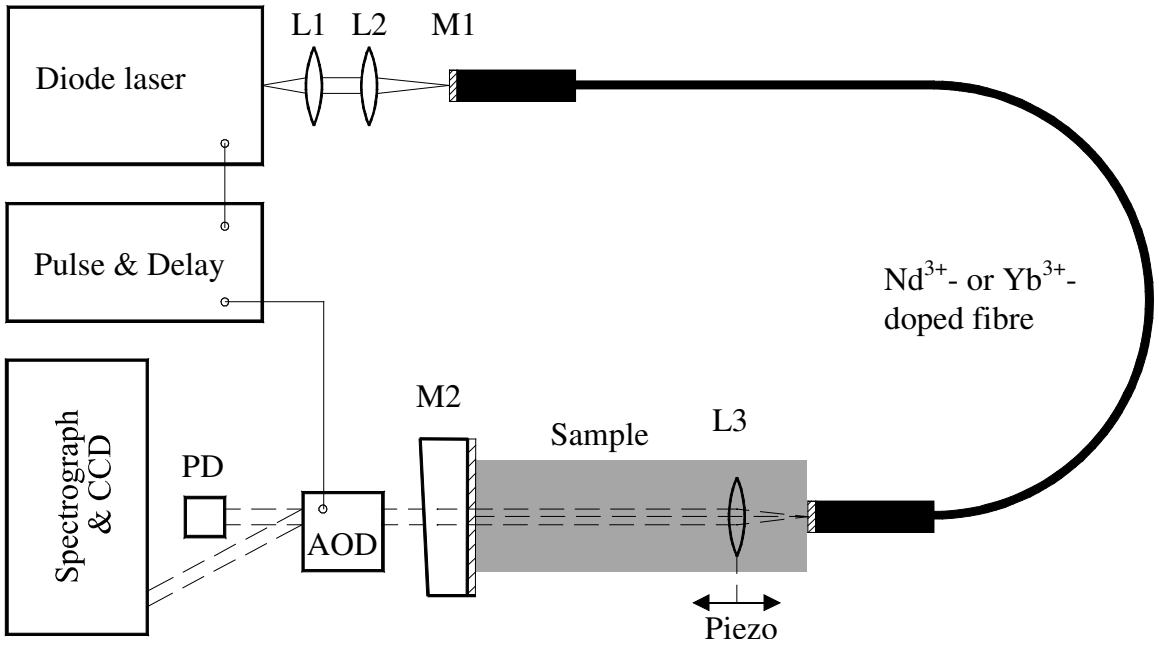

Fig. 3.8: Experimental set-up

The cavity of an Yb-doped fibre laser with L_{cav} =307 cm optical path length is made up of a 78 cm-long fibre, and a 190 cm-long open space L_{ext} filled with air. The cavity of an Nd-doped fibre laser L_{cav} =270 cm optical path length is made up of a 106 cm-long fibre, and a 111 cm-long open space L_{ext} filled with air. The air shows weak absorption in the spectral range of the laser emission, predominantly caused by third overtones of vibronic transitions of the atmospheric water vapour. In order to calibrate the recorded absorption spectra, moisture and temperature of the air have been recorded during the experiment.

The output beam of the fibre laser is deviated by an acoustic-optical deflector (AOD), spectrally analysed by a 1-m Czerny-Turner spectrograph with 17.28-mm-long 1728-channel CCD array (Thompson CSF TH 7803), and stored in a digital oscilloscope having 10-bit dynamical resolution (Krenz TRB 7803). The spectral resolution of the recoding is 0.035 nm; the CCD pixel separation amounts to 0.0034. Time-resolved spectra of laser emission are recorded by setting a detection window, as it is illustrated in Fig.3.9.

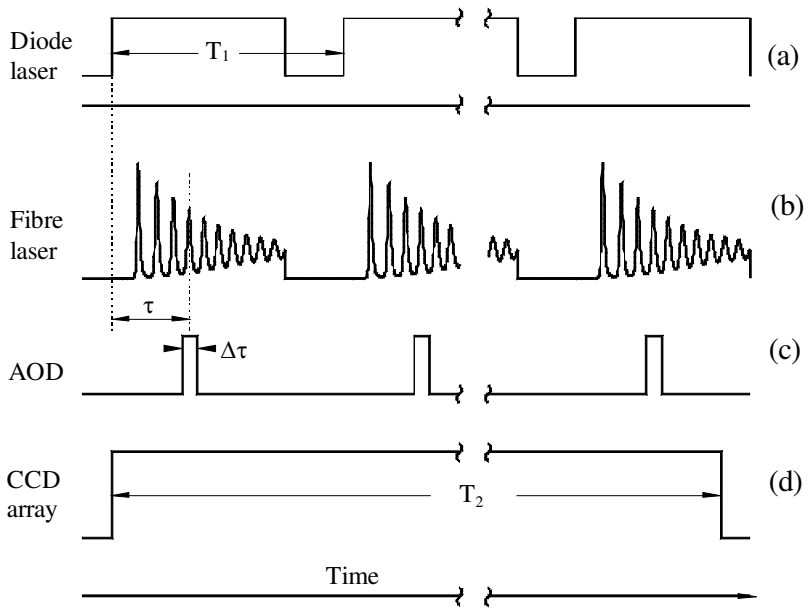

Fig. 3.9: Switching cycle for data acquisition. (a) Emission of the pump diode laser is modulated with the period T_1=1 ms; for 0.8 ms the power is above threshold, and for 0.2 ms below threshold of the fibre laser. (b) Emission of the fibre laser showing relaxation oscillations. (c) Detection window: AOD deflects the beam to spectrograph during the interval $\Delta\tau$ after delay τ against onset of pumping. (d) CCD array integrates light over T_2 = 140 ms, not synchronized with above timing.

The fibre laser emission is turned on and off by step modulation of the pump power P above and below the threshold, P_{thr} ,of the fibre laser. The period of modulation is set to T_1=1 ms (Fig.3.9(a)), and the duration of the pump laser at $P > P_{thr}$ is 0.8 ms. After switching the pump laser to $P > P_{thr}$, the fibre laser starts with the emission showing relaxation oscillations

as they are typical with solid state lasers (Fig.3.9(b)). The AOD, synchronised with the modulation of the pump power, deflects the beam of the fibre laser to the spectrograph for a short time interval $\Delta\tau$ = 8 μs after the adjustable delay τ with respect to the onset of the pump laser (Fig.3.9(c)). The CCD array accumulates emission spectra of 140 laser pulses during the recording time T_2 = 140 ms (Fig.3.9(d)). These spectra become additionally averaged by the storage oscilloscope over 512 successive reading cycles of the CCD array and get finally stored in a computer. The time required for one recording is 512×140 ms ≈ 72 s. The stored signal represents the spectrum of the laser emission at a certain time delay τ after onset of laser oscillation averaged over 71680 laser pulses. The full spectral dynamics is represented by plots of the emission spectra of the laser recorded at successive time delays τ. The time window $\Delta\tau$ of the spectral recording is usually set such as to overlap with one of the relaxation peaks of the laser emission. The emission spectrum of a cw fibre laser is recorded by switching off the pump modulation. The undeflected beam is monitored by a Si-photodiode (PD, Fig.3.8).

Fig 3.10 demonstrates the characteristic relaxation oscillation obtained with the Nd-fiber laser. The rate of cavity loss, γ, of the fibre laser is determined from measurements of the frequency ω of relaxation oscillations by using the relation $\gamma = \omega^2 T_1 / (\eta\text{-}1)$ [21,22], where T_1 is the lifetime of the upper laser level, and $\eta = P/P_{thr}$ is the pump rate normalized to the threshold. Since the above relation holds for four-level configurations it is applicable for both Nd^{3+} - and Yb^{3+} -doped lasers at $\lambda_{em} > 1.04$ μm. Taking into account the lifetimes of the upper laser levels T_1= 460 μs (Nd^{3+}) [21] and T_1= 850 μs (Yb^{3+}), we have measured γ =$9\cdot10^6$ s^{-1} (17 % loss per cavity round trip) with Yb^{3+}-doped fibre laser and $\gamma = 4.6\cdot10^6$ s^{-1} (8 % loss per cavity round trip) with Nd^{3+}-doped fibre laser. This loss is determined by three principal contributions: the output light (1%), reflection from the open end of the fibre, and imperfect coupling of light from the external mirror to the fibre.

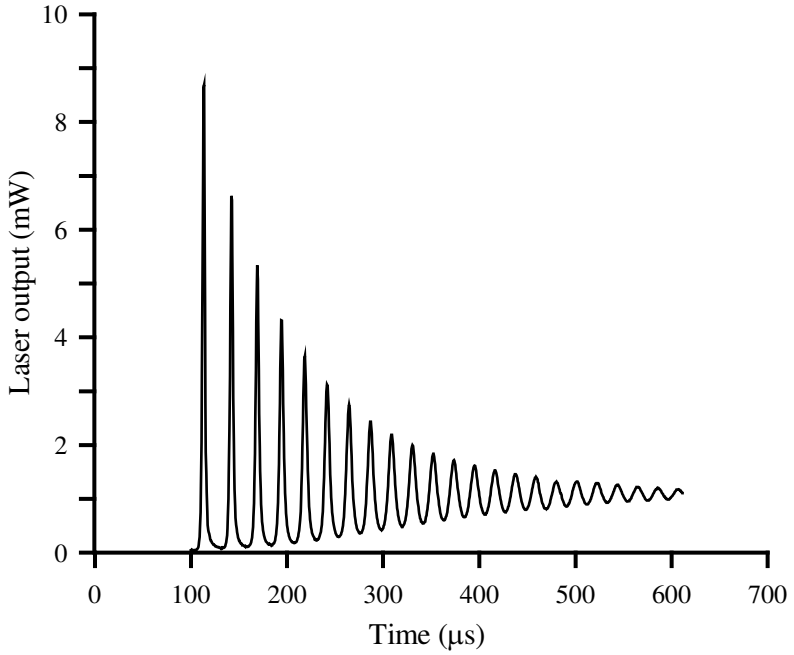

Fig. 3.10: Output power of the Nd^{3+}-doped fibre laser after the pump has been switched above threshold at time zero, pump rate $\eta = 11$.

Fig.3.11 shows the emission spectra of the Yb^{3+}- doped fibre laser at the pump rate η = 5.6 recorded at different times t after onset of laser oscillation [23]. The cavity loss is 17% per round trip. With the data acquisition of the top three spectra, the recording window has been set such as to coincide with one of the first three maxima of the relaxation oscillation of the total power. The spectra are normalized to the maximum signal in each record. The spectral dynamic of the laser follows closely the dynamic of other lasers with homogeneously broadenrd gain, such as the dye laser [24], the diode laser [25] or the Ti:sapphire laser [26]. The emission starts within a broad spectral range and condenses into a narrow range with time advancing. However, this condensation is not as pronounced as with those other lasers since here substantial inhomogeneous broadening is present. Fig. 3.11 also shows the absorption dips of water growing with the time of laser oscillation, since the effective absorption length increases. The condensation of the laser emission is possible if the laser gain is homogeneously broadened, i.e. all the oscillating modes compete for the common population inversion. The width of the stationary spectrums is determined by: spontaneous emission, mode coupling and inhomogeneity of the gain.

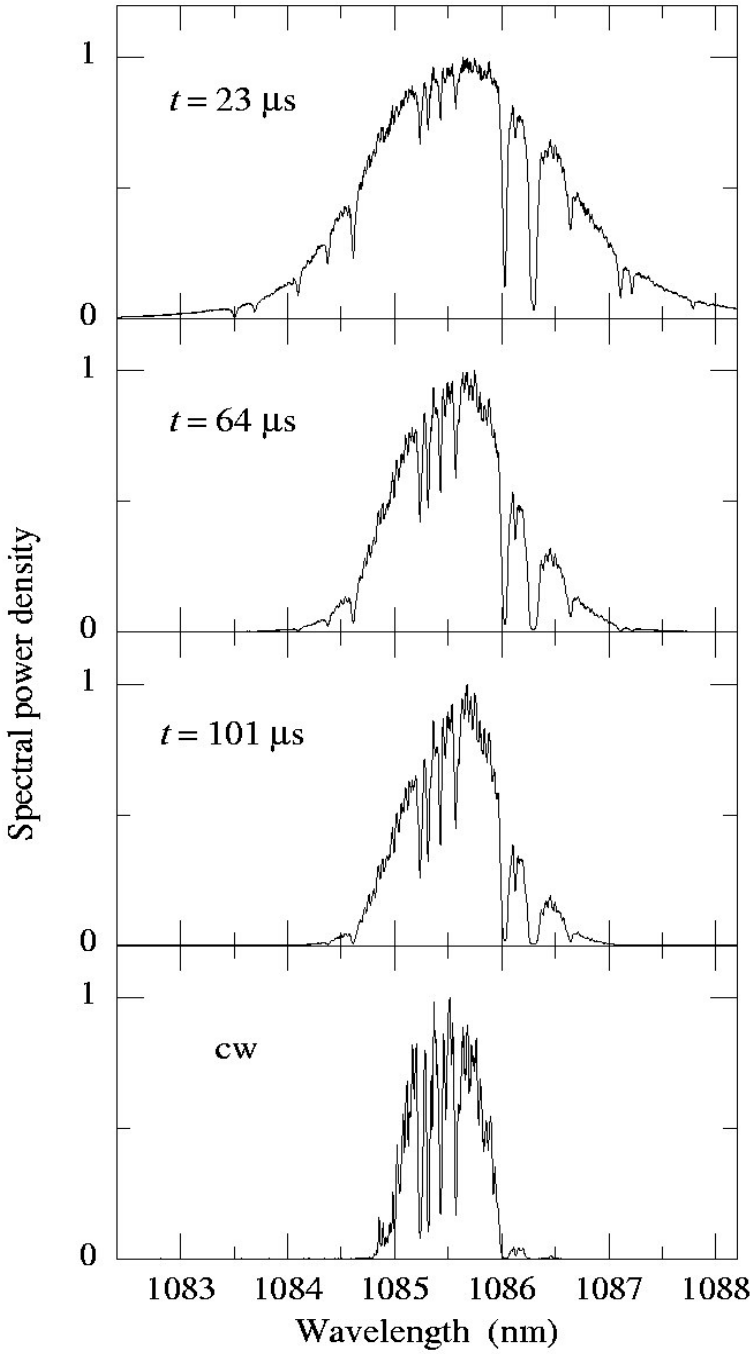

Fig. 3.11: Normalized spectra of the Yb^{3+} doped fibre laser with atmospheric ICA recorded at three different times t after the onset of laser oscillation, and in cw operation; L_{fib} = 78 cm, L_{cav} = 308 cm, $\gamma = 9 \cdot 10^6$ s^{-1}, $\eta = 5.6$.

The spectral dynamic of the Nd^{3+}-doped laser at the pump rate $\eta = 5$, is demonstrated in Fig. 3.12. The emission spectrum is shown on a compressed spectral scale with lower resolution than the spectra of the Yb^{3+}-doped laser, since it is much broader. It shows the spectral dynamics typical for inhomogeneously broadened lasers [27]. The laser emission starts at the spectral position where the net gain is maximum. When this gain becomes saturated, gain in neighbouring regions continues growing, since the corresponding ion classes are not yet saturated. At 60 μs after the onset of laser oscillation, two neighbouring ion classes, spectrally separated from the initially oscillating central class of ions by one homogeneous linewidth $\Delta\nu_{hom}$, dominate the emission spectrum of the laser. The separation between the emission maxima at t = 60 μs is 6 nm (Fig.3.12). This span corresponds to $2\Delta\nu_{hom}$ as proven by independent measurements of the homogeneous broadening of Nd^{3+} ions in silicate glass that yield $\Delta\nu_{hom}$=30 cm^{-1} [28]. At 123 μs, the emission of these neighbouring ion classes has almost vanished, whereas the central class of ions and more distant classes appear oscillating in the laser spectrum. There is no further spectral broadening since the width of the net laser gain is determined by the chromatic aberration of the collimating lens L3 (see Fig. 3.8). The alternation of the emission of neighbouring ion classes that gives rise to transient spectral waves in the laser emission, disappears when the relaxation oscillations become damped. The subsequent cw emission spectrum is broad and reflects the width of the net gain profile. Thus the emission spectrum of this laser broadens with time, in contrast to the spectrum of lasers with homogeneous broadening. This feature, typical for inhomogeneously broadened lasers, is a considerable asset since it allows the simultaneous recording of ICA in a far broader spectral range. The total number of oscillating modes in the emission spectrum of the cw Nd-doped laser in Fig.3.12 is up to 60000.

Fig. 3.13 shows the spectral dynamics of the Nd-doped laser with the pump rate η = 5.6, recorded at a higher spectral resolution. Here the cavity loss is 15 % per round trip. The emission of this laser is tuned to the spectral region of the Yb-doped laser shown in Fig.3.11.

Two features are obvious from comparing the two sets of spectra: (i) The absorption signals in both lasers grow with the duration of laser emission, and this grows is independent on the presence of relaxation oscillations. This finding agrees with the results of measurements on a bulk Nd-doped glass lasser [29], and it is in contrast with other claims [30]. (ii) The sensitivity of the Nd-doped fibre laser in cw operation is higher than that of the Yb-doped fibre laser. The situation changes for strong absorption lines.

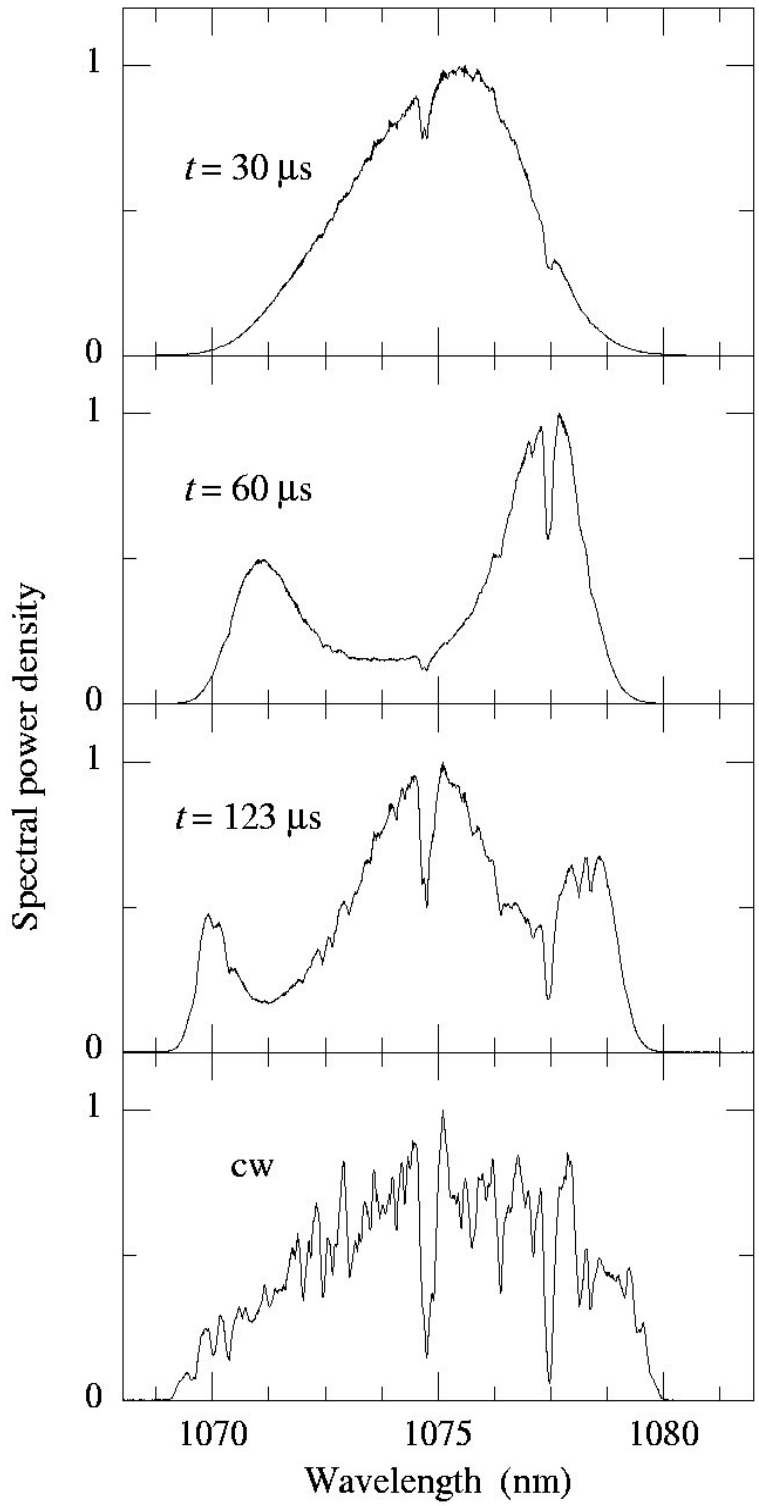

Fig. 3.12: Normalized spectra of the Nd^{3+} doped fibre laser with atmospheric ICA recorded at three different times t after the onset of laser oscillation, and in cw operation, L_{fib} = 78 cm, L_{cav} = 308 cm, $\gamma = 9 \cdot 10^6$ s^{-1}, $\eta = 5$.

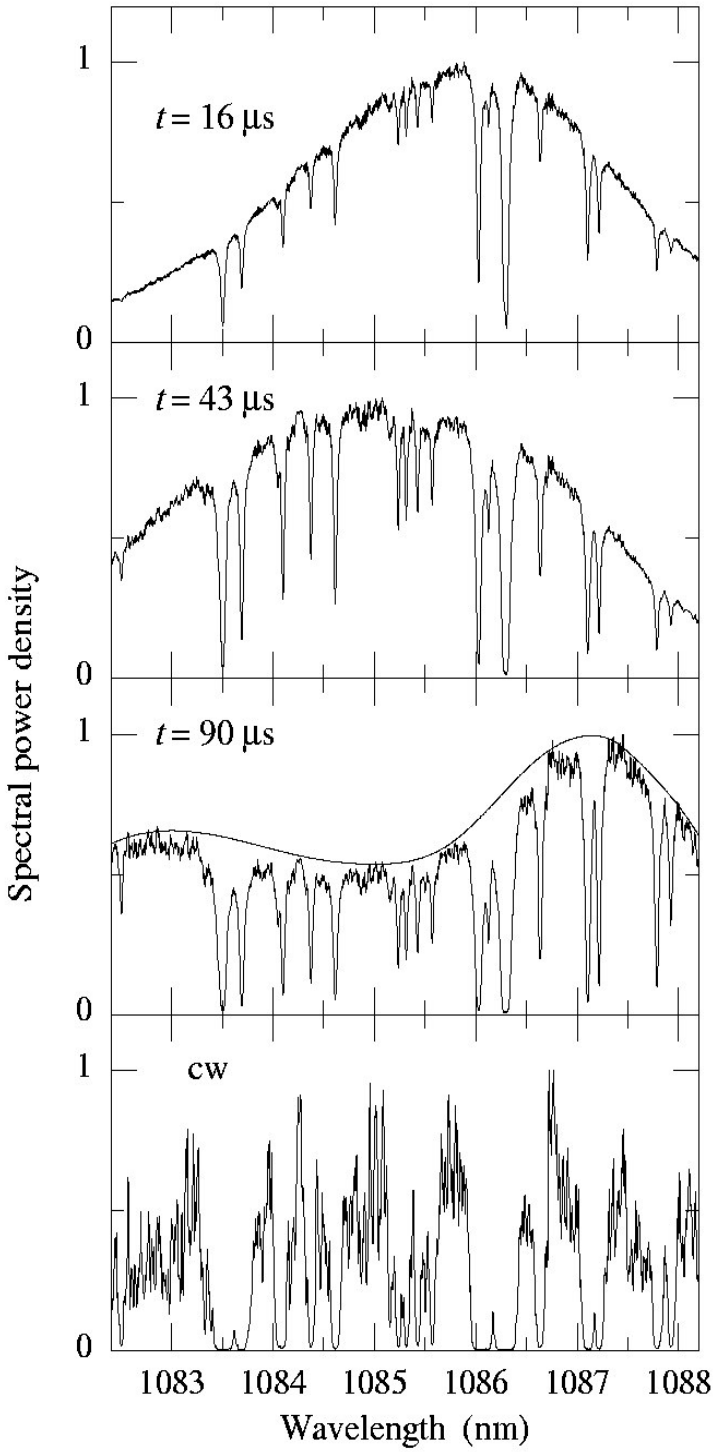

Fig. 3.13: Normalized spectra of the Nd-doped fibre laser with atmospheric ICA recorded at three different times t after the onset of laser oscillations and in cw operation on an extended spectral scale, as compared with Fig. 3.12. Pump rate: $\eta = 5.6$. As an example, the envelope of the emission spectrum without absorption that it required for normalization of the emission spectra is shown at $t = 90$ µs.

Fig. 3.14 shows the experimental values of the effective absorption path length achieved with the Yb^{3+}-doped laser for three strong absorption lines, as a function of duration of the laser emission. The line $L_{\text{eff}} = ct$ is plotted for comparison; its slope is the velocity of light. One can note the deviation from the linearity of the effective path length L_{eff} that is similar to that obtained from simulations (see Figs. 3.4, 3.5) with the absorption line $\kappa = 1.1 \cdot 10^{-6}$ cm^{-1}. The effective path length of $L_{\text{eff}} = 31.3$ km was measured in the 10-th maximum, while according to the $L = ct$ the effective path length is $L_{\text{eff}} = 96$ km. This observation shows that the sensitivity of ICAS measurements with strong absorption lines is limited by spontaneous emission. In the spectral region of the strong absorption lines the intensity of laser emission is small. Therefore the main factor limiting the sensitivity in this case is the spontaneous emission. This factor is not as strong for the weak lines because the intensity of the laser emission is high.

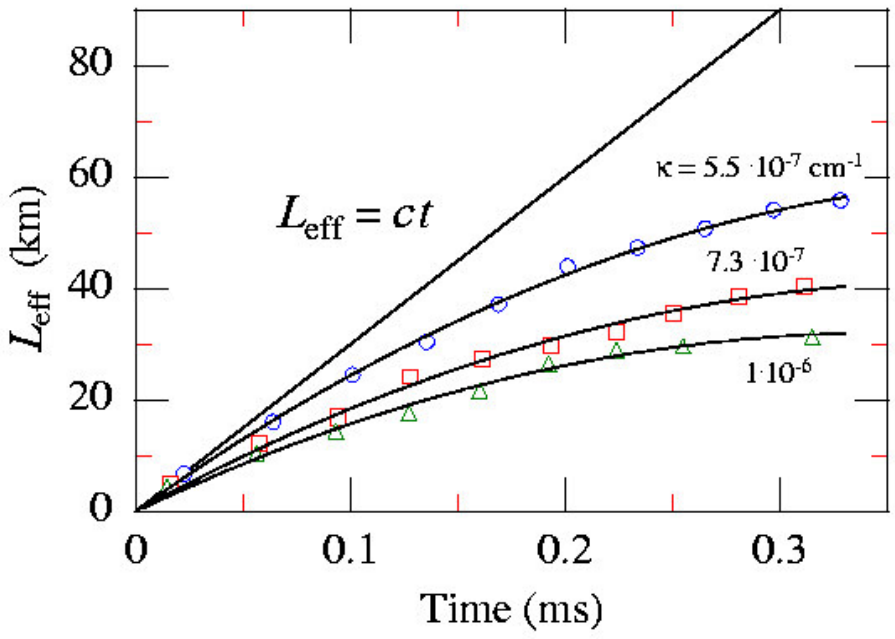

Fig. 3.14: Measured values of effective absorption path length, L_{eff}, obtained with a Yb-doped fibre laser at different absorption lines at pump rate $\eta = 5.6$, cavity loss $\gamma = 9 \cdot 10^6$ s^{-1}, L_{cav}=307 cm, L_{fib}=78 cm.

Even larger deviation from the linearity is observed with simulations at smaller pump rates and larger cavity losses. One can see it in the Fig.3.15 where it is shown the simulation of effective absorption path length with $\eta = 1.9$ and $\gamma = 2.85 \cdot 10^7$ s^{-1}. The diagrams reproduce well the experimental curves in Fig. 3.14. The effective path length deviates from the linear dependence $L=ct$. One can see that this deviation is especially strong for absorption lines with large absorption coefficient.

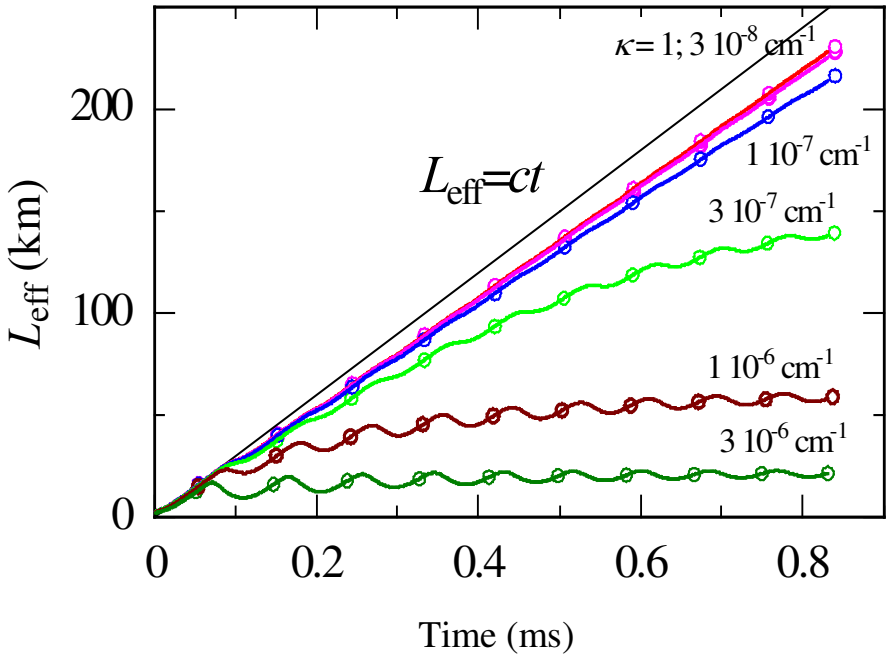

Fig. 3.15: Effective path length L_{eff} simulated for Yb-doped fibre laser for different absorption lines with $\eta = 1.9$ and $\gamma = 2.85 \cdot 10^7$ s^{-1}as a function of time.

Similar phenomenon has been observed with Nd^{3+}- doped fibre laser. Fig.3.16 shows the experimental values of the effective absorption path length, L_{eff}, obtained with the Nd^{3+}-doped laser at five different absorption lines, as a function of time. The data points correspond to different maxima of relaxation oscillations. It was possible to make the pictures of the emission spectrums only in these points of time, but not in the minima and any other intermediate points of time. One can observe the growth of the effective absorption path length with time. The value of the deviation of effective path length from the theoretical value $L_{\text{eff}} = ct$

depends on the absorption coefficient. The lines with the larger absorption coefficient deviate stronger from the linearity. The reason of this behaviour is the influence of spontaneous emission on the absorption signal.

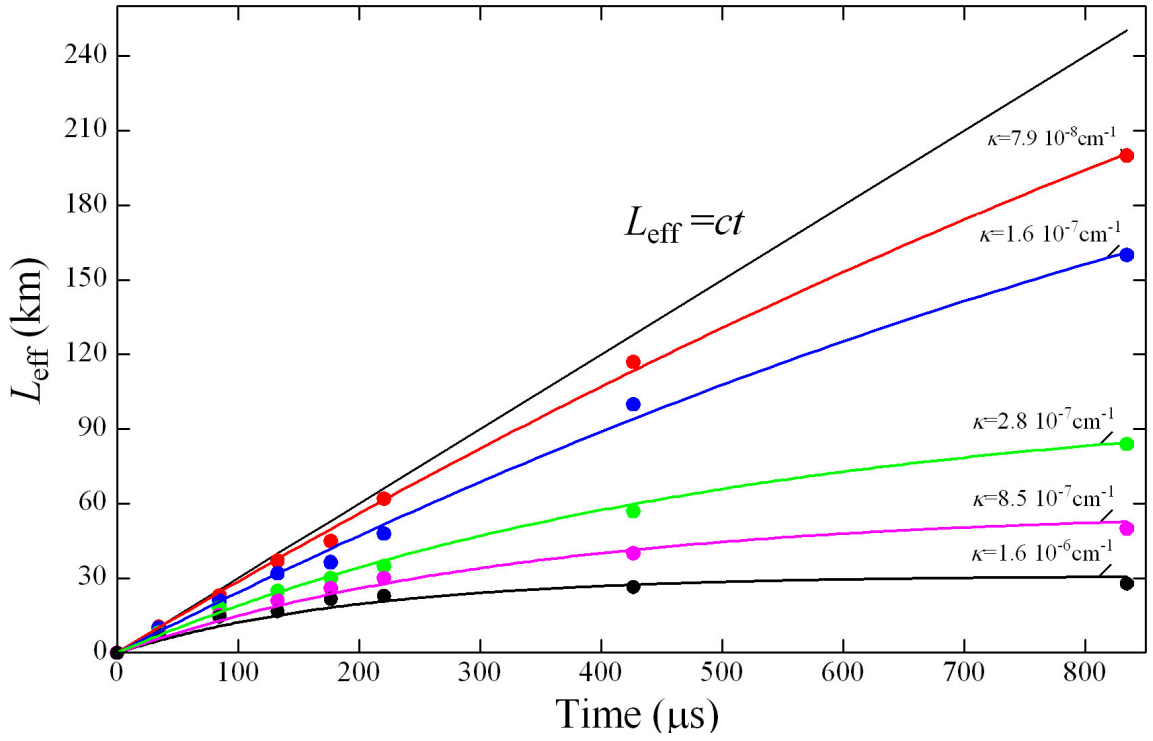

Fig.3.16: Measured values of effective absorption path length, L_{eff}, in the cavity of the Nd-doped fiber laser at different absorption lines, at pump rate η=3.1, cavity loss γ=4.6·10^6 s^{-1} (8% loss per cavity round trip), L_{cav} = 270 cm, L_{fib} = 106 cm.

4. Influence of longitudinal inhomogeneities of the gain on the emission dynamics of solid-state lasers and on the sensitivity of ICAS

4.1. Model description of the laser with longitudinal inhomogeneities of the gain and with ICA

Inhomogeneous distribution of the population inversion leads to the interaction between the lasing modes that may cause sensitivity limitation to intracavity absorption. An increase of the number of lasing modes within homogeneous gain profile leads to the reduction of the ingomogeneous part of the inversion. In this case a higher sensitivity of intracavity absorption measurements can be expected. The number of oscillating longitudinal modes in a fibre laser can vary in a wide range from several modes to several tens thousand modes. That would mean large variations of sensitivity of these lasers to ICA.

If the spatial inhomogeneity of the gain in the fibre laser is the main reason for sensitivity limitation of intracavity absorption spectroscopy, the sensitivity should depend on the number of oscillating modes within the homogeneous linewidth of the gain. Since various fibre lasers show different homogeneous linewidth of the gain, they may have different sensitivities to ICA. This phenomenon can be investigated experimentally by controlling the number of oscillating modes in the laser with intracavity etalon.

The pump power may also affect the spectral sensitivity. When it increases the intensities of the individual oscillating modes also increase. Therefore the spectral modulation of the gain grows which is equivalent to the increase of the spatial inhomogeneities of the inversion in the laser cavity. As a result, the spectral sensitivity of intracavity absorption measurements may decrease when the pump increases.

There are two kinds of spatial inhomogeneities in the laser cavity: longitudinal and transversal. Transversal inhomogeneity arises from the nonuniform saturation of the population inversion in the plane, orthogonal to the laser axis and will be considered later. The reason of the longitudinal ingomogeneity is the saturation of the population inversion in the longitudinal direction, so called „spatial hole burning“. The laser field in the cavity is represented by standing waves (see Fig. 4.1). The eigen functions for Fabry-Pero cavity are

$$\psi_q(z) = 1 - \cos(k_q z) \tag{4.1}$$

where $k_q = 2\pi q / L$, q – number of half-waves in the laser cavity, L – the length of the cavity.

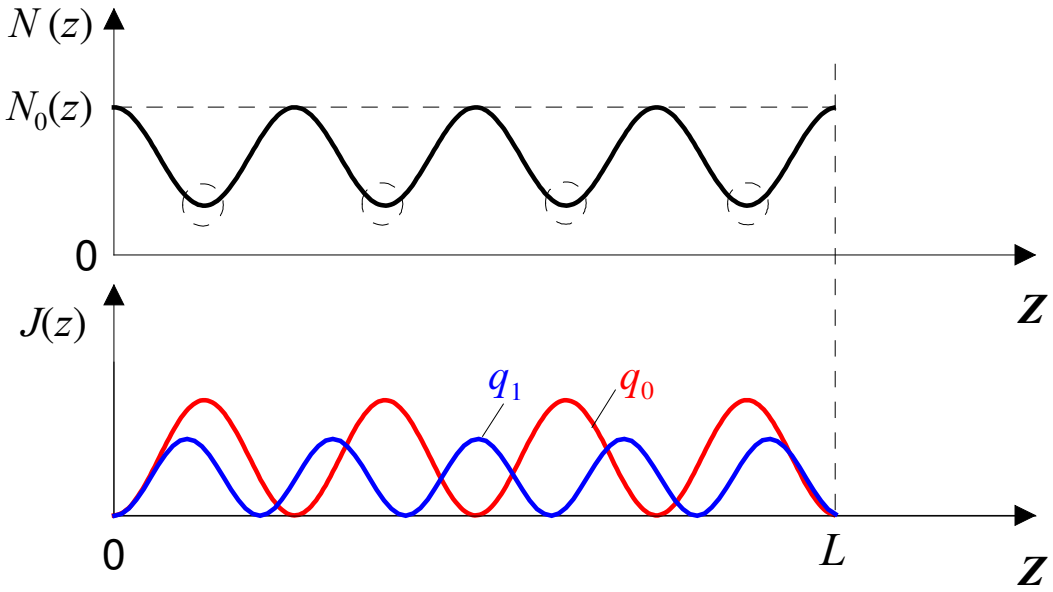

Fig. 4.1: Population inversion $N(z)$ (top) and intensity of laser emission $J(z)$ (bottom) versus axial coordinate. Spatial holes burned by laser emission of the mode q_0 in the inversion are shown by circles.

Inhomogeneous distribution of the intensity of laser field along the laser cavity leads to nonuniform longitudinal saturation of the population inversion. The inversion is minimum in the antinodes of standing waves of laser radiation because of a stronger saturation in these points whereas it is maximum in the nodes of the laser field. As a result, in addition to the central mode with maximum gain the other modes with smaller gain become also oscillating. Fig. 4.1 demonstrates this effect. The distribution of laser intensity $J(z)$ (bottom) and corresponding distribution of the population inversion $N(z)$ (top) are shown along the laser cavity (0-L). For simplicity only two axial modes are shown here. q_0 is the mode with a maximal gain, q_1 is the mode with a smaller gain. The inversion is saturated by the mode q_0 in its antinodes ("circles"). Mode q_1 saturates the inversion in other spatial points of the cavity. Nonuniform saturation of the population inversion along the cavity is one of the reasons of multimode oscillations in the laser.

The population inversion N including the pump rate P is described through Fourier expansion:

$$Y(z,t) = Y_0 + 2 \sum_{i=1/2,1,...}^{\infty} Y_i \cos(k_i z), \tag{4.2}$$

where

$$Y_i(t) = \frac{1}{L} \int_0^L dz Y(z) \cos(k_i z) \tag{4.3}$$

Substitution of $N \rightarrow N(z)$, $P \rightarrow P(z)$ and $M_q \rightarrow M_q \psi_q(z)$ into the rate equations (2.8) and (2.9) gives the following equations:

$$\dot{M}_q = B_q (M_q + 1) \int_0^L dz \, \psi_q N(z) - \gamma(1 + \beta_q) M_q \tag{4.4}$$

$$\dot{N}(z) = P(z) - AN(z) - N(z) \sum_q B_q M_q \psi_q(z) \tag{4.5}$$

where

$$\beta_q = \kappa_q c/\gamma + Z(q - q_0)^2 \tag{4.6}$$

are losses in the mode q, including narrowband absorption ($\kappa_q c$) and parabolic extended loss caused by dispersion of the intracavity lens (L3 in Fig. 3.8), Z is the parabolic function.

Substitution the expansions (4.2) and (4.3) into Eq. (4.4) and (4.5) gives [23]:

$$\frac{d}{dt} m_q(\tau) = G[b_q (m_q + \frac{B_0}{A})(n_0 - n_q) - (1 + \beta_q) m_q], \tag{4.7}$$

$$\frac{d}{dt} n_0(t) = \eta_i - n_0 (1 + \sum_q b_q m_q) + \sum_q \frac{b_q m_q}{2}, \tag{4.8}$$

$$\frac{d}{dt} n_i(t) = -n_i (1 + \sum_q b_q m_q) + \frac{b_i m_i n_0}{2}. \tag{4.9}$$

where the following dimensionless values are used:

$$\begin{aligned}
&\eta_i = P_i / P_{0,thr},\\
&n_i = N_i / N_{0,thr},\\
&b_q = B_q / B_0,\\
&m_q = M_q B_0 / A,\\
&\tau = tA \qquad \Rightarrow \qquad \frac{d}{d\tau} = \frac{1}{A}\frac{d}{dt}\\
&G = \gamma / A.
\end{aligned} \tag{4.10}$$

In Eg. (4.9) is $i = (q_0 - \frac{\mathcal{N}\text{-}1}{2})...(q_0 + \frac{\mathcal{N}\text{-}1}{2})$. Eqs. (4.7-4.9) are the classical equations of Tang, Statz and de Mars [31] for the mode number m_q, averaged value of the population inversion n_0 and the spatial harmonics of the population inversion n_i.

From Eqs. (2.5), (2.6), (2.11) and (4.10) follows the expression for spectral saturation time:

$$t_s = \frac{\ln(M_q / M_{q,\kappa})}{\kappa c} = \frac{\ln(m_q / m_{q,\kappa})}{\kappa c} \tag{4.11}$$

where $m_{q,\kappa}$, m_q are the normalized photon numbers with narrowband absorption and without narrow band absorption.

From Eq. (4.7) with $\dot{m}_q = 0$ the population inversion is:

$$n_q = \eta_0 - \frac{1+\beta_q}{b_q}\frac{m_q}{(m_q + B/A)}. \tag{4.12}$$

From Eg. (4.8) with $\dot{n}_0 = 0$ the stationary value of the population inversion is:

$$n_0 = n_0 - \sum_q m_q (1+\beta_q)\frac{m_q}{(m_q + B/A)}. \tag{4.13}$$

Solution of Eq. (4.9) relative to m_i ($\Leftrightarrow m_q$) and substitution n_q from Eg. (4.12) gives the expression for the mode number:

$$m_q = \frac{2}{n_0 b_q}\left(n_0 - \frac{1+\beta_q}{b_q}\frac{m_q}{(m_q + B/A)}\right)\left(1 + \sum_j b_j m_j\right). \tag{4.14}$$

The comparison Eqs. (4.11) and (4.14) gives the expression for the spectral saturation time:

$$t_s = -\ln\left(\frac{n_0 - \frac{1+\beta_{q,\kappa}}{b_q}\frac{m_{q,\kappa}}{m_{q,\kappa} + B/A}}{n_0 - \frac{1}{b_q}\frac{m_q}{m_q + B/A}}\right)\frac{1}{\beta_{q,\kappa}\gamma}. \tag{4.15}$$

By neglecting spontaneous emission [$m_q/(m_q+B/A) \approx 1$] and in the middle of a spectrum (b_q=1) t_s becomes:

$$t_s \approx \frac{-\ln\left[1 - \frac{\beta_{q,\kappa}}{n_0 - 1}\right]}{\beta_{q,\kappa}\gamma} \approx \frac{1}{\gamma}\left(\frac{1}{n_0 - 1} + \frac{\beta_{q,\kappa}}{2(n_0-1)^2} + \frac{\beta_{q,\kappa}^2}{3(n_0-1)^3} + \ldots\right). \tag{4.16}$$

From Eq. (4.16) the spectral saturation time increases when the cavity loss γ decreases and the absorption coefficient ($\propto \beta_{q,\kappa}$) increases. The less the value of n_0 differs from 1, the larger the saturation time becomes. With larger number of oscillating modes the value n_0-1 becomes small. Without the spatial hole burning n_0=1. For classical Tang-Statz-DeMars rate equations [31] the value of n_0 is evaluated as (neglecting the spontaneous emission):

$$\frac{1 - 1/\eta}{2 \cdot \mathcal{N}} < (n_0 - 1) < \frac{1 - 1/\eta}{1 \cdot \mathcal{N}} \tag{4.17}$$

The saturation time is estimated from the upper limit of Eg. (4.17) and by taking into account only of the first term of Eq. (4.16):

$$t_s \approx \frac{1}{\gamma}\frac{\mathcal{N}}{(1 - 1/\eta)} \tag{4.18}$$

In addition, one can see from (4.18) that spectral saturation time is proportional to the number of oscillating modes. Besides that t_s does not depend on pump rate when it is large.

For a passive cavity without the gain the saturation time is $t_s \approx 1/\gamma$, in an active cavity $t_s \approx \mathcal{N}/\gamma$, i.e. the mode number determines how much γt_s can exceed the unity (Eq. 4.18).

Comparison with limitation by spontaneous emission

The sensitivity limitation caused by the spatial hole burning can be compared with fundamental sensitivity [1] $L_{\text{eff}} = \frac{cM_q^s}{\gamma}$. The sensitivity is limited by the spontaneous emission if the spectral saturation time resulting from the spontaneous emission is smaller than the sensitivity limitation resulting from the spatial hole burning:

$$\frac{M_q}{\gamma} < \frac{1}{\gamma}\frac{\mathcal{N}}{1-1/\eta} \quad \Leftrightarrow \quad M_q < \frac{\mathcal{N}}{1-1/\eta} \tag{4.19}$$

From Eq. (3.7) the average value of the photon numbers in all modes is:

$$M_q \approx \frac{1}{\mathcal{N}}\frac{A}{B}(\eta - 1) \tag{4.20}$$

Eqs.(4.19) and (4.20) result in

$$\frac{A}{B} < \frac{\eta \mathcal{N}^2}{(\eta-1)^2} \tag{4.21}$$

The sensitivity limitation resulting from the spontaneous emission is present closely to the laser threshold and with many oscillating modes. With the given parameters η and $\mathcal{N}$ the sensitivity of the laser is limited by the spontaneous emission if A/B is small.

Influence of the mode number

Fig. 4.2 shows the stationary emission spectra for different number of laser modes calculated with Eqs. (4.7)-(4.9). With smaller number of laser modes (left), the distribution of the population inversion along the laser cavity is more inhomogeneous. In this case the gain saturation is stronger for the stronger oscillating modes, whereas it becomes weaker for weak modes. A small absorption line of intracavity absorption can be observed in the emission spectrum. The population inversion get more homogeneous along the laser cavity at the larger number of oscillating modes. In other words the ingomogeneity of the population inversion is gradually smoothed with the increase of the number of lasing modes. In this case the competition between the lasing modes increases. As a consequence, the emission spectrum condenses stronger and the absorption dip in the spectrum is larger.

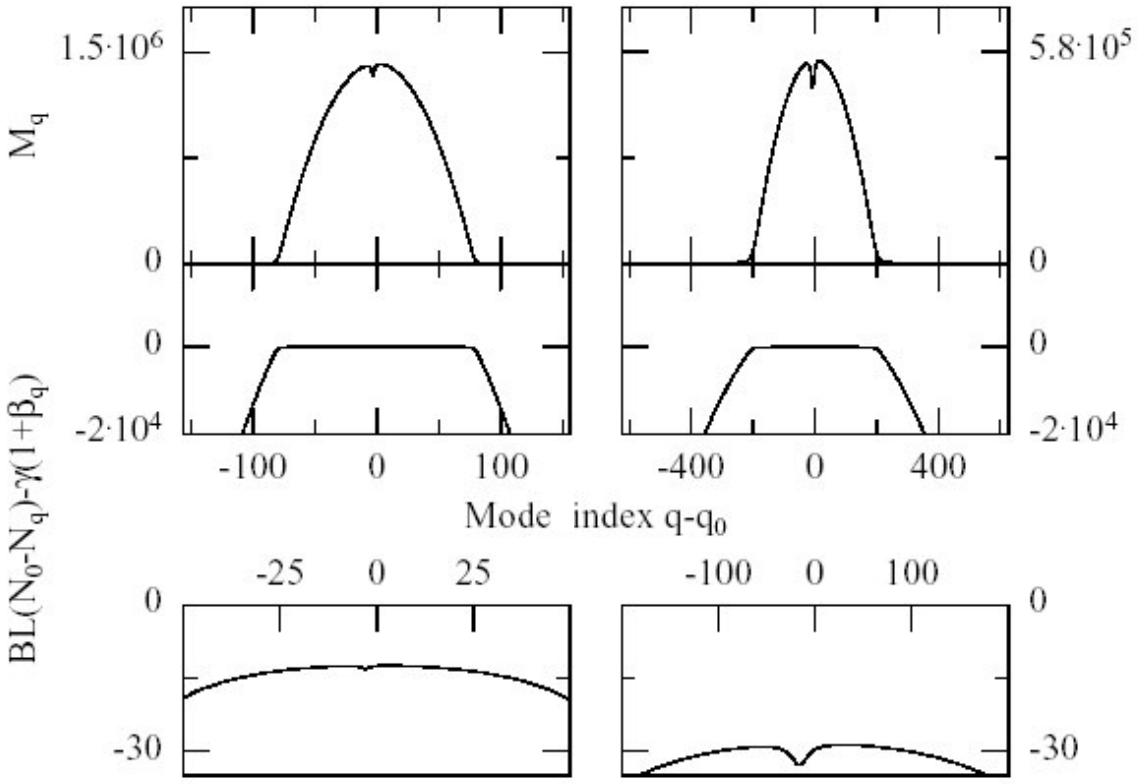

Fig.4.2: Stationary spectra (top) and netto-gain (bottom) of the laser with two different number of oscillating modes at pump rate $\eta = 1.5$.

Influence of the pump parameter

Fig. 4.3 shows the stationary emission spectrum (top) calculated with Eqs. (4.7)-(4.9) for two different pump rate. One sees that the higher sensitivity is observed with the smaller pump parameter. In this case the narrow-band losses is less compensated by the inhomogeneous gain. With smaller pump rate the inhomogeneity of the population inversion along the laser cavity is reduced. That is the reason of the higher sensitivity of intracavity absorption measurements. With the increase of the pump rate the spatial ingomogeneity of the population inversion grows. As a result the depth of the absorption line in the emission spectrum significantly drops. In this case the intracavity absorption is partially compensated by spatial inhomogeneities of the gain.

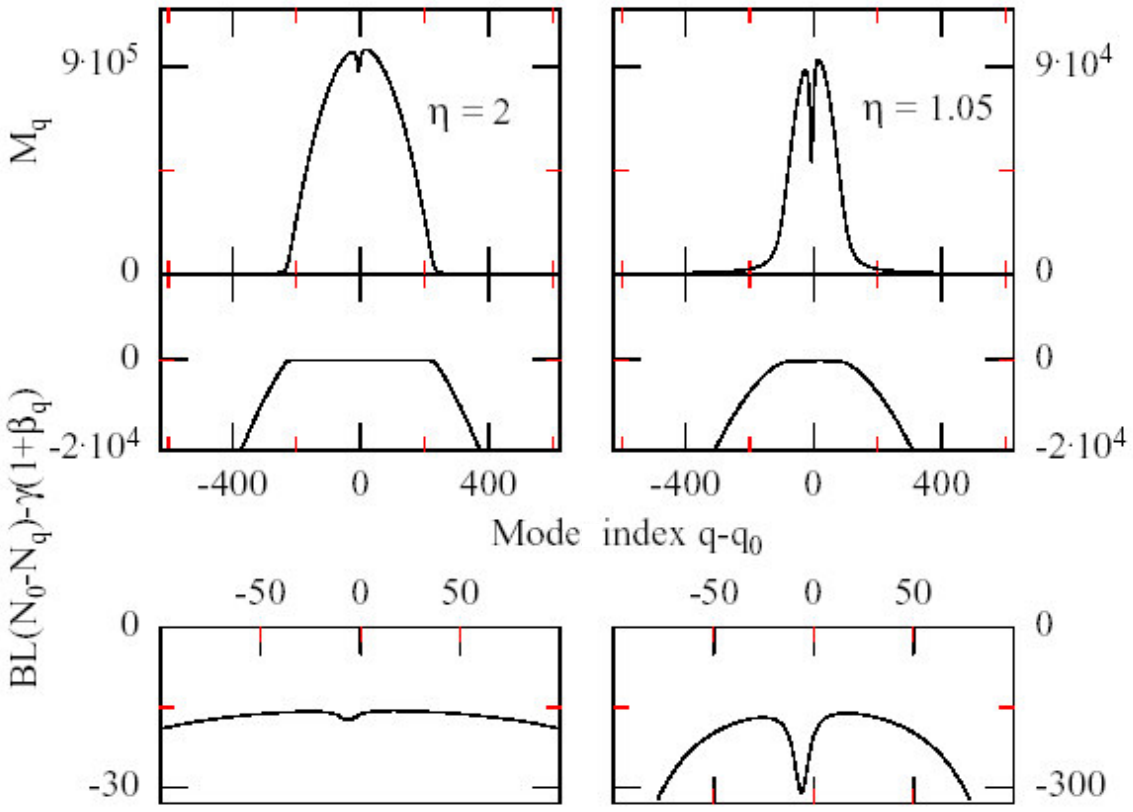

Fig. 4.3: Stationary spectra (top) and netto-gain (bottom) for two different pump parameter η.

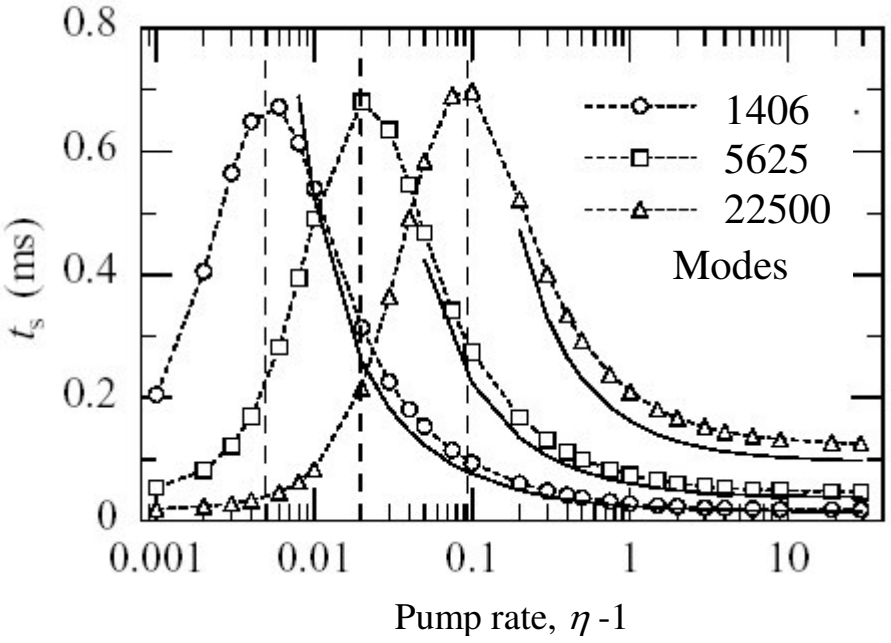

Fig. 4.4: Spectral saturation time, t_s, vs. pump rate η and mode number.

Figure 4.4 shows the calculated dependence (dotted lines) of the saturated time t_s derived from Eq. (4.15) on the pump rate η -1, at different number of oscillating modes. The calculation has been made when different number of longitudinal modes participated in the laser process: 1406, 5625 and 22500. The sensitivity increases with a pump rate up to the maximal value shown in the figure by the dotted vertical lines and then decreases down to the nearly constant value at η -1 >>1. The increase of the spectral saturation time with the pump rate near the threshold is caused by the spontaneous emission. The increase is observed up to the value of the pump rate at which the contributions to the sensitivity limitation by the spatial hole burning and by the spontaneous emission are about the same. With further increase of the pump rate the spatial hole burning becomes the most important factor for sensitivity limitation. The continuous lines indicate the spectral saturation time t_s obtained with Eq (4.18), describing the case when the spontaneous emission is not taken into account at the estimation of the sensitivity. One can see that well above the laser threshold the sensitivity is larger for the laser with the larger number of oscillating modes. The calculated behaviour of the sensitivity agrees with the experimental data as it is shown in the next section.

4.2. Influence of laser parameters on the sensitivity of ICA measurements with a Nd-doped fibre laser

According to Eqs. (2.7) and (4.18) spectral sensitivity determined by spatial inhomogeneities is:

$$L_{\text{eff}} = c\,t_s \approx \frac{c}{\gamma}\frac{\mathcal{N}}{1-1/\eta} \tag{4.22}$$

From this expression the sensitivity should grow with the number of oscillating laser modes and decrease with increasing pump power. In the following experiment these features are proved experimentally.

The experimental set-up is shown in Fig. 4.5. The input mirror M_1 of the laser cavity is placed directly on the input face of the Nd-doped fibre and has reflectivity near unity in the operation range of the fibre laser, and high transmission at the wavelength of the pump radiation. The length of the fibre is L_{fib} = 105 cm. The aspheric lens L is employed for the collimation the fibre laser beam exiting from the open end of the fibre. The laser emission is tuned by moving the lens L along the optical axis using the effect of chromatic aberration. The output plane dielectric mirror M_2 has 1% transmission in the operation range of the fibre laser. The intracavity etalon is used to select a small number of oscillating modes. It consists of two glass substrates with back faces cut at the Bruster angle. The front faces of both etalon substrates have the reflectivity near 4%. Two glass substrates is adjusted perpendicular to the optical axis of the cavity with variable separation L_{et}. Variation of L_{et} is used to select a required number of laser modes. Intermode frequency spacing, $\Delta\nu = 1/2L_{\text{et}}$, decreases with an increase of the etalon length L_{et}. The number of oscillating modes can be increased by increase of the total optical length of the cavity L_{cav} up to 8 m with a help of 2 additional cavity mirrors M_3, M_4. The intracavity etalon is absent in this case. The output beam is analysed by the spectrograph with CCD array and a digital oscilloscope.

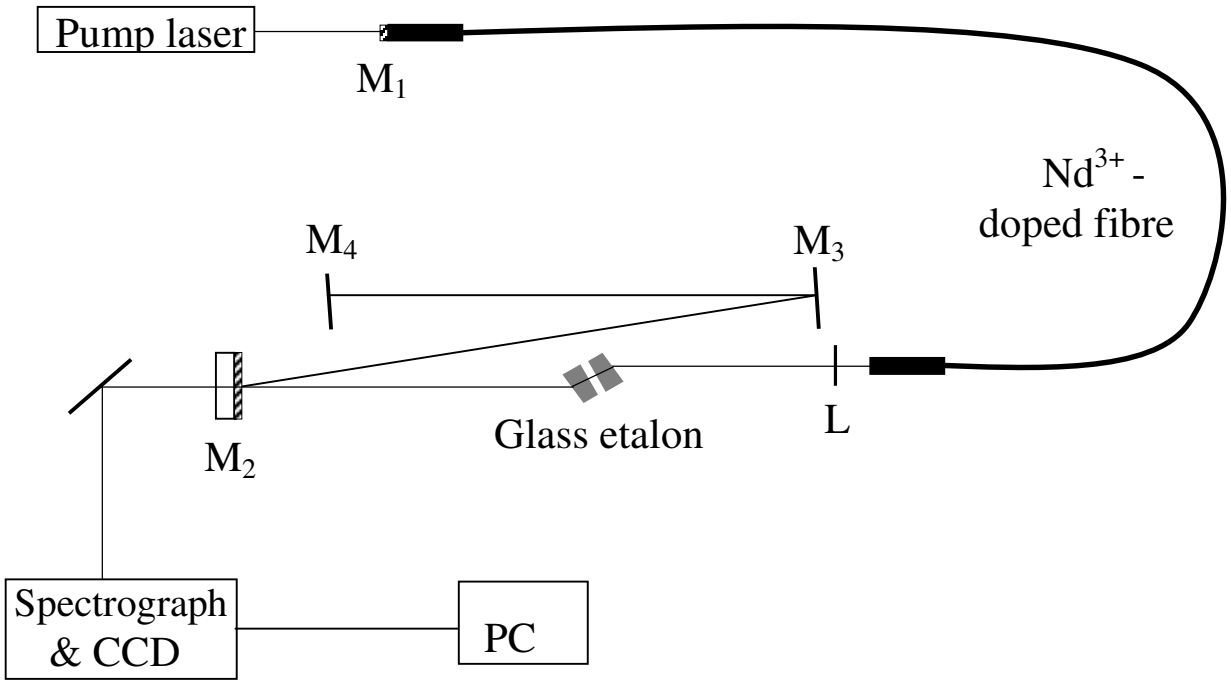

Fig. 4.5: Experimental set-up

Fig. 4.6 shows 4 graphs of the emission spectra of the Nd-doped fibre laser at the different number of oscillating modes within homogeneous spectral width of the gain: 1700, 20000, 35000, 48000 at the pump rate η=2.3. The small number of oscillating modes, 1700, was selected by intracavity etalon with a base L_{et} = 1.5 mm. In this case the spectral sensitivity is reduced. It corresponds to the effective path length of 8 km. The reason for this reduction is the increase of spatial inhomogeneities along the laser cavity for small number of modes. Emission spectra in the 2–4 diagrams were recorded without intracavity etalon, but with different length of the cavity: 3.3 m, 5.8 m, 7.9 m. The number of oscillating modes in the cavity grows when the cavity length increases. One can see from the Fig. 4.6 that the effective path length increases from 8 km to 63 km with the increase of the mode number from 1700 up to 48000. The reason of larger spectral sensitivity at larger number of oscillating modes is the decrease of longitudinal spatial ingomogeneity. Fig. 4.7 demonstrates this phenomenon.

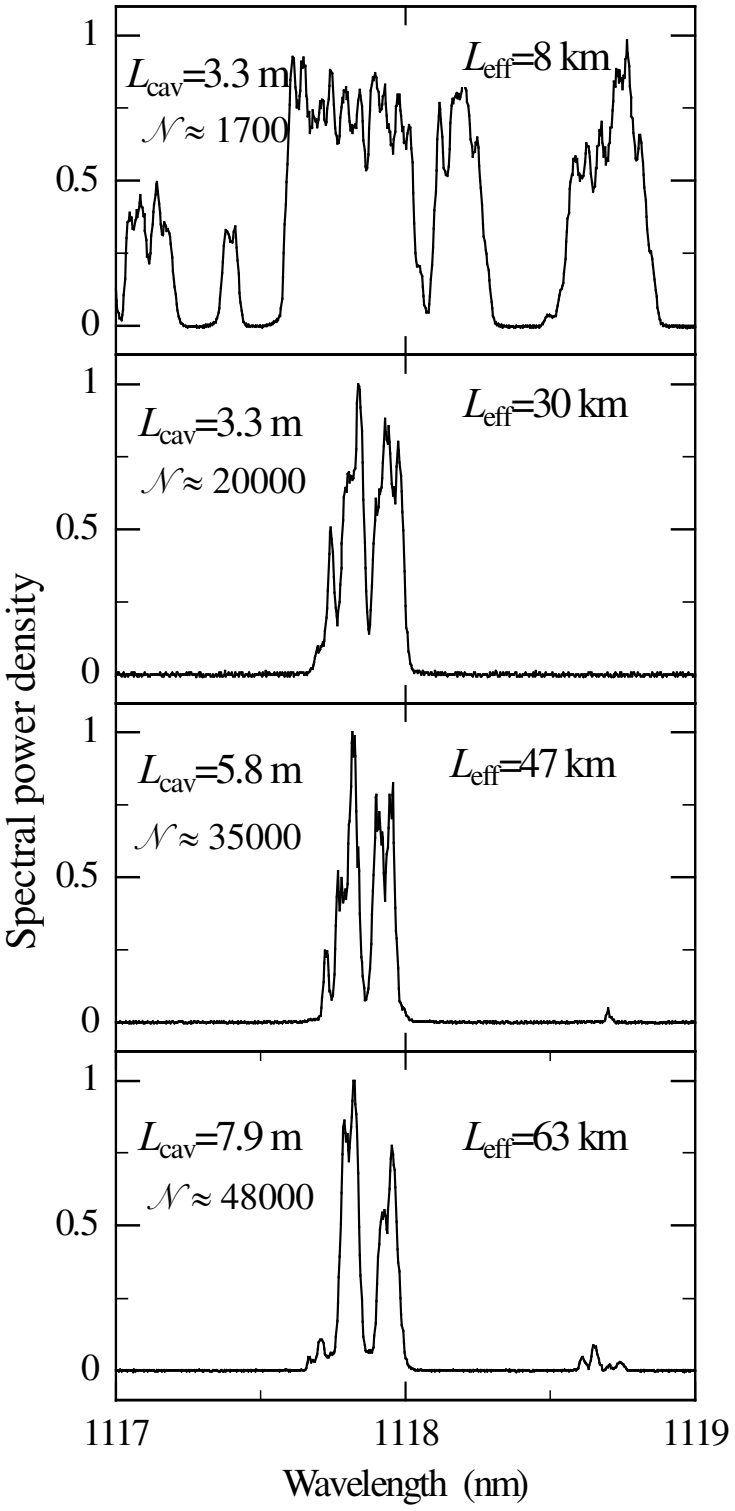

Fig. 4.6: Emission spectra of the Nd^{3+}-doped fibre laser with the different number of oscillating modes, $\mathcal{N}$, at pump rate $\eta = 2.3$.

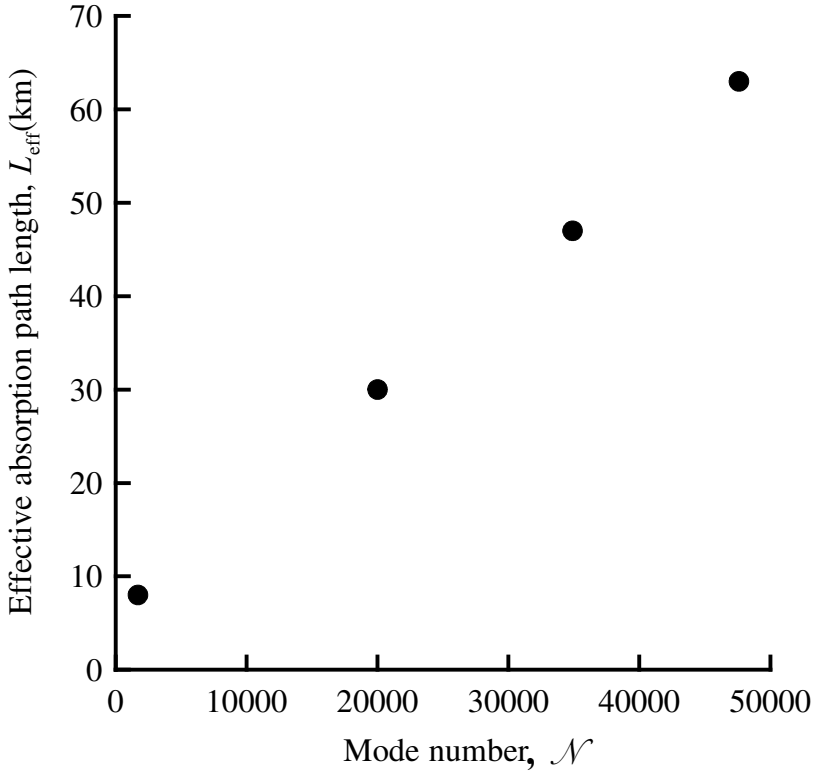

Fig. 4.7: Experimental values of the effective absorption path length, L_{eff}, of ICAS with Nd^{3+}-doped fibre laser vs. the mode number, $\mathcal{N}$, at pump rate $\eta = 2.3$.

The second experiment is made in order to prove the dependence of the spectral sensitivity on the pump rate. Figure 4.8 shows the emission spectra of the Nd-doped laser at different pump rate in the case of the largest number of modes (laser cavity L_{cav} = 7.9 m). The corresponding transmission spectrum obtained with HITRAN data base (top graph) is shown for comparison. One can see the increase of the absorption signal at the decrease of the pump rate from $\eta = 23$ to $\eta = 1.07$. The effective path length L_{eff} grows here up to the value of 101 km at the pump rate $\eta = 1.07$. The reason for this growth of L_{eff} is the evident decrease of the longitudinal spatial inhomogeneity in the laser cavity at the small pump rate.

Figure 4.9 shows the emission spectra of the Nd-doped laser at the change of pump rate in the case of the shortest laser cavity L_{cav} = 3.3 m. The corresponded transmission spectrum obtained with HITRAN data base (top graph) is shown for comparison. One sees from Fig. 4.9 the increase of the absorption signal at the decrease of the pump rate. The effective path length increases from 6 km to 57 km at the decrease the pump rate from $\eta = 66$ to $\eta = 1.4$.

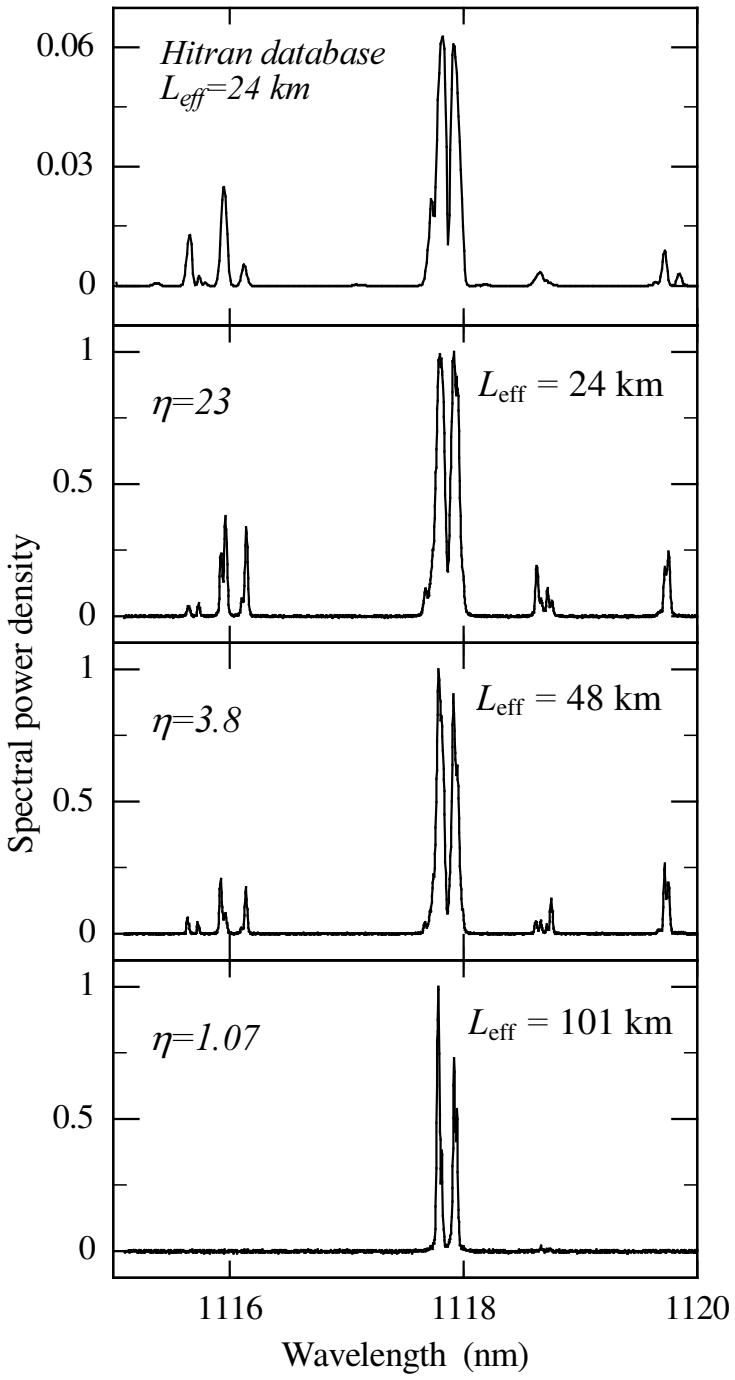

Fig. 4.8: Emission spectra of the Nd^{3+}-doped fibre laser with the number of oscillating modes $\mathcal{N}$ = 48000 (L_{cav} = 7.9 m), at three values of pump rate, η, and corresponding transmission spectrum from HITRAN data base (top).

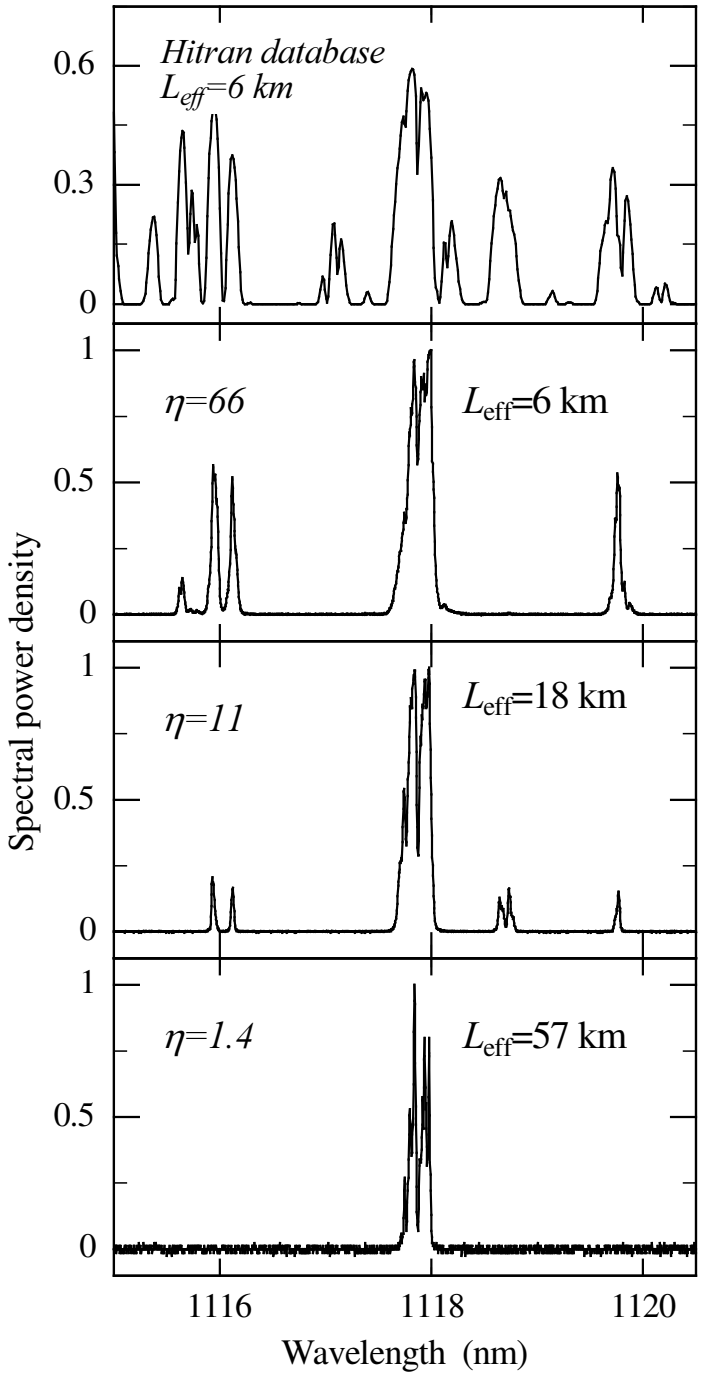

Fig. 4.9: Emission spectra of the Nd^{3+}-doped fibre laser with the number of oscillating modes $\mathcal{N}$ = 20000 (L_{cav} = 3.3 m), at three values of the pump rate, η, and corresponding transmission spectrum from HITRAN data base (top).

Fig. 4.10 demonstrates the dependence of the effective absorption path length on the pump rate at 4 values of the number of oscillating modes. These results generally agree with

theoretical estimations shown in Fig. 4.4. Unfortunately the pump rate smaller than $\eta < 1.05$ was not used in the experiments because of insufficient stability of the system.

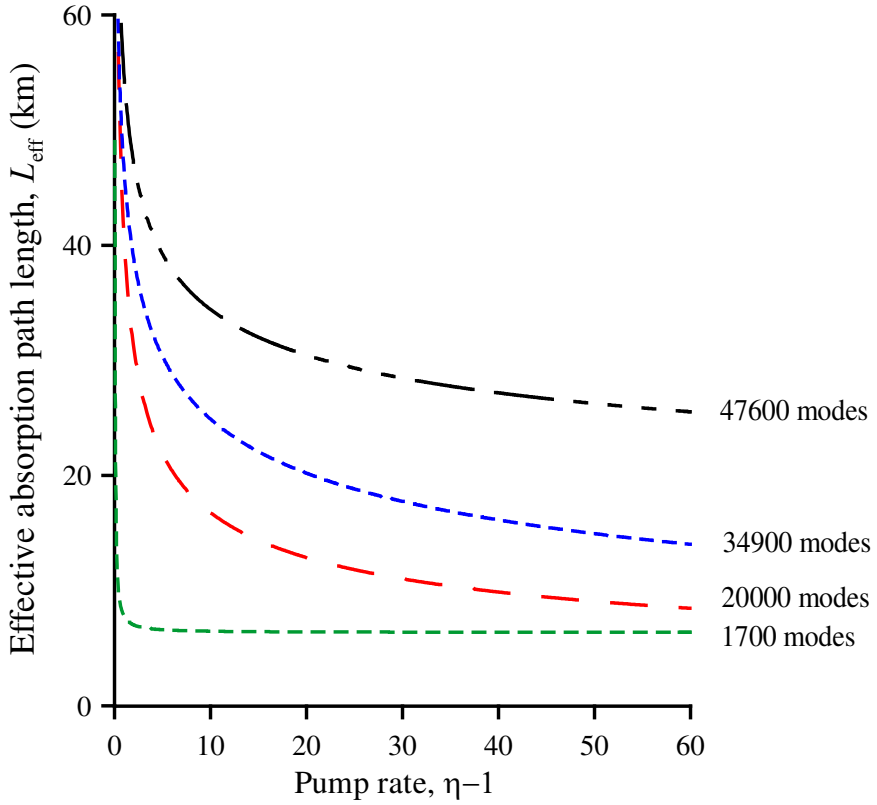

Fig. 4.10: Experimental values of the effective absorption path length, L_{eff}, of ICAS with Nd^{3+}-doped fibre laser vs. pump rate, η-1, at the different number of oscillating modes.

4.3. Emission dynamics of a multimode solid-state lasers

Another feature affected by mode coupling in the laser is emission dynamics in individual laser modes. Experimental investigation of emission dynamics of individual laser modes is possible by using lasers with short cavity [32]. In this section a chip solid-state laser is investigated. In this laser a gain medium is made out of 4-mm-thick disk of Schott LG680 silicate-based laser glass, doped with 3% of Nd. Both sides of the disk are coated with dielectric mirrors. The optical length of the cavity is 6 mm. The Nd:glass laser is optically pumped by a cw Ti:sapphire laser at 810 nm. In the laser the gain medium fills the entire length of the cavity, and both linear polarizations are excited. Since the number of oscillating modes is small, spatial inhomogeneity („hole burning“) of the gain in longitudinal [33, 34] and azimuthal directions [35] provides strong mode coupling in this lasers. It results in antiphase cross-saturation dynamics of the transient modal emission featuring low-frequency relaxation oscillations. Measurements performed with short cavities that are partly filled with gain medium [36–39] show similar features but less pronounced.

In cw operation the total laser power and the power in individual laser modes show characteristic fluctuations around their mean values as it is demonstrated in Fig. 4.11. The emission in the individual laser mode (bottom) has been selected by the spectrograph and recorded simultaneously with the total power (top) by a two-channel digital oscilloscope. In the fluctuations of the individual laser mode (bottom), one recognizes two types of oscillations: (i) in-phase oscillations of all modes with a characteristic time scale of ≈ 10 ms and an amplitude of up to 3%, and (ii) antiphase oscillations with a characteristic time scale of ≈ 100 ms and an amplitude of up to 15%. The total laser power does not show slow oscillations of the second type, confirming the perfect cancellation of these oscillations in different laser modes. In contrast, the fast oscillations of the total laser power (first type), show the same amplitude as oscillations in individual modes, proving their in-phase nature.

Figure 4.12 shows the power spectra of the observed fluctuations of the total output (top) and of the output in one of the central laser modes at η =1.19. They are Fourier transformations of long (≈64 ms) experimental records and are normalized to their component at zero frequency. Therefore, all power spectra show fluctuation amplitudes relative to the corresponding mean power and are compatible.

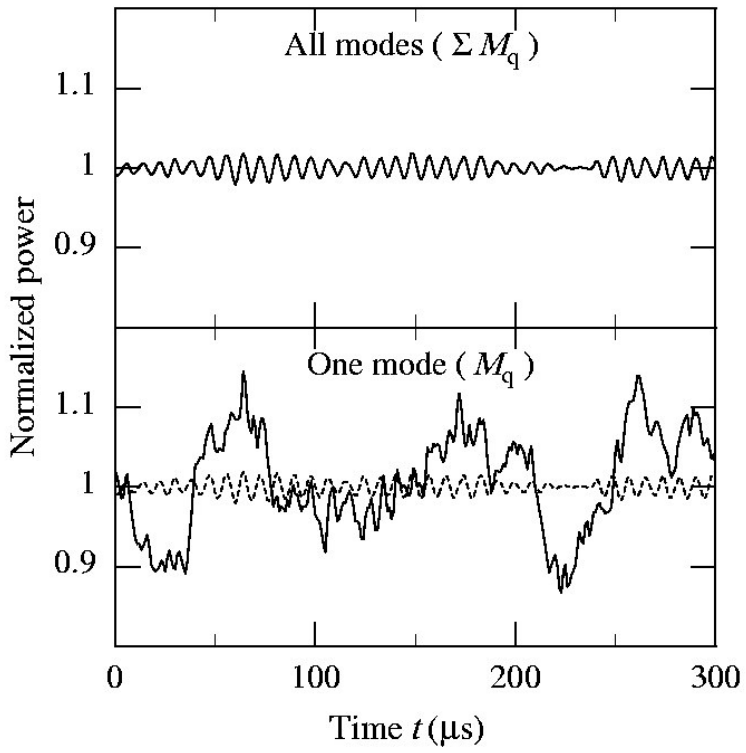

Fig. 4.11: Amplitude fluctuations of the total laser power (top) and of the power in one individual mode (bottom), recorded simultaneously at η=1.19. Emission power is normalized to the corresponding mean value. Total power is additionally shown in the bottom diagram by the dashed lines.

In previous experiments with a small number of oscillating modes [33, 34, 40] power spectra of the modal intensities revealed many low-frequency peaks. The number of these peaks was observed to be as large as the number of modes, $\mathcal{N}$, oscillating in the laser. In the present experiment spectra of the modal powers show only two peaks, one at the frequency (ν_0) of in-phase oscillations and another one, 10 times stronger, at the frequency (ν_q) of anti-phase oscillations, which depends upon the modal power. Fluctuations of the total laser power (Fig. 4.11, top) are much weaker than fluctuations of the modal power (Fig. 4.11, bottom) since the dominant fluctuations are antiphase oscillations that cancel in the total output. The power spectrum of the total output reveals just weak residual oscillations at ν_q with less than 1% of the amplitude of anti-phase modal oscillations.

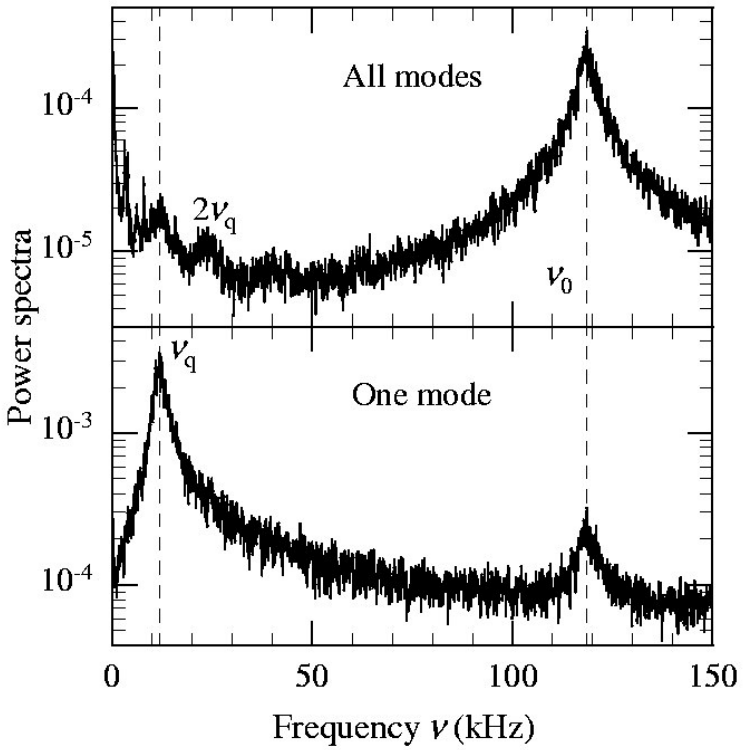

Fig. 4.12: Low-frequency power spectra of the total (top) and of the modal (bottom) power calculated from experimental records of laser emission at η=1.19 and normalized to the zeroth Fourier component. Frequency positions of in-phase (ν_0) and antiphase (ν_q) relaxation oscillations are shown by dashed lines.

In the total output also oscillations at $2\nu_q$ show up. These second-harmonics oscillations are very weak and are not clearly visible in the modal power because of the strong and broad peak at the fundamental frequency, ν_q . However, in the total output the second-harmonics oscillations are not compensated and appear almost as strong as oscillations at ν_q. The strongest fluctuations of the total laser power take place at the frequency of the in-phase oscillations (ν_0). The relative amplitudes of these oscillations in the total and modal laser power are about the same ($2\text{x}10^{-3}$).

These experiments show that longitudinal inhomogeneity of the gain is indeed very important mechanism coupling the laser modes. It should be taken into account in various practical applications, e.g. by measurements of intracavity absorption.

4.4. Emission spectrum of a Nd:YAG laser

If only a few laser modes are oscillating the longitudinal spatial inhomogeneity is very strong. Emission spectrum can be significantly modified in this case. It is especially pronounced with solid-state lasers, if a doped crystal is used as a gain medium. In these cases the laser mostly shows a spectrally narrow gain, that is usually homogeneously broadened. As a result the laser emission spectrum condenses into a few longitudinal modes.

The problem of the influence of spatially nonuniform gain profile on dynamical characteristics of solid-state lasers (optical spectrum, polarization, etc.) has a long history, especially as regards the relation between the longitudinal nonuniformity of gain and the emission spectrum [41-47]. It was found that when an active medium is situated close to cavity mirrors the competition of longitudinal modes is maximal and, as a result, the optical spectrum changes. This increased competition of laser modes has a simple qualitative explanation. Spatial structures of cavity eigenmodes are most strongly overlapped near a cavity mirror since nodes of all modes meet there. How this effect is manifestied quantitatively depends on the longitudinal nonuniformity of the gain.

The emergence of solid-state longitudinally pumped lasers renewed the interest to the specific features of their dynamical behavior caused by nonuniform gain profile inside the laser cavity. One case of the longitudinal gain nonuniformity is that the cavity is filled by the active medium only partially. Another natural case is the exponential absorption of pump intensity when a pump beam propagates along the active element. The influence of each type of the gain nonuniformity was studied in Refs. [48,49]. In work [49], it was shown both experimentally and theoretically that the partial filling of a cavity by the active medium may lead to suppression of the longitudinal modes with potentially large gain (for example, the central mode) by weaker modes. Analogous conclusions were drawn in [48] where the exponential decrease in the population inversion from one end of crystal (from which the laser is pumped) to another was considered.

In this section the stationary emission spectra of a Nd:YAG laser with a small number (up to 10) of oscillating modes will be investigated. In this laser the nonuniformity of the gain along a cavity is caused by the inhomogeneous saturation of the gain by a partial filling of the cavity with gain medium and by the exponential decay of the pump radiation along the crystal. These inhomogeneities may lead to redistribution of the photons among the laser modes.

The behaviour of miltimode solid-state lasers is well described by the rate equations of Tang, Statz and deMars for two-level medium (TSdM-model) [31, 50]. The laser cavity is supposed to be filled entirely by the two-level active medium. Spectral broadening of the gain is considered to be homogeneous.

$$\frac{\mathrm{d}\, I_k(\tau)}{\mathrm{d}\,\tau} = G I_k(\tau)\left[g_k \int_0^L n(z,\tau)\psi_k^2(z)\mathrm{d}\, z - 1 \right], \tag{4.23}$$

$$\frac{\partial\, n(z,\tau)}{\partial \tau} = \eta(z) - n(z,\tau)\left[1 + \sum g_j \psi_j^2(z) I_j(\tau)\right]. \tag{4.24}$$

Here the following dimensionless notations are used: $I_k(\tau)$ is the normalized intensity of an individual mode; $n(z, \tau)$ is the density of the population inversion; $\tau = t/T_1$ is the time measured in the units of the inversion decay rate; z is a longitudinal coordinate; L is the cavity length; $\eta(z)$ is the pumping parameter, which reflects the unsaturated inversion distribution along the cavity; $\psi_k(z)$ is the resonator eigenfunction, and $\psi_k(z) = \sqrt{2}\sin(\pi q_k z / L)$ for longitudinal modes of a Fabry-Perot cavity; $\pi q_k/L$ is the wave number (where q_k is a large integer corresponding to the number of half wavelengths of the k-th mode in the cavity) and k = 1,2,...,K, where K is the full number of laser modes included in the model; $G = T_1/T_c$, T_c is the photon lifetime in the laser cavity; g_k is the kth mode gain coefficient.

In the simplest case when pump is uniform along the cavity ($\eta(z) = \eta_0$) the inversion can be expanded into Fourier series:

$$n(z,\tau) = N_0(\tau) - 2\sum_{k=1}^{K} N_k(\tau)\cos(2\pi q_k z / L) + \ldots \tag{4.25}$$

Coefficients of this expansion are the population inversion averaged over the cavity length N_0 and the amplitudes of spatial inhomogenities (spatial harmonics) of the inversion N_k with the scale of nonuniformity of ~$\lambda/2$, reflecting the effect of spatial hole burning by each longitudinal mode. The inhomogeneous distribution of the intensity of laser radiation along the laser cavity is a reason of nonuniform longitudinal saturation of the population inversion. The inversion is minimal in the antinodes of standing waves of the laser radiation because of a stronger saturation in these point. It is maximal in the nodes of laser radiation because the laser field of the modes equals zero in these places and the inversion is not re-

duced due to the interaction with the field. As a result, in addition to the central mode with maximum gain other modes with smaller gain become also oscillating. It is one of the reasons of multimode simulated emission in the laser with homogeneously broadened gain.

By substituting the expansion (4.25) into the rate equations (4.23), (4.24) we obtain the following set of 2*K*+1 equations:

$$\begin{aligned}
\frac{dI_k}{d\tau} &= GI_k\left[g_k\left(N_0 + N_k\right) - 1\right], \\
\frac{dN_0}{d\tau} &= \eta_0 - N_0\left(1 + \sum_{m=1}^{K} g_m I_m\right) - \sum_{m=1}^{K} g_m I_m N_m, \\
\frac{dN_k}{d\tau} &= -\left(1 + \sum_{m=1}^{K} g_m I_m\right) N_k - \frac{1}{2} g_k I_k N_0
\end{aligned} \tag{4.26}$$

where

$$N_0(\tau) = \frac{1}{L}\int_0^L N\left(z,\tau\right)\mathrm{d}\,z\,,\; N_k(\tau) = \frac{1}{L}\int_0^L N\left(z,\tau\right)\cos(2\pi q_k z / L)\mathrm{d}\,z \tag{4.27}$$

It's necessary to note that the TSdM model does not take account of large-scale spatial ingomogenities of population inversion with nonuniformity on the scale of a cavity length as well as small-scale gratings with nonuniformity on the scale of ~λ/4, ~λ/8. This approximation is valid to describe low-frequency dynamics of multimode solid-state lasers in the case of a uniform unsaturated gain along the cavity. In real lasers, however, the pumping of the active medium is not uniformly distributed along the cavity. For this case D. Pieroux and P. Mandel [51] use the expansion of the population inversion of the active medium into the infinite Fourier series in terms of cosine functions:

$$n(z,\tau) = N_0(\tau) + 2\sum_{p=1}^{K-1} Y_p(\tau)\cos\left(2\pi p z / L\right) - 2\sum_{k=1}^{K} X_k(\tau)\cos\left(2\pi q_k z / L\right) \tag{4.28}$$

Here X_k are the the amplitudes of small-scale spatial inhomogenities of population inversion reflecting the effect of spatial hole burning by each longitudinal mode, and Y_p are the amplitudes of large scale spatial inhomogenities, which take account of nonuniform pump

profile along the cavity and the saturation effect of the population inversion by the lasing modes. In this approach the dimension of the equations increases up to $3K$:

$$\begin{aligned}
&\frac{dI_k}{d\tau} = GI_k\left[g_k\left(N_0 + X_k\right) - 1\right], \\
&\frac{dN_0}{d\tau} = \eta_0 - N_0\left(1 + \sum_{m=1}^{K} g_m I_m\right) - \sum_{m=1}^{K} g_m I_m N_m, , \\
&\frac{dY_k}{d\tau} = \eta_0 - Y_p\left(1 + \sum_{m=1}^{K} g_m I_m\right)X_k - \frac{1}{2}\sum_{m=1}^{K} g_m I_m Y_{m+p} - \frac{1}{2}\sum_{m=1+p}^{K} g_m I_m X_{m-p},
\end{aligned} \tag{4.29}$$

where k=1,2,...,K, p=1,2,...,K-1.

One can suggest a such consideration of longitudinal pump nonuniformity, where the dimension of the model is the same as in a simple case of uniform longitudinal pump distribution ($2K$+1). TSdM equations provide the expression for the saturated population inversion in steady state. One can see from Eq. (4.24) that the saturated inversion $n(z)$ is proportional to the unsaturated population inversion $\eta(z)$:

$$\overline{n}(z) = \eta(z) \cdot \left[1 + \sum g_j \psi_j^2(z) \bar{I}_j\right]^{-1} \tag{4.30}$$

It's quite natural, therefore, to represent the population inversion in the form of two multipliers:

$$n(z, \tau) = \Phi(z) D(z, \tau), \tag{4.31}$$

where $\Phi(z)$ is the unsaturated gain profile, reflecting slow changes in the population inversion along the cavity length. It's determined only by the geometry of the system, for example, by crystal size and by exponential change of pumping along the crystal rod. The new variable $D(z, \tau)$ is fast spatial frequency function, responsible for the effect of saturation of the population inversion by the lasing field. One can expand the multipliers of the expression (4.31) into Fourier series:

$$D(z,\tau) = D_0(\tau) - 2\sum_{k=1}^{K} D_k(\tau)\cos(2\pi q_k z/L) - 2\sum_{k=1}^{K} N_k(\tau)\sin(2\pi q_k z/L) + \ldots, \quad (4.32)$$

$$\Phi(z) = 1 + 2\sum_{j=1}^{K} \Phi_j \cos(2\pi j z/L) + 2\sum_{j=1}^{K} \Psi_j \sin(2\pi j z/L) + \ldots \quad . \quad (4.33)$$

By substituting these expansions into the rate equations we obtain the following set of $3K+1$ equations:

$$\begin{aligned}
\frac{dI_k}{d\tau} &= GI_k\left[g_k\left(D_0 + \sum_{m=1}^{K} (D_m \Phi_{|\kappa-m|}) + N_m \Psi_{|\kappa-m|} \right) - 1 \right], \\
\frac{dD_0}{d\tau} &= \eta_0 - D_0\left(1 + \sum_{m=1}^{K} g_m I_m \right) - \sum_{m=1}^{K} g_m I_m D_m, \\
\frac{dD_k}{d\tau} &= -\left(1 + \sum_{m=1}^{K} g_m I_m \right) D_k - \frac{1}{2} g_k I_k D_0 , \\
\frac{dN_k}{d\tau} &= -\left(1 + \sum_{m=1}^{K} g_m I_m \right) N_k ,
\end{aligned} \quad (4.34)$$

One can see in the last equation (4.34) that the expression $\left(1 + \sum_{m=1}^{K} g_m I_m \right)$ is always positive. Therefore all the expansion coefficients N_k will disappear in the limit of large time and will not participate in the dynamics of a multimode laser. Hence the variables N_k may be set equal to zero and eliminated from the set of equations (4.34). Eventually, we have the following set of ordinary differential $2K+1$ equations:

$$\begin{aligned}
\frac{dI_k}{d\tau} &= GI_k\left[g_k\left(D_0 + \sum_{m=1}^{K} (D_m \Phi_{|\kappa-m|}) \right) - 1 \right], \\
\frac{dD_0}{d\tau} &= \eta_0 - D_0\left(1 + \sum_{m=1}^{K} g_m I_m \right) - \sum_{m=1}^{K} g_m I_m D_m, \\
\frac{dD_k}{d\tau} &= -\left(1 + \sum_{m=1}^{K} g_m I_m \right) D_k - \frac{1}{2} g_k I_k D_0
\end{aligned} \quad (4.35)$$

It's necessary to emphasize that the model of the solid-state laser, described by means of Eqs. (4.35), is developed in approximation commonly used for the simplest case of homogeneous longitudinal distributions of unsaturated population inversion (Eq. (4.26). The developed model Eqs. (4.35) allows to consider the spatial longitudinal inhomogenities produced by nonuniform pump profile along the laser cavity, but for all that the dimension of the model remains the same (2*K*+1). Obviously, it's more convenient to use a model with initially lower dimension for description the specific features of the laser. The only difference between the equations (4.26) and (4.35) are the additional terms $\sum_{m=1}^{K}(D_m \Phi_{|\kappa-m|})$ in Eqs. (4.35) for the modal intensities. The terms take into account the nonuniform pump profile. In contrast to the equations (4.29), obtained by Pieroux and P. Mandel [51], the equations (4.35) do not take account of the influence of large-scale spatial inhomogeneities of the population inversion induced by the saturation effect of the inversion.

Numerical computations of the model (4.35) were made in the limit of possible 20 oscillating modes that corresponded to real experimental conditions of Nd:YAG laser. A concrete type of longitudinal inhomogeneity was analyzed. The inhomogeneity caused by the exponential absorption of the pump field along a active medium that fills the laser cavity only partially.

$$\Phi(z) = \begin{cases} \alpha L \exp(-\alpha z)/[1-\exp(-\alpha l)] & 0 \le z \le l, \\ 0 & l < z \le L, \end{cases} \tag{4.36}$$

where L is the length of the laser cavity, l - the length of the active element, α - the absorption coefficient of the pump, z – longitudinal coordinate.

A Lorenzian gain profile is:

$$g_k = \left\{ 1 + \left[\left(\frac{K}{2} + 1 - k \right) \delta - \delta_0 \right]^2 \right\}^{-1}, \quad k = 1,2,\ldots K, \ (K=20), \tag{4.37}$$

where δ and δ_0 are the longitudinal mode spacing and the detuning of the mode nearest to the centre of the gain line (k=11) from the line centre, respectively, normalized to the half width of the gain spectrum. To have a real situation of asymmetry, when all the oscillating modes

have different gain coefficients, the detuning was introduced $\delta_0 \approx \delta / 4$. Gain line width was considered to be 160 GHz that was typically for Nd:YAG rod crystal. The experimental conditions L_{opt}=8.3 cm and L_{opt}=5.7 cm result $\delta = 0{,}021$ and $\delta = 0{,}03$, correspondingly. According to the experimental measurements, the absorption coefficient α=3–4.5 cm^{-1}. In numerical simulations the parameter αl was taken equal to 3.5.

Figs. 4.13 and 4.14 show the calculated emission spectra versus the pump parameter η for two filling factors l/L =0.2 and l/L =0.3. In the first case the frequency spacing between oscillating modes are changed from 3 to 4 elementary frequency spacing when the pump parameter increases from 1 up to 1.5. In the second case the frequency spacing between oscillating modes vary from 2 to 3 elementary frequency spacing. The both cases are in good agreement with the corresponding experimental results. Besides that, both figures clearly demonstrate that the changes in the pumping lead to the hopping on adjacent oscillating modes.

Fig. 4.15 shows the behaviour of the modal intensities when the filling factor l/L is varied. A decrease of l/L from 0.4 up to 0.2 leads to an increase the distance between the oscillating modes from 2 up to 4 elementary intermode spacing in good accordance with the experimental data. It should be note that in this case the total emission bandwidth is practically not changed because a twofold decrease in the filling factor is accompanied by a twofold decrease in the intermode spacing.

In Figs. 4.16 and 4.17 one can see the dependence of the modal intensities versus the absorption coefficient of the pump α for two filling factors. The theoretical behaviour of the modal intensities here is very similar to those in the experiments within the interval of α from 2 cm^{-1} up to 4 cm^{-1} . It is evident that the appearance of the exponential absorption ($0<\alpha<0.1$) leads to a rarefaction of the emission spectrum. A further increase in α is accompanied by abrupt hops between the adjacent modes, with jumps in the intensities of oscillating modes.

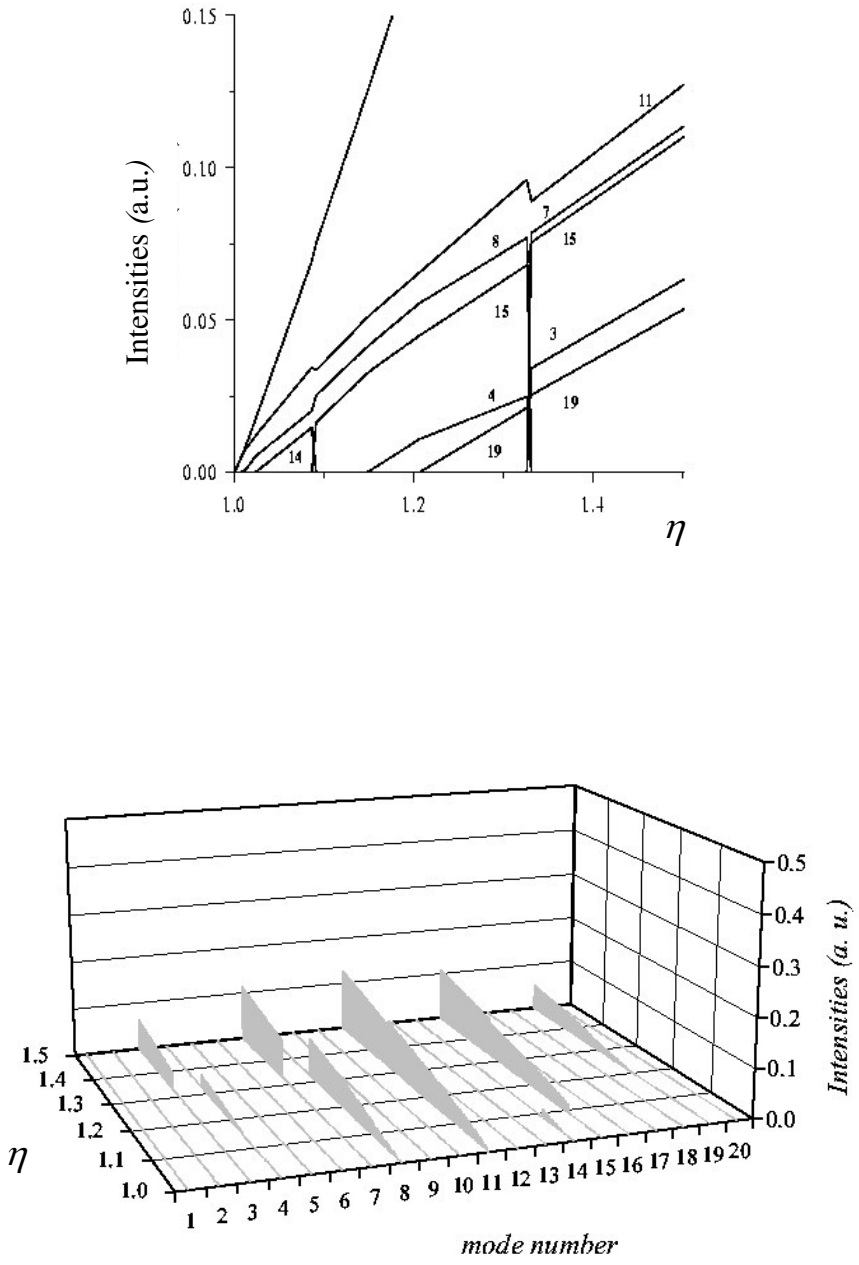

Fig. 4.13: Dependence of the modal intensities on the pump parameter η [(top) two–dimensional presentation, (bottom) three-dimensional presentation] for G = 2500, l/L = 0.22, δ=0.021, $\delta_0 = \delta/4$, and $\alpha = 3.5$ cm^{-1}, calculated with Eqs. (4.35).

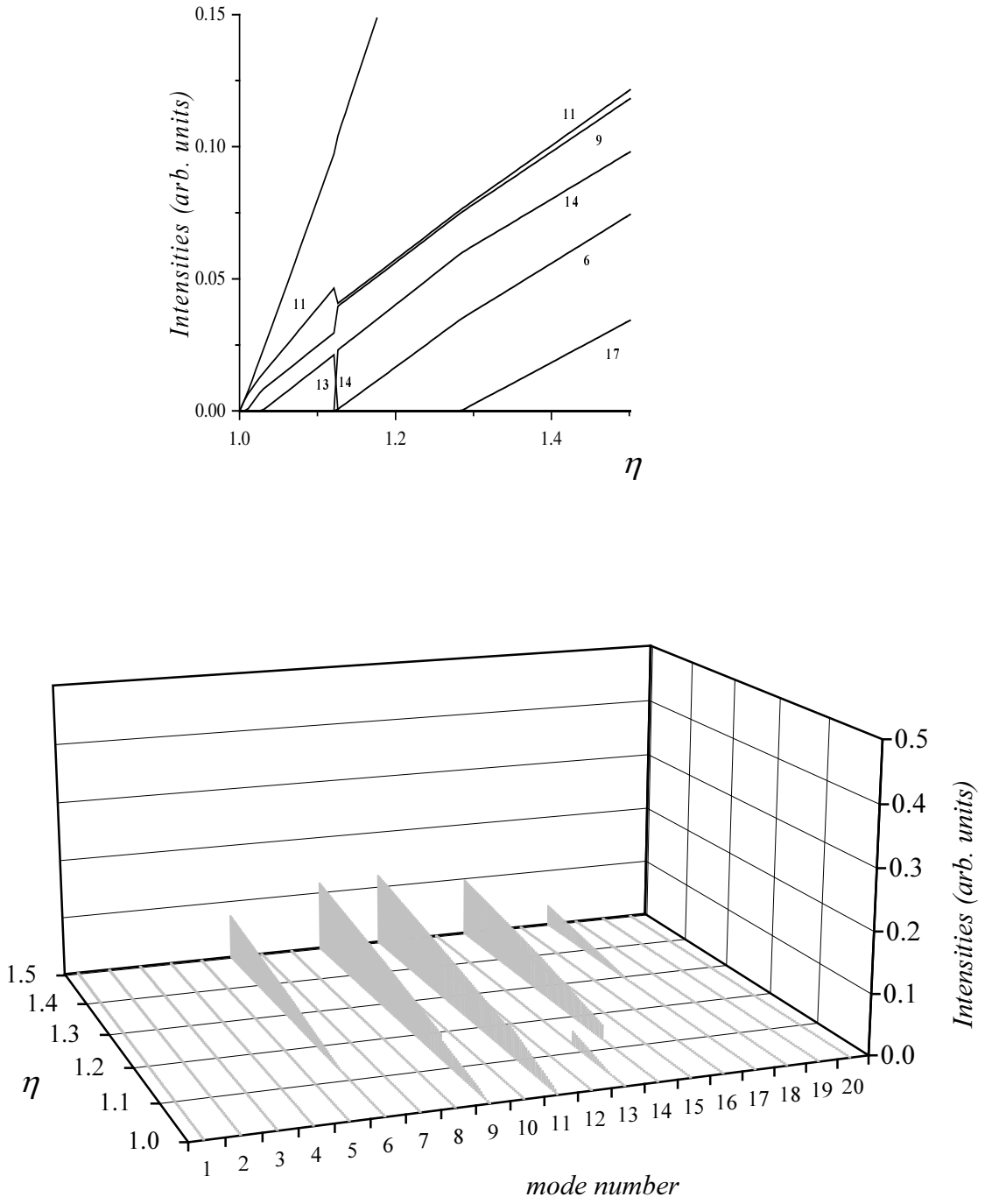

Fig. 4.14: Dependence of the modal intensities on the pump parameter η [(top) two–dimensional presentation, (bottom) three-dimensional presentation] for G = 2500, l/L = 0.32, δ=0.03, $\delta_0 = \delta/4$, and $\alpha = 3.5$ cm^{-1}, calculated with Eqs. (4.35)

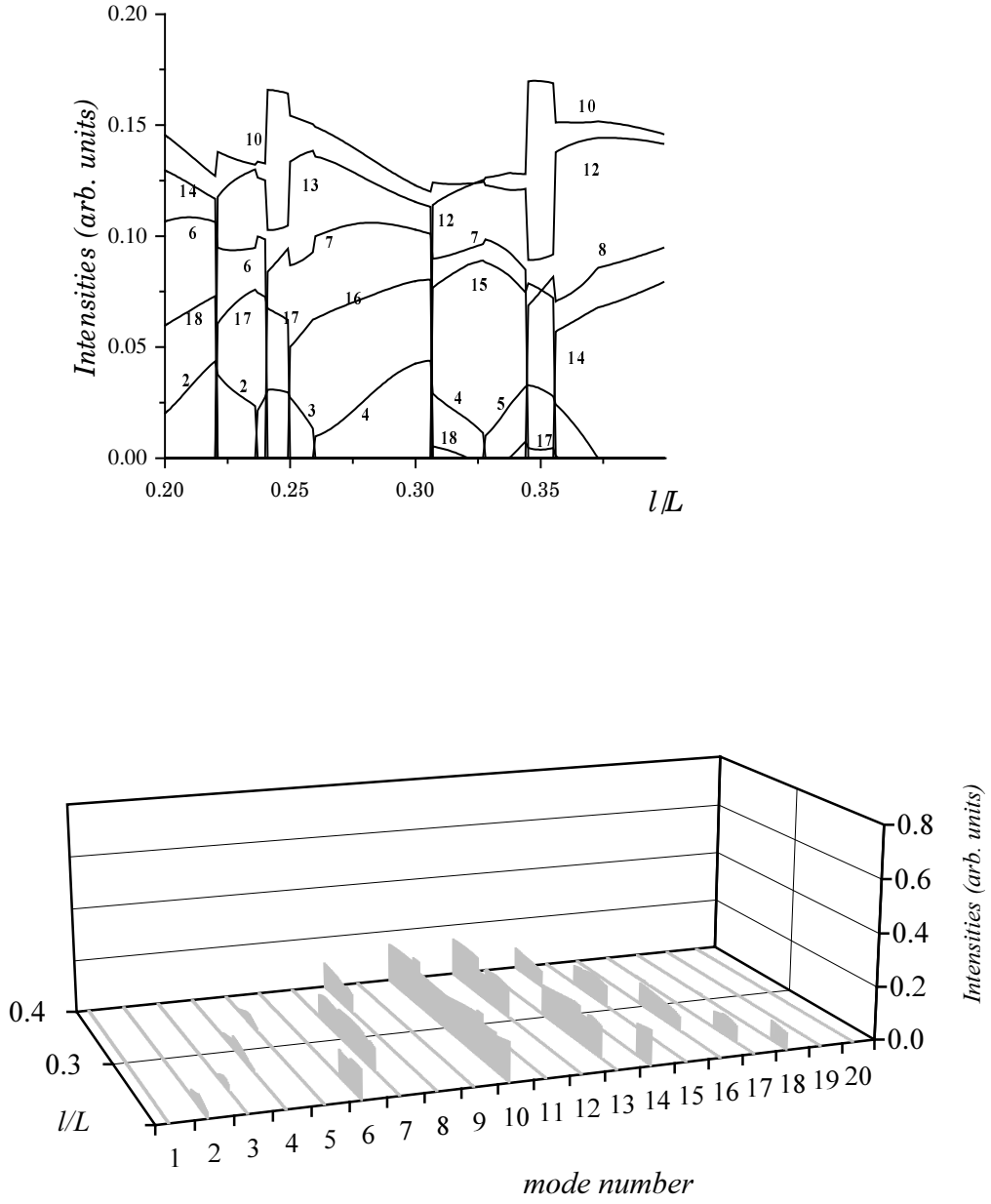

Fig. 4.15: Dependence of the modal intensities on the filling factor l/L [(top) two–dimensional presentation, (bottom) three-dimensional presentation] for $G = 2500$, $\eta = 1.5$, δ=0.03, $\delta_0 = \delta/4$, and $\alpha = 3.5$ cm^{-1}, calculated with Eqs. (4.35).

Note that in the absence of the exponential pump nonuniformity ($\alpha = 0$) the changes in the filling factor (see Fig.4.18) are accompanied by non-monotonic changes in the modal intensities but still there are no intensity jumps. The same is in the case of an entirely filled laser cavity ($l/L = 1$): changes in α are not accompanied by intensity jumps [2]. Thus, jumps in the

modal intensities including hops of adjacent modes are characteristic only of the joint action of two mechanisms of longitudinal nonuniform pump profile along the laser cavity: the pump decay along the crystal and the partial filling of the laser cavity by the active medium.

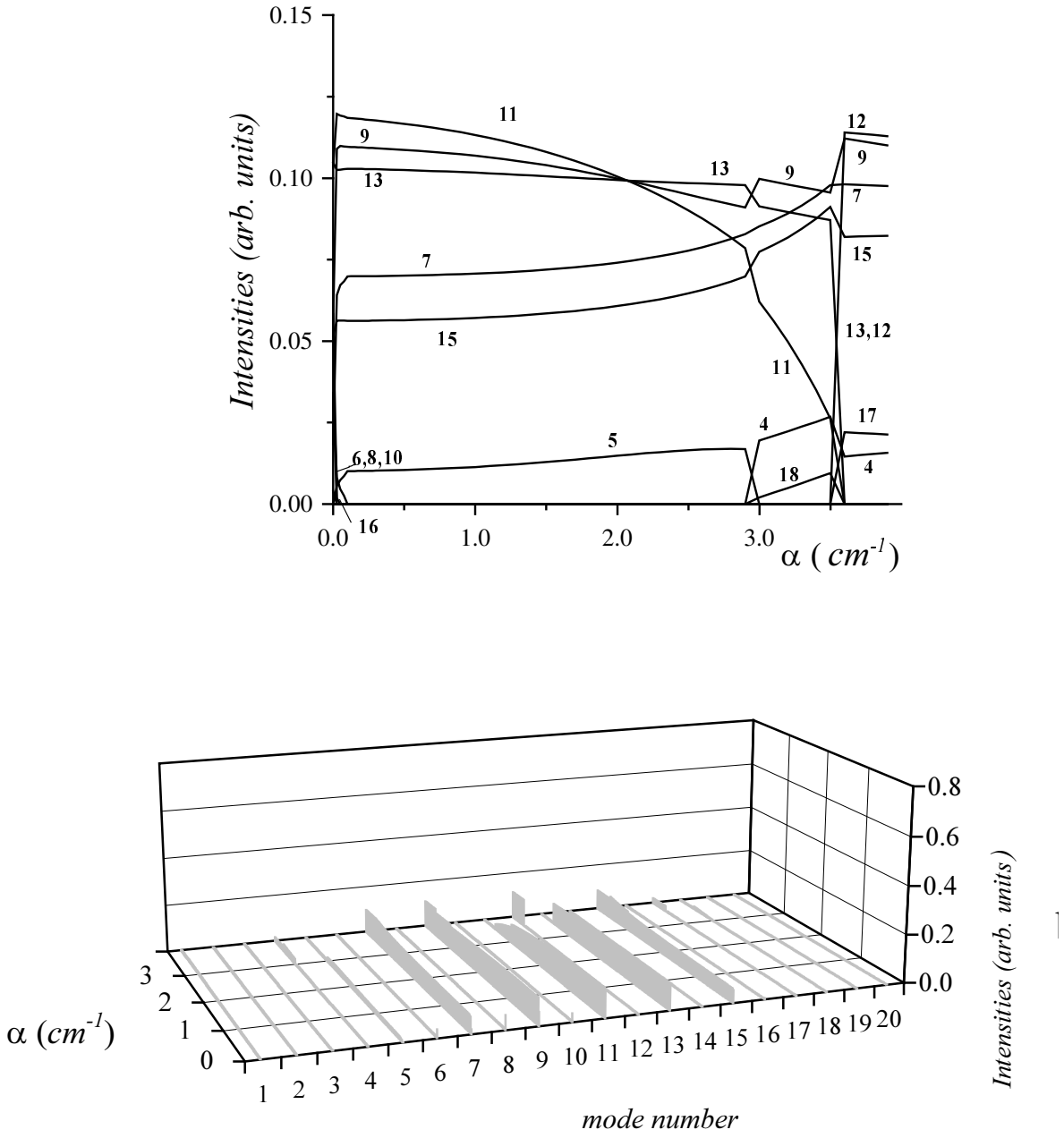

Fig. 4.16: Dependence of the modal intensities on the absorption coefficient α [(top) two–dimensional presentation, (bottom) three-dimensional presentation] for $G = 2500$, $\eta = 1.5$, $l/L = 0.021$, δ=0.03, and $\delta_0 = \delta/4$, calculated with Eqs. (4.35).

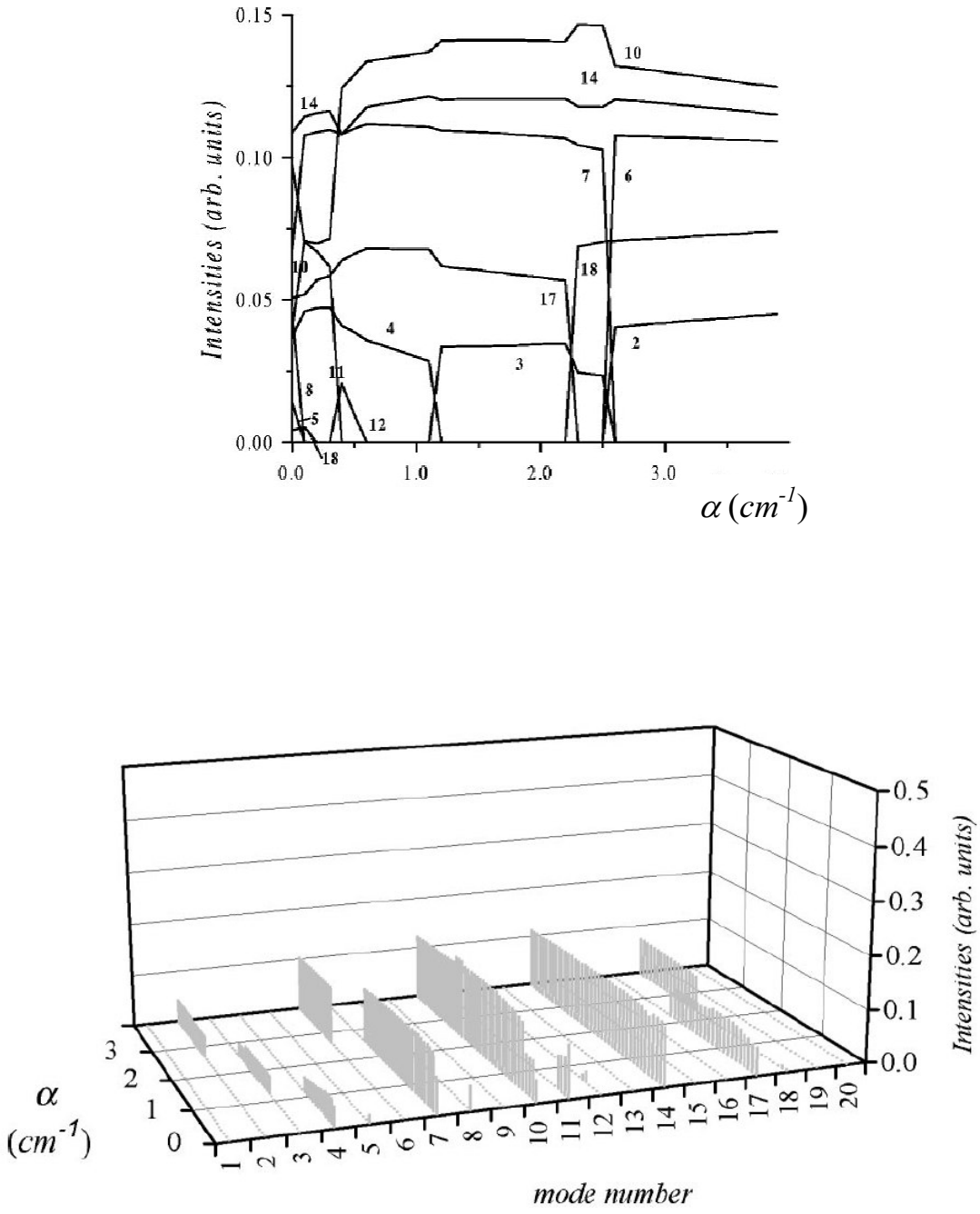

Fig. 4.17: Dependence of the modal intensities on the absorption coefficient α [(top) two–dimensional presentation, (bottom) three-dimensional presentation] for $G = 2500$, $\eta = 1.5$, $l/L = 0.032$, $\delta = 0.03$, and $\delta_0 = \delta/4$, calculated with Eqs. (4.35).

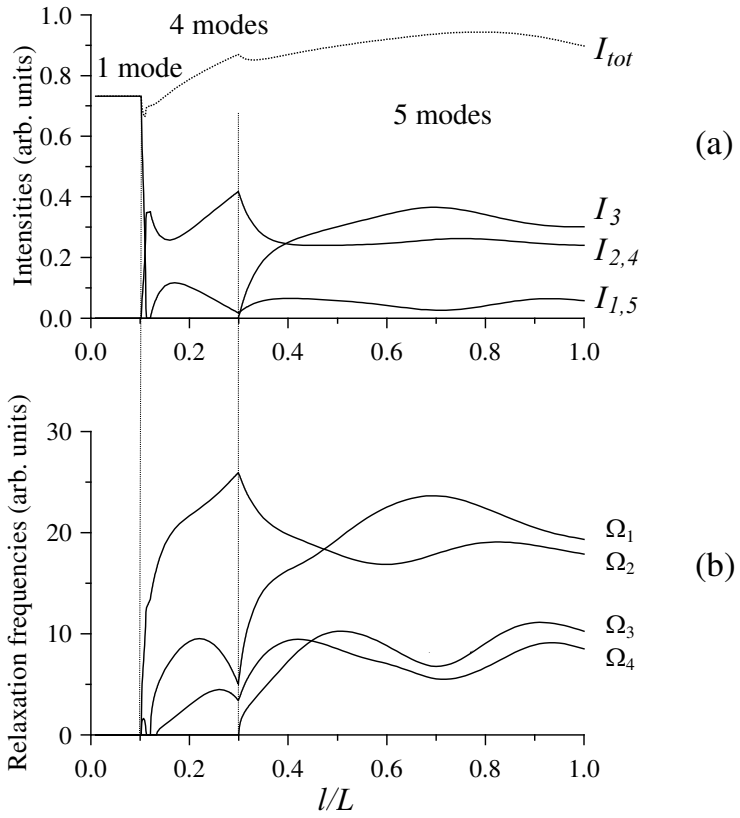

Fig. 4.18: Dependencies of the modal intensities (top) and corresponding relaxation frequencies (bottom) on the filling factor l/L at the absorption coefficient $\alpha = 0$ for $G = 2500$, δ=0.03, $\delta_0 = \delta/4$.

Experimental results

The experimental setup is shown schematically in Fig.4.19. The pump source is a semiconductor laser 1 that generated linearly polarized radiation at the wavelength of λ=810 nm. The active element 5 is a 10 mm Nd:YAG crystal rod, 6 mm in diameter with faces tilted at an angle of ≈ 1.5° relative to each other. The input face 4, being perpendicular to the rod axis, had a multilayer dielectric coating with ≈ 0.995 reflectivity at the operating wavelength of a Nd:YAG laser, λ = 1064 nm, and relatively high transmission at the wavelength of pump radiation 810 nm. The other crystal face has an antireflective coating at the wavelength of λ = 1064 nm. The output laser mirror 6 is a spherical isotropic mirror with 99% reflectivity at the operating wavelength and a radius of curvature of 30 cm.

The experiments were carried out for two laser cavity lengths of 5.7 cm and 8.3 cm, with filling factors of 0.32 and 0.22, accordingly. Half-wave plate 8 and Glan prism 10 were used to study the emission spectrum of different polarization modes. The emission spectrum of the Nd:YAG laser was monitored correspondingly by Fabry-Perot optical spectrum analyser 15 with cavity lengths of 2.4 mm and 4.1 mm, which corresponded to the free spectral ranges of ~ 63 GHz and ~ 37 GHz, respectively. Fineness of the Fabry-Perot analyser was F = 119.

In the experiments lasing on two orthogonally polarized modes was observed: strong and weak, which could be selected by the polariser. By means of a half-wave plate at λ = 810 nm (not shown in the figure) the orientation of the pump polarization was chosen such as to have maximum selection of the polarization modes.

Fig. 4.20 is characteristic photos of the emission spectrum of strong polarization modes of a Nd:YAG laser with the cavity length L_{opt} = 8.3 cm, the filling factor of 0.2 and intermode frequency spacing of 1.8 GHz. Fig. 4.20 shows that the emission spectrum is non-equidistant. The frequency spacing between the central mode and the nearest modes $\Delta\nu'_{las}$ is larger than between two lateral modes $\Delta\nu''_{las}$. The frequency spacing between the oscillating modes was compared with the free spectral range of the Fabry-Perot spectrum analyzer $\Delta\nu_{f\text{-}p}$ = 37 GHz (see Fig. 4.20, bottom). The frequency spasings between the oscillating modes were evaluated as $\Delta\nu''_{las}$ = 5.6 GHz and $\Delta\nu'_{las}$ = 7.4 GHz. This approximately corresponds to three (1.8 × 3 = 5.4 GHz) and four (1.8 × 4 = 7.2 GHz) elementary longitudinal mode spacing

$\Delta\nu$. It means that two or three longitudinal modes were suppressed between the oscillating modes.

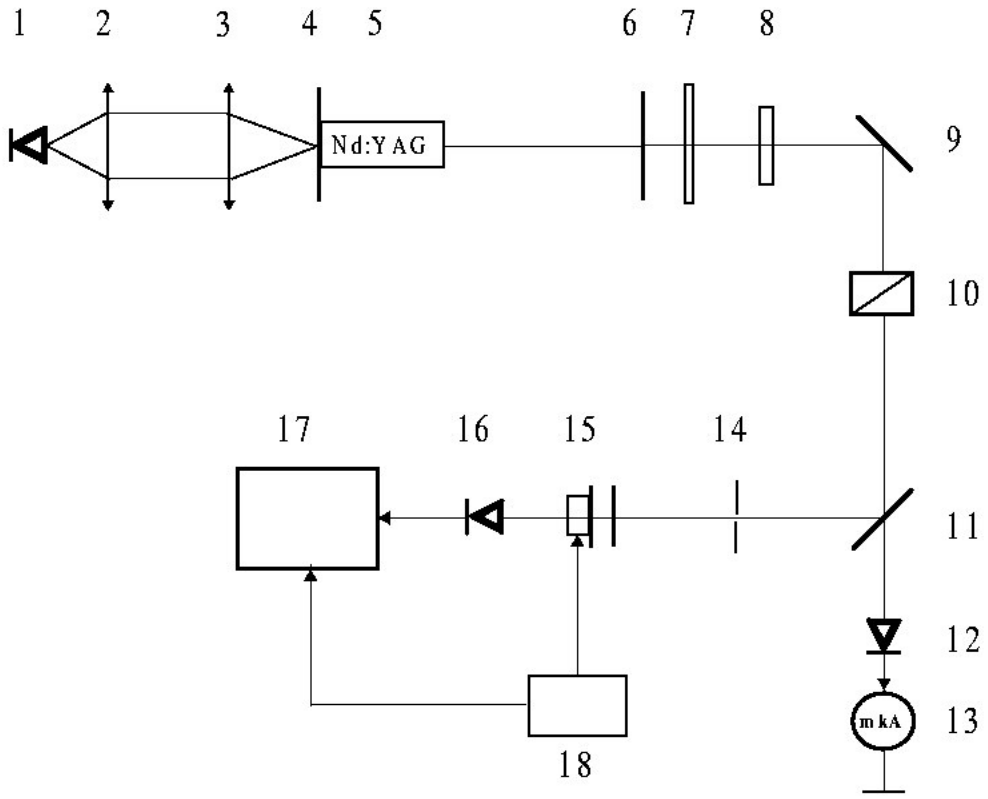

Fig. 4.19: Experimental set-up. (1) pump laser, 810 nm; (2 and 3) collimating lenses; (4 and 6) cavity mirrors; (5) yttrium aluminium garnet crystal; (7) filter λ = 810 nm; (8) $\lambda/2$ plate, λ = 1064 nm; (9 and 11) mirrors; (10) Glan prizm; (12 and 16) photodiodes; (13) microammeter; (14) aperture; (15) Fabry-Perot spectrum analyzer; (17) oscilloscope; (18) scanning unit of a Fabry-Perot interferometer.

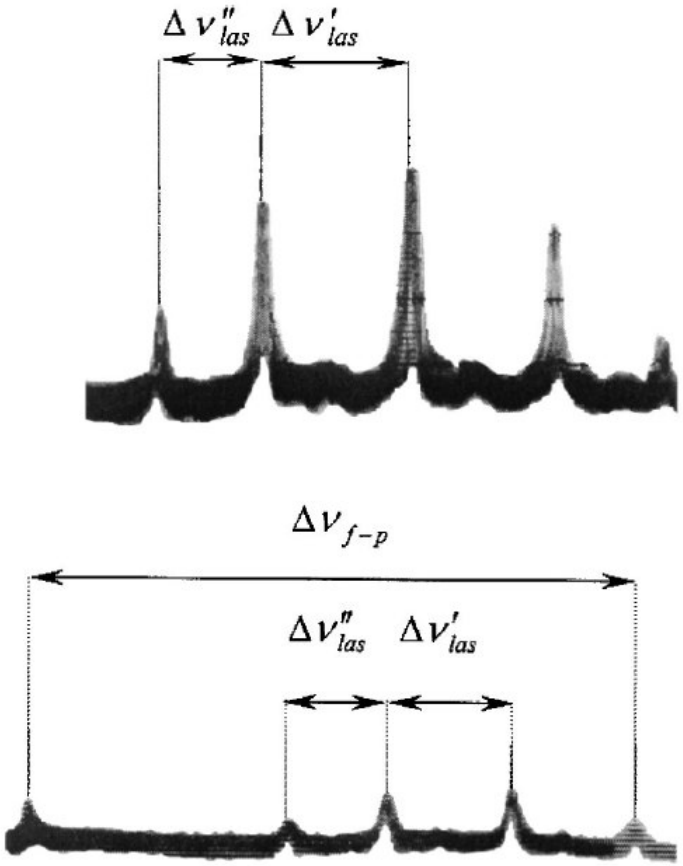

Fig. 4.20: Optical spectra for dominating polarization at $L_{\text{opt}} = 8.3$ cm for two values of pump parameter $\eta = 1.22$ (top), $\eta = 1.16$ (bottom). $\Delta\nu'_{las}$ and $\Delta\nu''_{las}$ are frequency spacing between lasing modes; $\Delta\nu_{f\text{-}p}$ is the free spectral range of the Fabry-Perot analyzer.

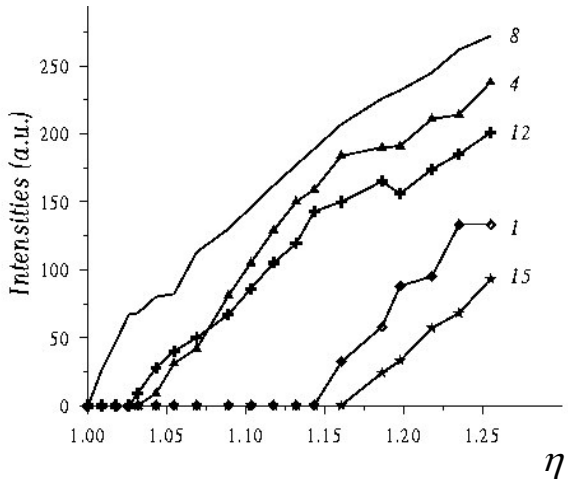

a

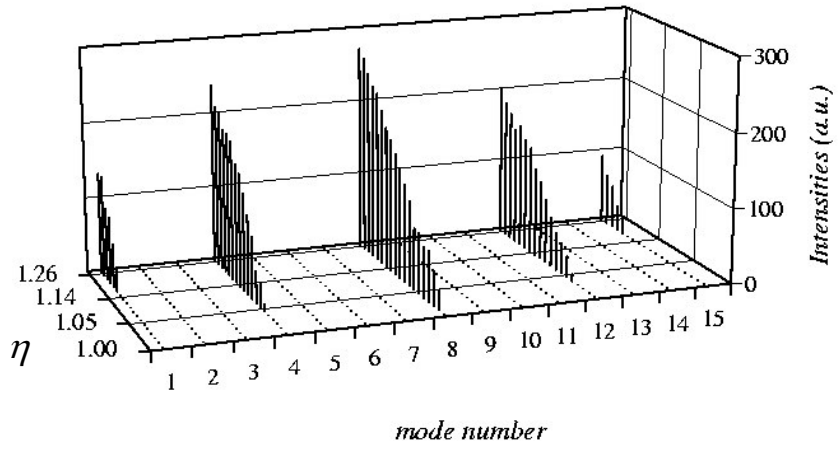

b

Fig.4.21: Modal intensities vs. pump parameter η [(a) two-dimensional presentation, (b) three-dimensional presentation] for L_{opt} = 8.3 cm. The numbers 1,2,...,15 show the numbers of cavity modes.

Fig. 4.21 shows the behaviour of the modal intensities versus pump parameter η in usual two-dimensional form (Fig. 4.21a) and in the three-dimensional presentation (Fig. 4.21b). In the latter case, the position of the oscillating modes on the frequency axis with account of the frequency spacing between them (in units of the elementary longitudinal mode spacing $\Delta\nu$) is shown schematically. The numbers of longitudinal modes of the laser cavity (1,2,...,15) are indicated along one axis in the horizontal plane (the frequency axis), and the

pump parameter η - along the other axis. The pump parameter was varied from η = 1.0 to η = 1.3. Along the vertical axis the intensity of the oscillating modes is given in arbitrary units. The plots show that at pump close to threshold only one mode is oscillating (mode number 8). When the pump is increased, the modes 12 and 4 at a distance of 4 longitudinal mode spacing from the central mode and then the modes 1 and 15 at a distance of 3 longitudinal mode spacing from the adjacent modes 4 and 12 almost simultaneously enter the lasing process. Figure 4.21 shows that the intensities of all oscillating modes nearly monotonically increase with increasing pump. Hopping between modes with adjacent longitudinal indices is not observed in the experiment. The spectrum was almost symmetric and stable.

A series of analogous measurements was carried out for a shorter cavity length of L_{opt} = 5.7 cm with corresponding cavity filling factor of 0.3 and intermode frequency spacing of 2.6 GHz. The optical spectrum of a Nd:YAG laser was monitored by a Fabry-Perot optical spectrum analyser with the cavity length of 2.4 mm, which corresponds to free spectral range of ~ 63 GHz.

Fig.4.22a shows the emission spectrum of a strong polarization mode when the pump parameter is changed from η = 1.0 to η = 1.5. The number of modes participating in the lasing was varied from 1 to 5. One can see that the emission spectrum is non-equidistant. Side modes enter the lasing process asymmetrically: when pump increases the centre of the optical spectrum shifts to the low-frequency region (left). The intervals between the lasing modes were 5.2 GHz and 7.8 GHz, which approximately correspond to two (2.6 × 2 = 5.2 GHz) and three (2.6 × 3 = 7.8 GHz) elementary longitudinal mode spacing $\Delta\nu$, respectively. It means that one or two longitudinal modes were suppressed between two lasing modes. Three-dimensional Fig. 4.23 shows the intensities of lasing modes versus the pump parameter, taking into account the position of the modes on the frequency axis. Analogous behaviour of weak polarization longitudinal modes is seen in Fig. 4.22b. In this figure the lasing threshold for a weak polarization mode is η = 1.3. The number of oscillating modes in weak polarization mode is smaller than in strong polarization mode, but frequency spacing between lasing modes in this polarization coincide with those in strong polarization.

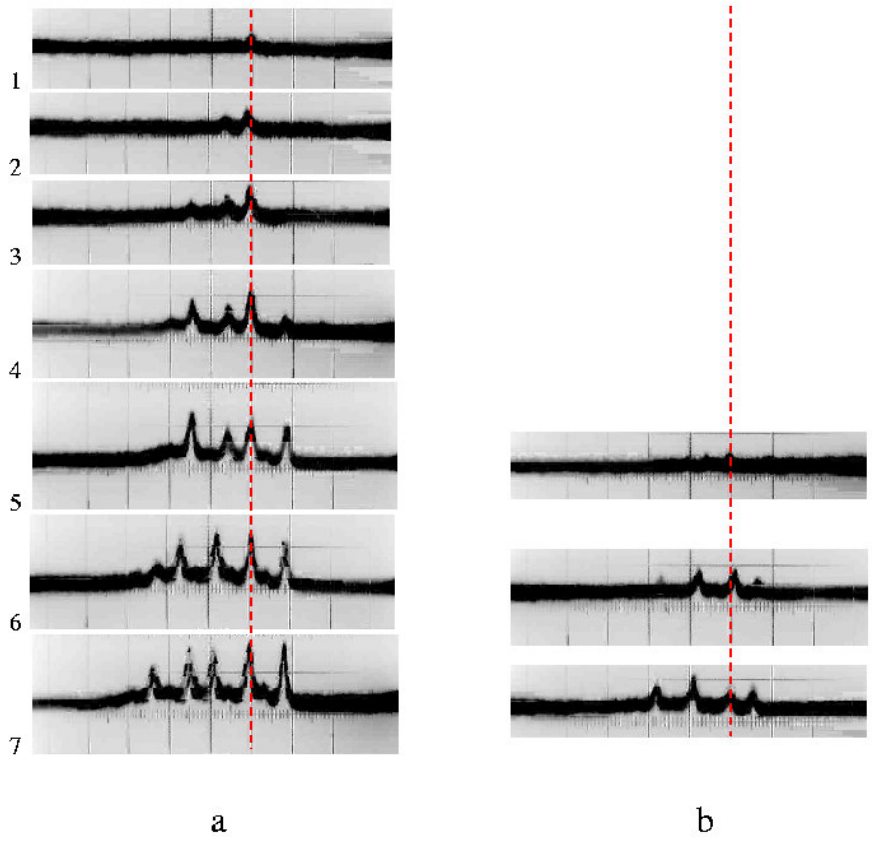

Fig. 4.22: Emission spectrum of the laser with L_{opt} = 5.7 cm when the pump parameter η is increased for (a) strong polarization mode, (b) weak polarization mode.

Note that in contrast to the case of a long laser cavity, in this configuration the emission spectrum shows considerable instability for both polarizations. This is manifested by frequent hopping from one longitudinal mode to adjacent modes. A reason for this may be that under these conditions the laser is more sensitive to uncontrolled changes in the cavity length. Figure 4.23 shows a non-monotonical change in the intensities of lasing modes versus the pump parameter.

Thus, the experimental study of the emission spectrum of a Nd:YAG laser has shown that a decrease in the filling factor from 0.3 down to 0.2 leads to rarefaction of the emission spectrum: the number of suppressed modes between adjacent oscillating modes increases from 1 up to 3. Frequency spacing between the modes vary from 2 to 4 elementary intermode spacing $\Delta\nu$ of the cavity. Oscillating modes become more stable to external perturbations and competing influence of adjacent longitudinal modes.

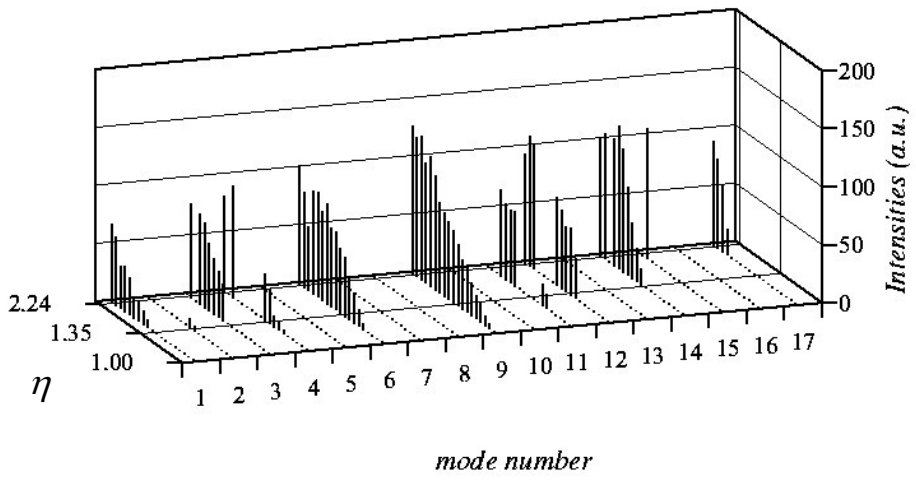

Fig. 4.23: Modal intensities vs. pump parameter η (three-dimentional presentation) for L_{opt} = 5.7 cm. The numbers 1,2,...,17 show the numbers of cavity modes.

The investigation of stationary emission spectra of a Nd:YAG laser with a small number of oscillating modes was carried out. The inhomogeneous distribution of the unsaturated gain along the cavity caused by a partial filling of the laser cavity with the active medium and by the exponential absorption of the pump radiation along the crystal. Inhomogeneous longitudinal distribution of the pump radiation is the reason of the change of the spatial distribution of the population inversion in comparison with the case of homogeneous distribution. The inhomogeneity leads to the change of the photon distribution among the oscillating modes. Stronger change of the photon distribution is observed both by the reduction of the filling factor of the cavity and by the increase of the absorption coefficient of the pump radiation. The increase of fluctuations of the modal intensities is observed at the increase of the filling factor. It is manifested in the change of the intensity of oscillating modes.

The interaction between the longitudinal modes by the joint effect of nonuniform longitudinal saturation of the inversion and of inhomogeneous longitudinal pump distribution may be a reason for the nonuniform distribution of modal intensities.

5. Influence of transversal inhomogeneities of the gain on the emission dynamics of solid-state lasers

5.1. Polarization dynamics of a Nd:YAG laser

This section presents the phenomena associated with azimuthal inhomogeneity of the saturation of the gain in a bipolarized laser.

The polarization of laser emission is determined by both the cavity anisotropy (birefringence, anisotropy of losses) as well as by the anisotropy of active medium gain (crystals with definite direction of dipole moments of active centers, active media in magnetic field, lasers with polarized pump laser). The absence of such a strong factor as anisotropy of losses for orthogonally polarized modes leads to the emission of both these modes. It was found [52-54] that in the weakly anisotropic cavity the excitation thresholds of orthogonally-polarized modes and their intensities depend on the orientation of the polarization of a pump laser. It was shown [55,56] using a dye laser (class A laser) that the use of the pump laser with linearly polarized emission leads to the gain anisotropy. This causes the influence of the pump polarization on the intensities of polarized modes. The model of the bipolarized class B laser with Fabry-Perot cavity [52,54] explains the observed effects in class B lasers. Unlike the class A lasers here the equation for population inversion can not be adiabatically excluded. Therefore the results of investigations [55,56] cannot apply directly to solid-state lasers. In the mentioned papers [52,54] gain anisotropy was taken into account phenomenologically via the pump parameter depending on the orientation of the pump polarization plane. When choosing the type of this dependence it was taken into account that the number of active centers is maximum for collinearly-oriented dipoles and has the minimum for orthogonally-oriented dipoles. Following the results [55,56], the attempt was made [40] to perform a more consistent quantum-mechanic derivation of the expression for the pump parameter. But here the authors did not take into account the effect of saturation in the azimuthal distribution of active centers due to the pump intensity leading to the decrease of the gain anisotropy with the increase of the pump intensity [55,56].

This section presents the theoretical investigation and experiments performed to study the effect of pump polarization on dynamical and fluctuation behavior of a solid-state Nd:YAG laser with a weakly anisotropic Fabry-Perot cavity. The developed model is shown

to be suitable to describe the specific features of polarization dynamics observed in the experiments. In the model the pump parameter takes into account the influence of the emission intensity of the pump laser on the gain anisotropy.

The experimental setup is shown in Fig. 5.1. The pump source is a semiconductor laser at 0.81 μm wavelength. Polarization is linear.

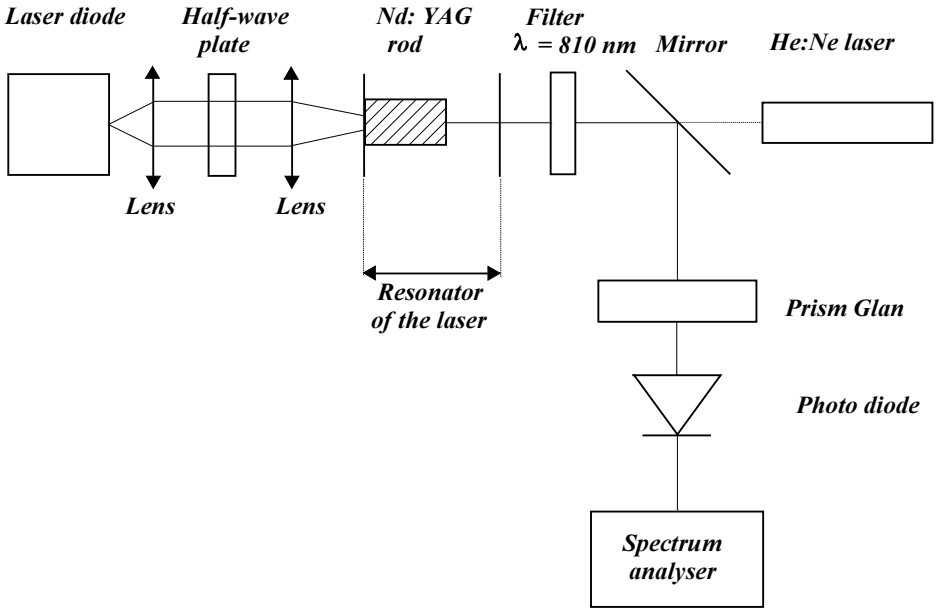

Fig. 5.1: Experimental set-up

A half-wave plate located between two focusing lenses is used to rotate the direction of pump polarization. A Nd:YAG crystal (1 cm long and 0.6 cm in diameter) is used as the active laser medium. One crystal face with dichroic coating acts as an input cavity mirror ensuring high reflection at 1.06 μm operating wavelength and high transparancy at the pump wavelength. The other crystal face with antireflection coating is transparent at 1.06 μm. An isotropic mirror with 99.5% reflection at 1.06 μm is used as an output cavity mirror. The cavity is 2.3 cm long. The refraction index of Nd:YAG crystal is 1.8. The optical length of the cavity is 3.1 cm. The interval between adjacent longitudinal cavity modes is about 5 GHz. A filter is placed at the cavity output to block the pump laser emission. The Glan prism is employed as an analyzer of the laser output. The Nd:YAG laser emission is detected by a photodiode whose output is connected to a spectroanalyzer. The maximum output power of the Nd:YAG laser is 2 mW. A He:Ne laser is used for the optical alignment of the system.

The experiment is made to study the effect of the pump polarization on the intensity of polarization modes of a Nd:YAG laser. The strong polarization mode corresponded to the position of the analyzer with maximal signal. The minimum analyzer transmission corresponds to a weak mode whose polarization is orthogonal to the strong mode. Rotation of the pump polarization Ψ_0 leads to the antiphase change of photocurrents I_1 and I_2 corresponding to strong and weak modes respectively.

Fig. 5.2 shows the dependence of the intensities I_1, I_2 of polarization modes on the pump polarization direction Ψ_0 when pump parameter $\eta = 1.2$ is constant. The dependence of I_1, I_2 on the pump parameter in two fixed positions of the half-wave plate $\Psi_0 = 0^0$ and $\Psi_0 = 90^0$ is presented in Fig. 5.3.

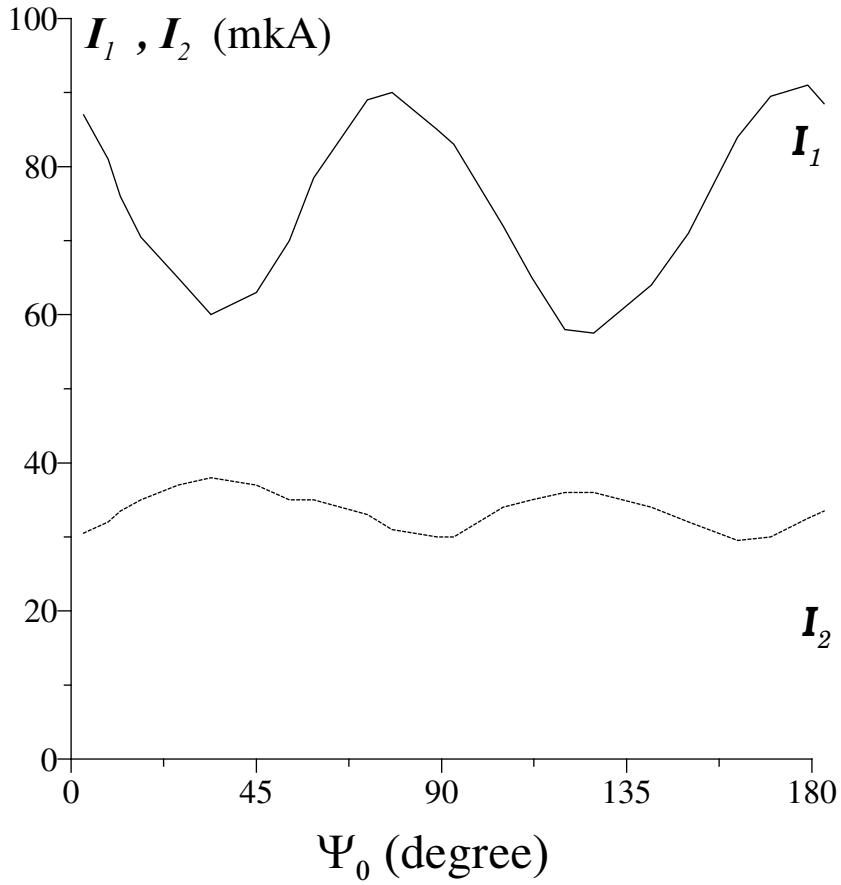

Fig. 5.2: Dependence of the intensities I_1, I_2 of polarization modes on the direction Ψ_0 of the pump polarization at $\eta = 1.2$.

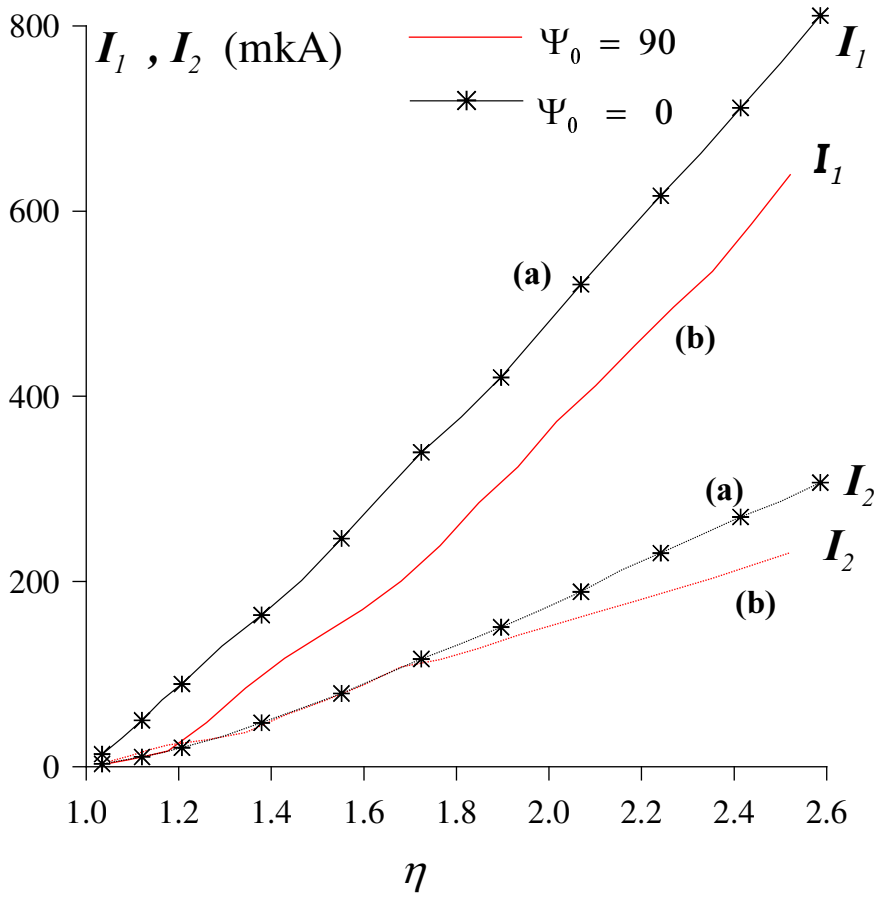

Fig. 5.3: Dependence of the intensities I_1, I_2 of polarization modes on the pump parameter η at (a) $\Psi_0 = 0^0$ and (b) $\Psi_0 = 90^0$.

The power spectra of the polarization modes I_1, and I_2 are shown in Fig.5.4. Along with a high-frequency peak at Ω_0 that corresponds to the main relaxation oscillation, there are two low frequency peaks at Ω_1, Ω_2 in the spectra. Fig. 5.4c shows the power spectrum I_{PR} measured at the intermediate position of the analyzer. The low frequency peaks are not present in this case indicating antiphase character of relaxation oscillations at frequencies Ω_1 and Ω_2.

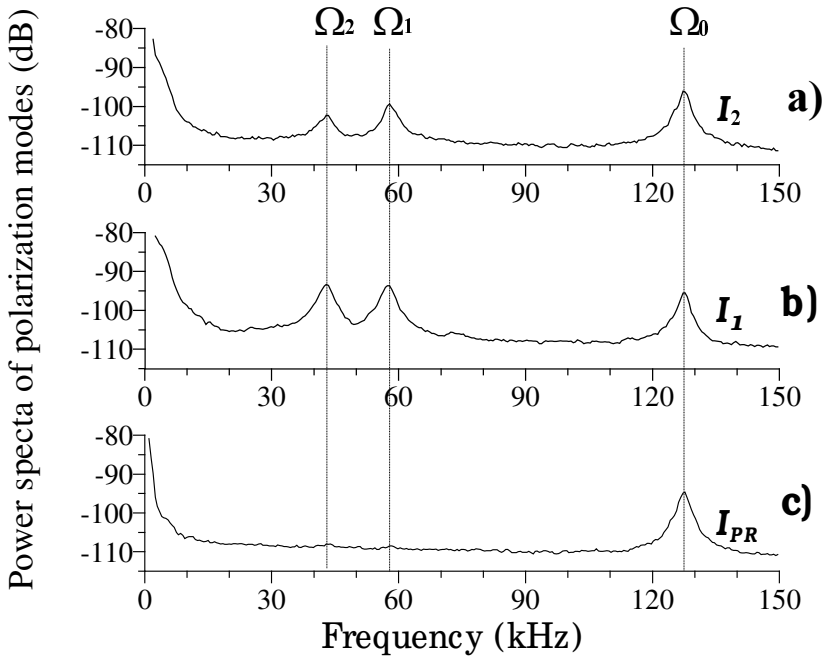

Fig. 5.4: The power spectra of the polarization modes at η =1.4. Here $I_{PR} \sim I_1 + I_2$.

Fig. 5.5 presents the dependence of relaxation frequencies $\Omega_{0,1,2}$ on pump parameter when position of the half-wave plate is fixed.

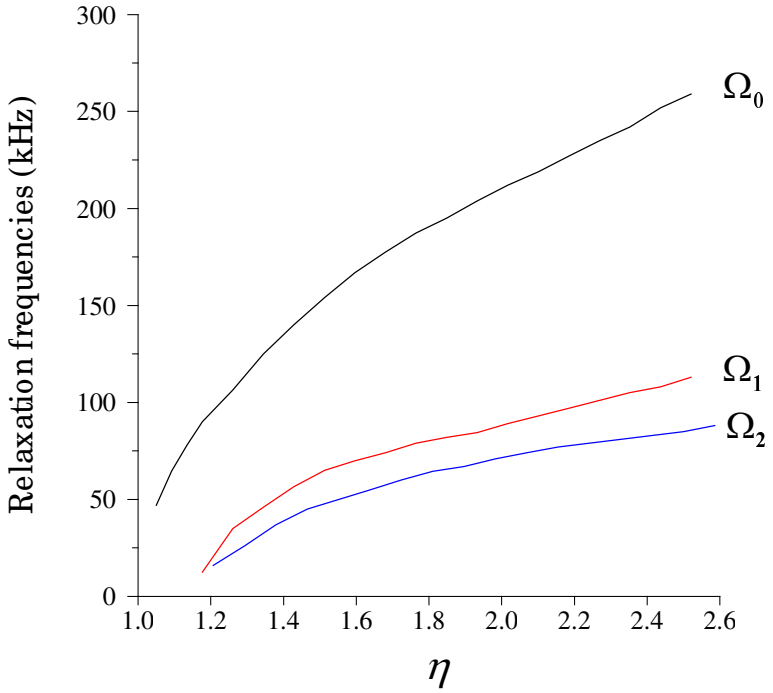

Figure 5.5: Dependence of relaxation frequencies on the pump parameter η at $\Psi_0 = 0^0$.

The influence of orientation of pump polarization on the laser threshold in different polarization modes η_1, η_2 is shown in Fig. 5.6.

The influence of pump polarization on the intensity of spontaneous emission is studied on an experimental setup with no output cavity mirror. During the rotation of the half-wave plate, the azimuth of maximum of spontaneous emission intensity is also rotated. When the position of the half-wave plate is fixed, the maximum and minimum of spontaneous emission are shifted at an angle close to 90^0. The ratio I^{min}/I^{max} of spontaneous emission is close to 0.7.

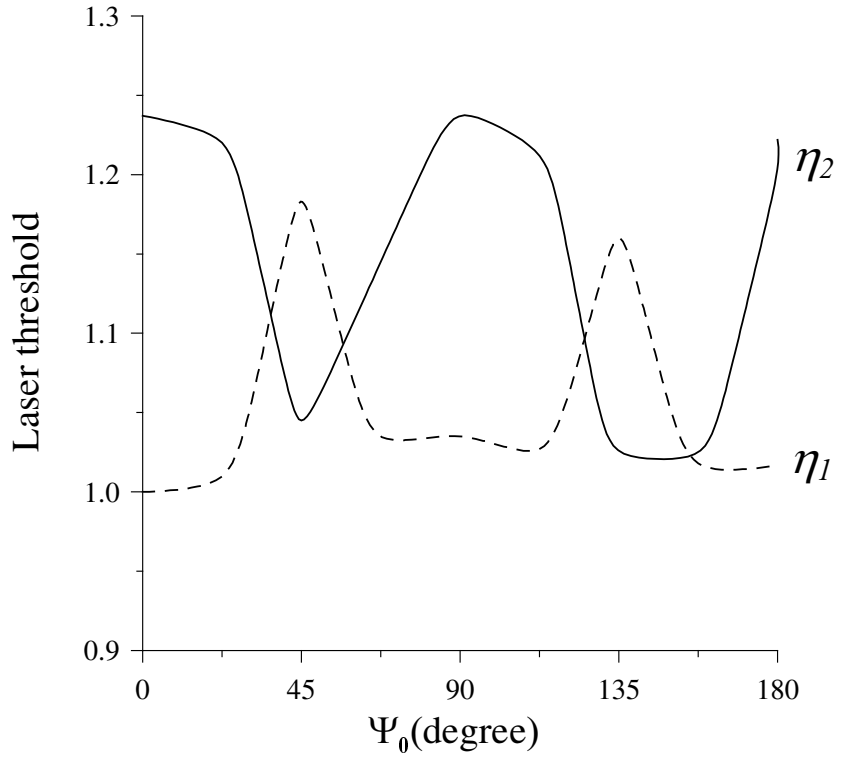

Fig. 5.6: Dependence of the laser threshold in different polarization modes η_1, η_2 on the direction of the pump polarization Ψ_0.

The main experimental results are as follows:

1) A strong dependence of the intensities of polarization modes on the direction of pump polarization is observed.

2) Two additional low frequency relaxation peaks, along with the high frequency relaxation peak, are observed in the power spectrum of each polarization mode.

3) There is a certain position of an analyzer when the low frequency relaxation peaks in the total laser output are absent indicating the antiphase character of these relaxation oscillations.
4) Maximum of spontaneous emission follows the rotation of the pump polarization plane.

An important factor in the dynamical behavior of solid-state lasers with a weakly anisotropic cavity is a collective interaction of all longitudinal modes of one polarization (first polarized mode) with the whole ensemble of modes of the orthogonal polarization (second polarized mode). The model considers interaction of two orthogonally-polarized modes. The field is composed of two orthogonally-polarized cavity eigenmodes [57]:

$$\vec{E} = (E_1\vec{U}_1 + E_2\vec{U}_2)e^{i\omega t} + c.c. \tag{5.1}$$

Here $\vec{U}_{1,2}$ are the orthogonal eigenmodes of the laser cavity, $E_{1,2}$ are the slowly varying amplitudes of fields with orthogonal polarizations, ω is the carrier optical frequency. Eigenmodes $\vec{U}_{1,2}$ are defined by the expression

$$\vec{U}_m = \sqrt{2}\vec{e}_m^{\,0} \sin k_m z, \qquad \text{m=1, 2} \tag{5.2}$$

where $\vec{e}_m^{\,0}$ are unit eigenvectors of the cavity:

$$\vec{e}_1^{\,0} = \vec{x}^{\,0} \cos R + \vec{y}^{\,0} \sin R, \tag{5.3}$$

$$\vec{e}_2^{\,0} = \vec{x}^{\,0} \sin R - \vec{y}^{\,0} \cos R \tag{5.4}$$

where $\vec{x}^{\,0}$, $\vec{y}^{\,0}$ are the Cartesian unit vectors, R is an angle between vectors $\vec{x}^{\,0}$ and $\vec{e}_1^{\,0}$ (see Fig.5.7).

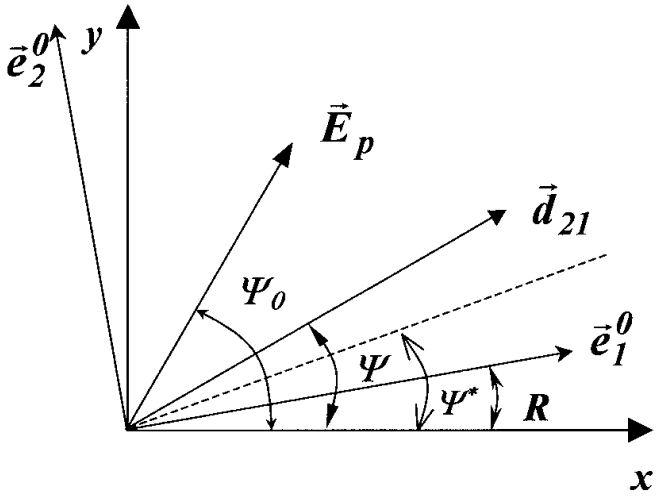

Fig. 5.7: The position of the eigenvectors $\vec{e}_1^{\,0}$, $\vec{e}_1^{\,0}$ the pump field vector $\vec{E}_p$, and the vector of active dipoles $\vec{d}_{21}$ in the Cartesian coordinates.

Active ions in crystals take definite positions inside the cell unit of crystal lattice. In Nd:YAG crystal there are 3 equal positions. Therefore the dipole moments of the active ions will be oriented around several definite directions in space preserving the isotropic properties of the crystal as a whole. Depending on the technology used to fabricate the active element its axis (that usually coincide with the cavity axis) may not coincide with the axis of isotropic dipole distribution. It is assumed for simplicity that active dipoles are linearly polarized and part of them is randomly oriented in the plane orthogonal to the laser axis:

$$\vec{\mathrm{d}}_{21}^{0} = \vec{\mathrm{d}}_{21} / \left|\vec{\mathrm{d}}_{21}\right| = (\vec{x}^{\,0} \cos\Psi + \vec{y}^{\,0} \sin\Psi) \tag{5.5}$$

(the angle-Ψ value ranges from 0 to π) and the rest part of dipoles is oriented along Ψ^* direction:

$$\vec{\mathrm{d}}_{21}^{0} = (\vec{x}^{\,0} \cos\Psi^* + \vec{y}^{\,0} \sin\Psi^*) \tag{5.6}$$

The angular distribution of dipoles is presented as a sum of isotropic and anisotropic parts:

$$f_{or}^{0}(\Psi) = \Phi_1/\pi + \Phi_2\,\delta(\Psi-\Psi^*). \tag{5.7}$$

The linearly polarized pump oriented along the direction Ψ_0 modifies the angular distribution of active dipoles [38,39] as follows:

$$f_{or}(\Psi) = f_{or}^{0}(\Psi)F(\Psi-\Psi_0) \tag{5.8}$$

$$F(\Psi-\Psi_0) = b\cos^2(\Psi-\Psi_0)/(1+b\cos^2(\Psi-\Psi_0)) \tag{5.9}$$

Here $b=E_p^{\,2}\tau_2\mu_p^{\,2}/h^2$, $E_p^{\,2}$ is the intensity of pump field, μ_p is the dipole moment of the absorption transition of the active ion and τ_2^{-1} is the homogeneous absorption line width of the absorption transition.

The laser model, which takes into account the interaction of the laser field (Eq. (5.1)) with the dipoles that have the angular distribution (Eqs. (5.8) and (5.9)), is described by the equations [27]:

$$\begin{aligned}
&\frac{dE_m}{d\tau} = i\frac{\Delta_{cm}}{2}E_m - \frac{G}{2}E_m + \frac{G}{2\pi L}\iint_{L\Psi}\vec{d}_{21}^{\,0}\left(\vec{d}_{21}^{\,0}\vec{E}\right)(N+D)U_m^*\,dz\,d\Psi \\
&\frac{dN}{d\tau} = \eta_1 - N\left(1+\left|\vec{d}_{21}^{\,0}\vec{E}\right|^2\right), \qquad \eta_1 = \Phi_1\eta F(\Psi-\Psi_0)/\pi \\
&\frac{dD}{d\tau} = \eta_2 - D\left(1+\left|\vec{d}_{21}^{\,0}\vec{E}\right|^2\right), \qquad \eta_2 = \Phi_2\eta F(\Psi^*-\Psi_0)
\end{aligned} \tag{5.10}$$

Here m=1, 2; $G=2\gamma/A$; $\tau=t\cdot A$; $\Delta_{cm} = (\omega-\omega_{cm})/2A_\perp$, where A, γ are the inversion and the field relaxation rates, respectively, $A_\perp$ is the homogeneous spectral half-width of the gain. The variables N, D describe the inversion of the randomly-oriented and unidirectionally oriented dipoles of the active ions, respectively.

The interaction of the linearly polarized field with the ensemble of randomly oriented dipoles results in the inhomogeneous azimuthal distribution of inversion N (the effect of angular hole burning):

$$N = N^0 + 2N^c \cos 2\Psi + 2N^s \sin 2\Psi + \dots \ . \tag{5.11}$$

Each angular harmonic of the inversion N^i (i = 0, c, s) and D consist of a space-uniform component and spatial harmonics. The spatial harmonics are determined by the individual action of each mode (spatial hole burning) and by the joint action of the modes whose wave numbers k_1 and k_2 are different:

$$N^{\mathrm{i}} = N_0^{\mathrm{i}} + 2N_1^{\mathrm{i}} \cos(2k_1 z) + 2N_2^{\mathrm{i}} \cos(2k_2 z) + 2N_{12}^{\mathrm{i}-} \cos(k_1 - k_2)\mathrm{z} + 2N_{12}^{\mathrm{i}+} \cos(k_1 + k_2)\mathrm{z} \tag{5.12}$$

$$D = D_0 + 2D_1 \cos(2k_1 z) + 2D_2 \cos(2k_2 z) + 2D_{12}^{-} \cos(k_1 - k_2)\mathrm{z} + 2D_{12}^{+} \cos(k_1 + k_2)\mathrm{z} \tag{5.13}$$

Neglecting the angular harmonics of spatial distribution of the gain the dynamics of laser emission can be described with the following rate equations [57]:

$$\begin{aligned}
\dot{I}_1 &= GI_1\left[N_0^0 + N_1^0 + N_0^c \cos 2R + N_0^s \sin 2R + D_0 + D_1 - 1\right] \\
\dot{I}_2 &= GI_2\left[N_0^0 + N_2^0 - N_0^c \cos 2R - N_0^s \sin 2R + D_0 + D_2 - 1\right] \\
\dot{N}_0^0 &= \eta_1 - N_0^0(1 + I_1 + I_2) - N_0^c(I_1 - I_2)\cos 2R - N_0^s(I_1 - I_2)\sin 2R - \left(N_1^0 I_1 + N_2^0 I_2\right) \\
\dot{N}_0^c &= \eta_1^c - N_0^c(1 + I_1 + I_2) - \frac{1}{2}N_0^0(I_1 - I_2)\cos 2R - \frac{1}{2}\left(N_1 I_1 - N_2 I_2\right)\cos 2R \\
\dot{N}_0^s &= -N_0^s(1 + I_1 + I_2) - \frac{1}{2}N_0^0(I_1 - I_2)\sin 2R - \frac{1}{2}\left(N_1 I_1 - N_2 I_2\right)\sin 2R \\
\dot{N}_1 &= -N_1(1 + I_1 + I_2) - \frac{1}{2}N_0^0 I_1 - \frac{1}{2}N_0^c I_1 \cos 2R - \frac{1}{2}N_0^s I_1 \sin 2R \\
\dot{N}_2 &= -N_2(1 + I_1 + I_2) - \frac{1}{2}N_0^0 I_2 + \frac{1}{2}N_0^c I_2 \cos 2R + \frac{1}{2}N_0^s I_2 \sin 2R \\
\dot{D}_0 &= \eta_2 - D_0\left[1 + I_1 + I_2 + (I_1 - I_2)F(\Psi^*)\right] - (D_1 I_1 + D_2 I_2) - (D_1 I_1 - D_2 I_2)F(\Psi^*) \\
\dot{D}_1 &= -D_1\left[1 + I_1 + I_2 + (I_1 - I_2)F(\Psi^*)\right] - \frac{1}{2}D_0 I_1\left(1 + F(\Psi^*)\right) \\
\dot{D}_2 &= -D_2\left[1 + I_1 + I_2 + (I_1 - I_2)F(\Psi^*)\right] - \frac{1}{2}D_0 I_2\left(1 - F(\Psi^*)\right),
\end{aligned} \tag{5.14}$$

where

$$\eta_1 = \eta\Phi_1$$

$$\eta_1^c = \left[\eta\Phi_1\left(\sqrt{1+2b_0}-1\right)/2b_0\right]\cos 2\Psi_0 \qquad (5.15)$$

$$\eta_2 = \eta\Phi_2\left\{1+\frac{\left(\sqrt{1+2b_0}-1\right)}{2b_0}\cos 2\left(\Psi_0-\Psi^*\right)\right\}$$

Figs. 5.8 and 5.9 display the behavior of the modes intensities I_1 and I_2 versus pump parameter η and pump polarization direction Ψ_0, respectively, obtained by numerical integration of Eqs. (5.14).

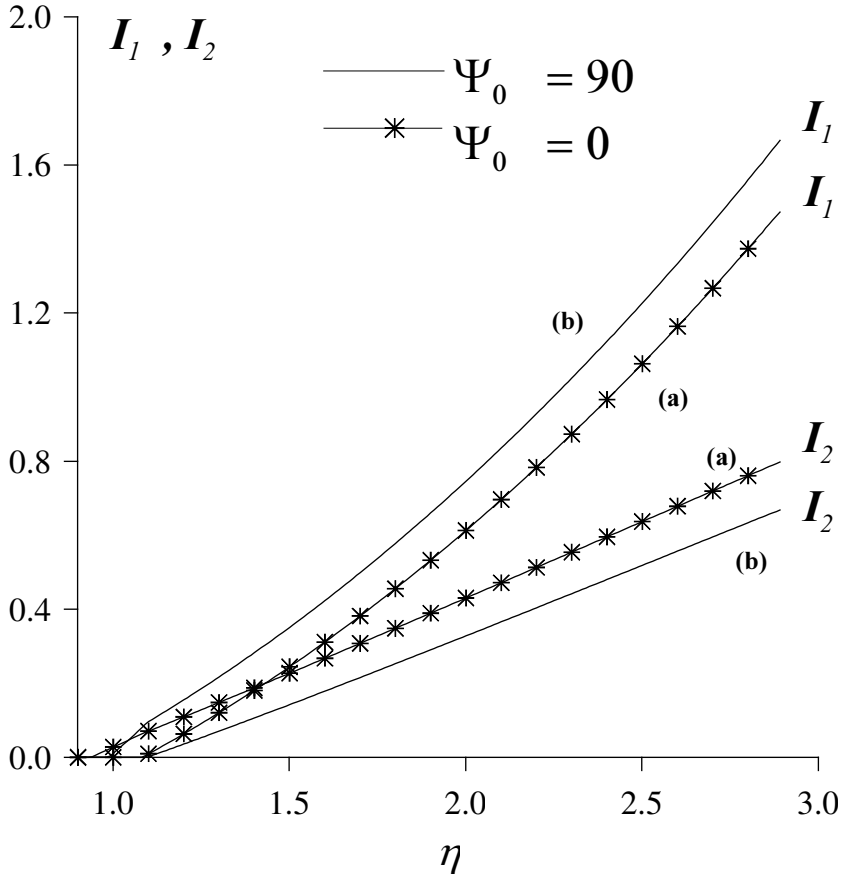

Fig. 5.8: Dependence of I_1, and I_2 on the pump parameter η at (a) $\Psi_0=0^0$ and (b) $\Psi_0=90^0$, calculated with Eqs. (5.14) and (5.15) at G=1000, b=100·η, and $\Psi^*= R =0^0$.

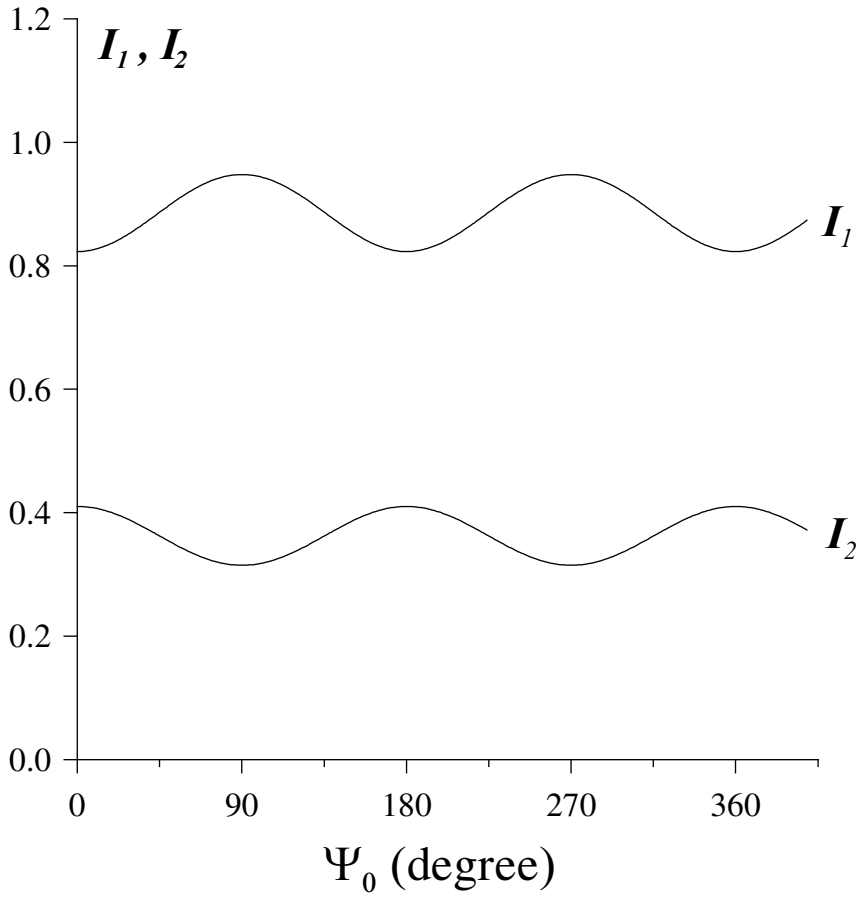

Fig. 5.9. Dependence of I_1, and I_2 on the direction Ψ_0 of the pump polarization at $\eta = 1.5$, $G = 1000$, $b = 100\eta$; $\Psi^* = R = 0^0$, $\Phi_1 = 0.5$; $\Phi_2 = 0.5$.

Comparison of these data with the experimental results (see Figs.5.2 and 5.3) proves that the model provides a good description of the behavior of laser emission. It should be noted that the separation of modes into a strong and a weak one observed in the experiment is provided in the present model by matching parameters Φ_1 and Φ_2 that determine the proportion of isotropically and anisotropically distributed dipoles of active medium.

A linear stability analysis of Eqs. (5.14) leads to the tenth-order characteristic equation whose roots are found numerically. They have two pairs of complex-conjugate roots defining relaxation oscillations. Fig. 5.10 shows the dependence of the relaxation oscillations frequencies on the pump parameter.

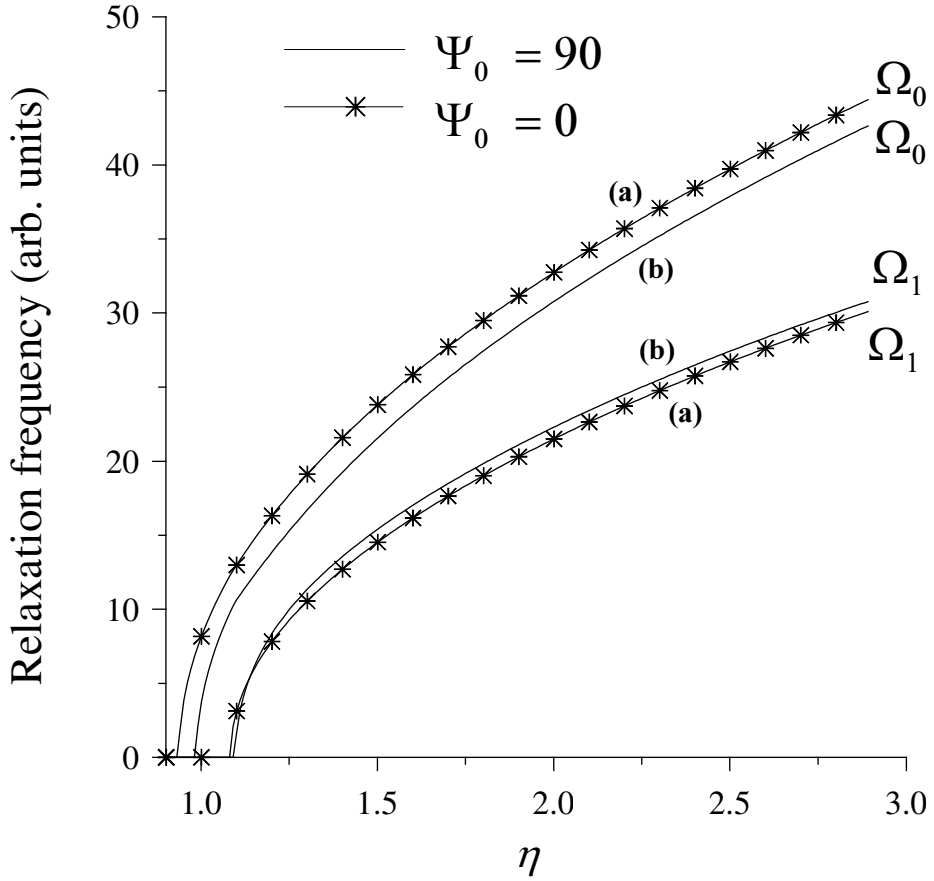

Fig. 5.10: Relaxation frequencies versus pump parameter, η, at (a) $\Psi_0=0^0$ and (b) $\Psi_0=90^0$, G=1000, $b=100\eta$; $\Psi^*= R =0^0$.

These results show that azimuthal inhomogeneity of the laser gain results in similar dynamics of laser emission as in the case of longitudinal inhomogeneity described in Sec. 4.

5.2. Polarization dynamics of a multimode solid-state lasers

This section presents the phenomena associated with azimuthal inhomogeneity of the saturation of the gain in a broadband multimode bipolarized laser. In contrast to previous section where only two modes are oscillating here many longitudinal modes in each polarization are excited. The Nd-doped microchip glass laser [4] mentioned in Sec. 4.3 emits in two polarizations and in many longitudinal modes. Since the glass facets are coated directly with mirrors, there is no selection of polarization, and the laser generally emits elliptically polarized light. Spatial inhomogeneity of the gain in the azimuthal direction gives rise to antiphase oscillations of polarization modes [52].

Figure 5.11 shows the emission in two orthogonal polarizations, measured behind of a polarizer. One can observe fast in-phase oscillations at ν_0, and slow antiphase oscillations at frequency ν_{pol}. Figure 5.12 shows power spectra of the total output at each polarization. The records of the emission at the two polarizations in Fig. 5.11 are not synchronized, therefore the antiphase character of slow oscillations does not show up in the diagrams. However, when the polarizer is removed a slow frequency component at ν_{pol} vanishes almost completely, as can be seen from comparison of Figs. 4.12 and 5.12. The absolute amplitude of the observed polarization oscillations is the same for both polarizations. However, the relative amplitude differs since the mean power in the two polarizations is different.

These experiments show that azimuzhal inhomogeneity of the gain causes fluctuations of the modal intensities that may limit the spectral sensitivity of intracavity absorption measurements.

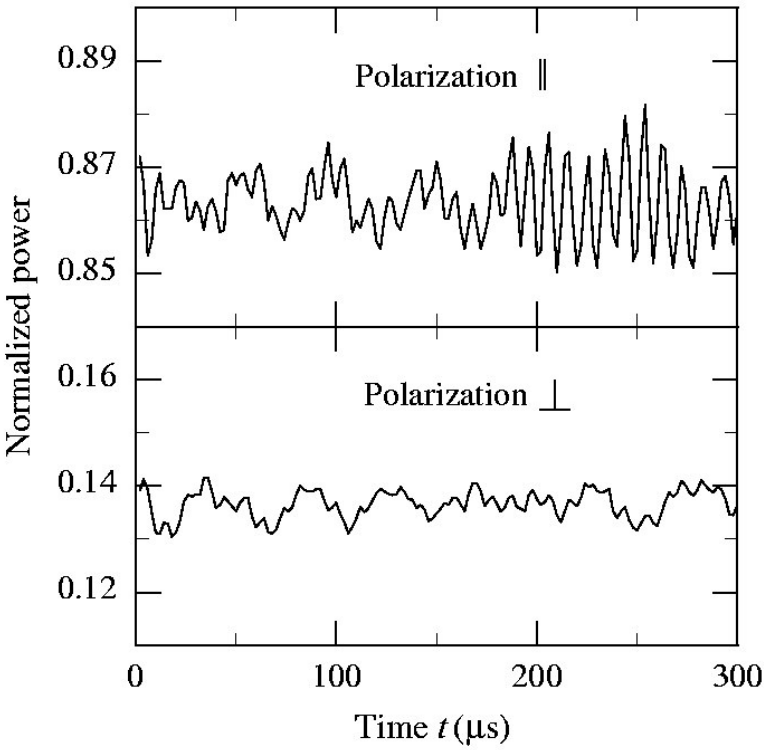

Fig. 5.11: Laser intensity measured in two orthogonal polarizations. The power in each polarization is normalized to the mean total power and not synchronized.

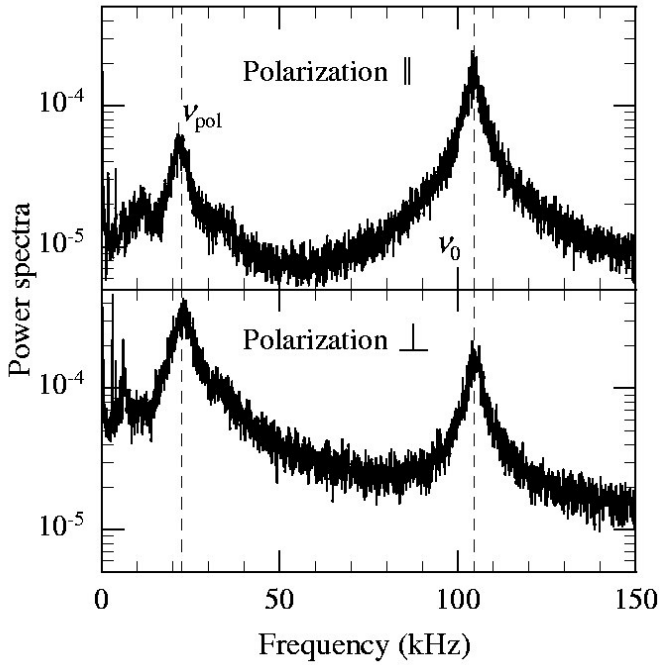

Fig. 5.12: Power spectra of the laser power emitted in two polarizations.

6. Sensitivity limitation of ICAS by spectral inhomogeneities of the gain

6.1. Single-mode and multimode ICAS

Different active ions in the Nd-doped fibre are subject to different Stark shifts and have different resonant frequencies [58]. Hence the active medium as a whole responds to a range of frequencies considerably larger than that for a single active ion, as shown in Fig. 6.1. This kind of response is called inhomogeneous spectral broadening, in contrast to the homogeneous broadening, when every active ion has the same resonance frequency and linewidth. The two types of broadening coexist in a real medium, but one kind can be dominant in a particular laser medium.

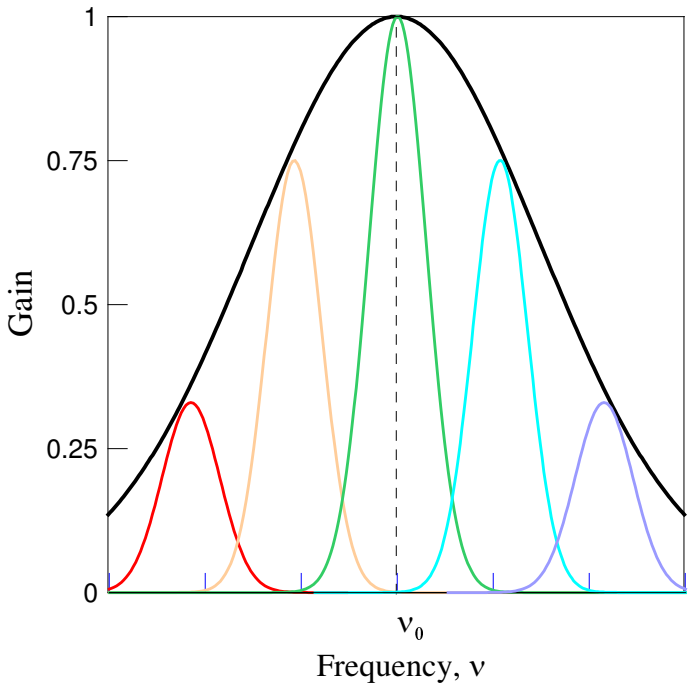

Fig. 6.1: The gain of individual active ions superimposed in the inhomogeneously broadened gain profile of a Nd–doped fibre laser medium. The homoheneous contribution to the medium line width is 30 cm^{-1}; the inhomogeneous contribution is appr. 10 time larger.

Fibre lasers show both homogeneous and inhomogeneous broadening of the gain in contrast to solid-state crystal lasers where homogeneous broadening is dominant. Homogeneous spectral broadening of the gain of fibre lasers is larger than the absorption linewidth of gases, which is prerequisite for high-sensitive measurements of absorption [1]. Fibre lasers allow for measurements of intracavity absorption in a broad spectral range even with no spectral tuning because of large contribution of inhomogeneous broadening of their gain.

The Yb^{3+}-doped and Nd^{3+}-doped silicate fibres lasers emit nearly in the same range from 1.07 μm up to 1.12 μm. The character of the gain broadening is different for these lasers. In Nd-doped fibre laser ingomogeneous spectral broadening is dominant, whereas in Yb-doped fibre laser homogeneous broadening is dominant. This difference might be the reason for different sensitivity limits of ICAS measurements.

The emission spectrum of a multimode laser is very sensitive to intracavity absorption, if the absorptive linewidth does not exceed the homogeneous linewidth of the gain [1]. If, however, the absorption linewidth exceeds the homogeneous broadening of the gain, the spectral sensitivity of ICA measurements is low. Figs. 6.2-6.6 demonstrate these two situations and their principal difference.

The case of narrowband absorption is shown in Figs. 6.2, 6.3. One can see (Fig.6.2) the spectral distribution of total cavity loss, including broadband cavity loss and narrowband cavity loss, and the spectral profile of the gain. The laser gain compensates only the broadband cavity loss, whereas the narrow line intracavity absorption is left uncompensated. Uncompensated loss leads to the reduction of the laser emission in the spectral range of ICA-line (Fig. 6.3).

When the absorptive linewidth exceeds the homogeneous linewidth of the gain (Fig. 6.4), the total cavity loss including the ICA-line is compensated by the increased laser gain. As a result the reduction of the laser emission in the spectral range of ICA-line is rather weak (Fig. 6.5). This case is equivalent to ICAS with a single-mode laser. Spectral sensitivity of ICA measurements with single mode lasers is significantly below than with multimode lasers.

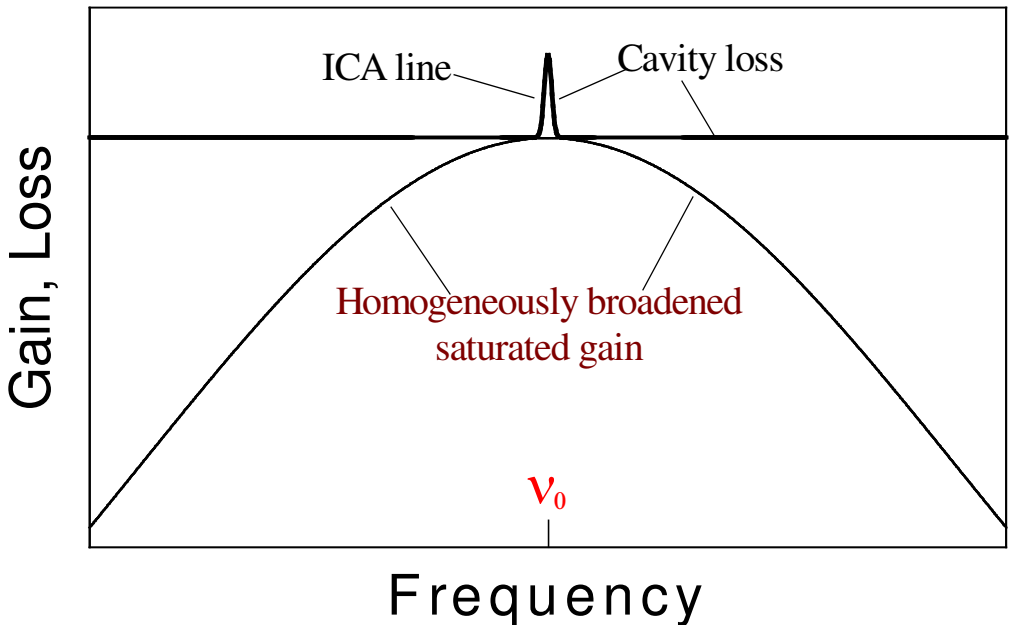

Fig. 6.2: Laser gain and cavity loss with narrowband intracavity absorption.

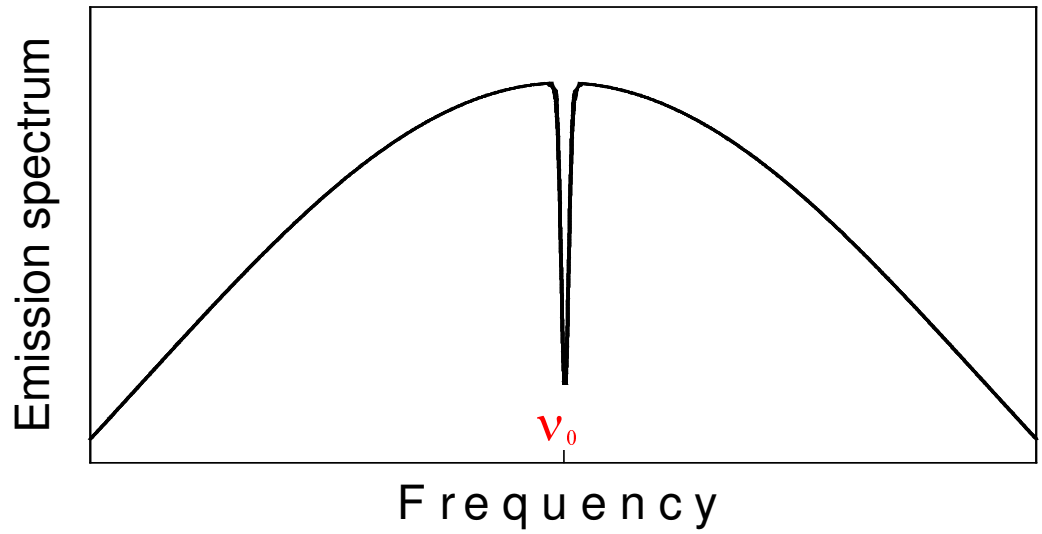

Fig. 6.3: Emission spectrum of a fiber laser with narrowband intracavity absorption.

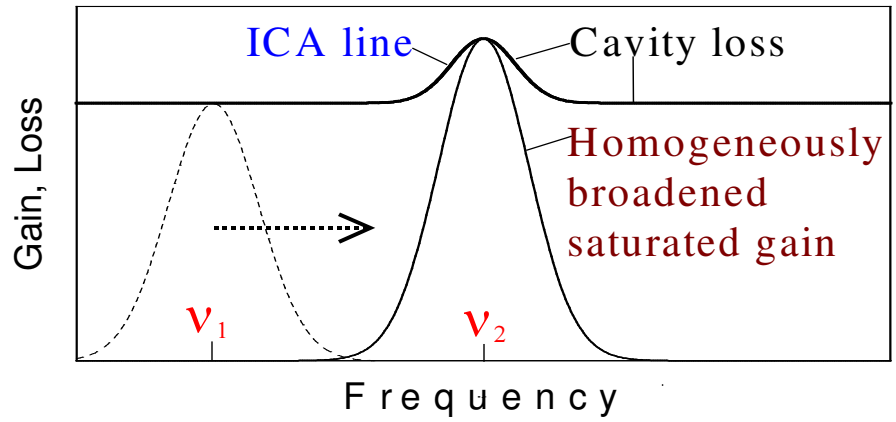

Fig. 6.4: Laser gain and cavity loss including broadband absorption.

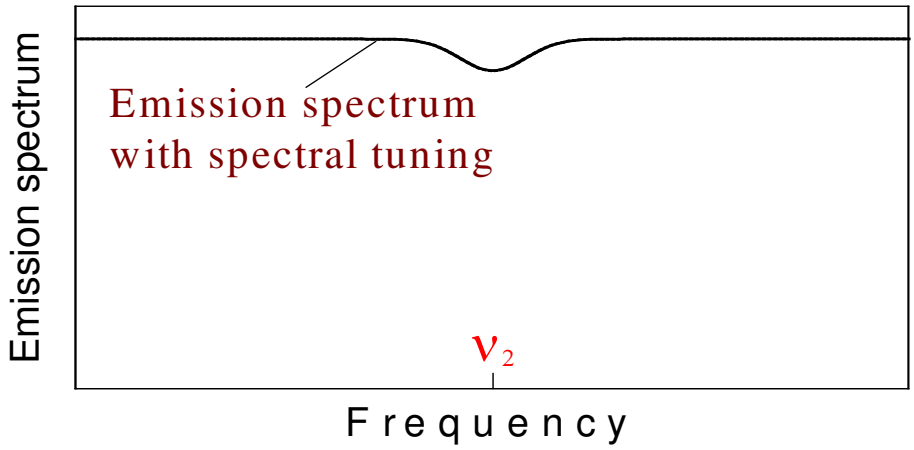

Fig. 6.5: Emission spectrum of the laser with broadband intracavity absorption.

Relation between effective absorption path lengths of multimode and single mode ICAS is described by the equation [1]:

$$L_{\text{eff}}^{mm} = M_q L_{\text{eff}}^{sm} \tag{6.1}$$

where M_q is the photon number in the laser mode q.

Fig. 6.6 shows the calculated output power of a cw laser versus the pump rate, for two different values of cavity loss $\gamma = \gamma_0 + \kappa c$ on two corresponding wavelengths ν_1, ν_2, with γ_0 being the internal cavity loss, and κ the extinction caused by the additional intracavity absorber. Absorption signal $K = \ln(I_1/I_2)$ is much smaller than in the case of ICAS with multimode laser.

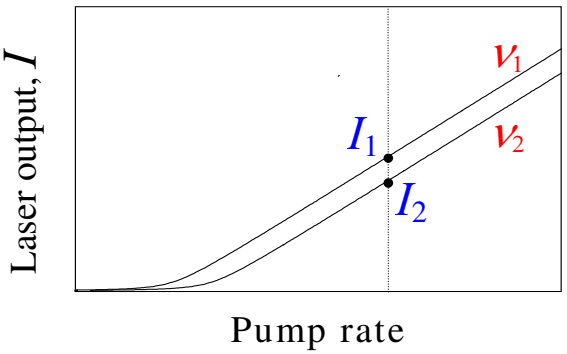

Fig. 6.6: Laser output at two different frequencies ν_1, ν_2 (Fig. 6.4).

Although the sensitivity of single-mode ICAS is smaller than that of multimode ICAS, it still exceeds the sensitivity of conventional absorption spectroscopy [1]. It may be useful for measurements of broadband absorbers.

6.2. Measurements of absorption with variable line width in the cavity of fibre lasers

The influence of the absorption linewidth on the spectral sensitivity to intracavity absorption was studied in the experiment. The experiment demonstrates the transition from the narrowband to broadband ICA. The absorption with variable linewidth is modelled by a glass etalon with variable base. The etalon provides the weak loss in the cavity of Nd- or Yb-doped fibre lasers.

The experimental set-up is shown in Fig. 6.7. The input mirror M_1 of the laser cavity is placed directly on the input face of the fibre and has reflectivity near unity in the operation range of the fibre laser, and high transmission at the wavelengths of the pump radiation. The

aspheric lens is employed for the collimation the fibre laser beam exiting from the open end of the fibre. The laser emission is tuned by moving the lens along the optical axis using the effect of chromatic aberration. The output plane dielectric mirror M_2 has 1% of transmission in the operation range of the fibre laser. The intracavity etalon consists of two simple glass substrates with back faces cut at the Bruster angle. The front faces of both etalon substrates have the reflectivity of 4%. The etalon produces a weak loss modulation (1.6 %) in the laser cavity. The change of the etalon length models the variation of the absorption line width. The open space of the cavity is filled with atmospheric air. The output beam is analysed by the spectrograph with CCD array and a digital oscilloscope. The measurements were made at the room temperature of the fibre and at temperature of liquid nitrogen. For this purpose the Nd-doped fibre was placed in the vessel with liquid nitrogen. It was done to decrease the homogeneous linewidth of the gain of the fibre laser and to see how it influences the sensitivity to intracavity absorption.

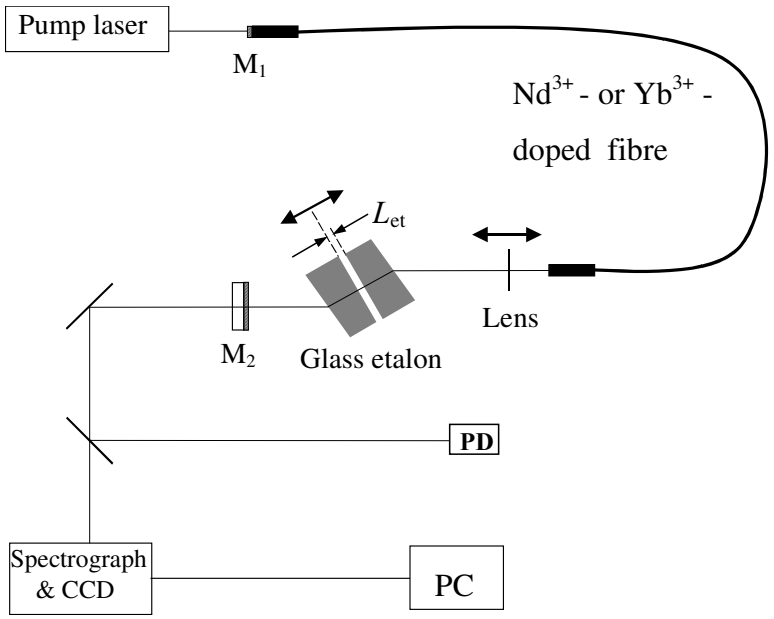

Fig. 6.7: Experimental set-up

Fig. 6.8 shows etalon reflectivity ΔR at two values of the etalon length L_{et} = 100 μm and L_{et} = 250 μm. One can see that the decrease of the etalon length leads to an increase of the period of the loss modulation. Fig. 6.8 demonstrates also the total cavity loss γ, which equals the sum of broadband cavity loss and the loss modulation inserted into the cavity by the etalon. The coupling efficiency of the etalon with the laser cavity is equal to $\alpha \approx 0.1$. It was measured by comparing of the absorption path length obtained for the experimental emission spectra with corresponding transmission spectum calculated with a help of HITRAN data base. The broadband cavity loss equals 15% per round trip. One can see that the etalon loss modulation is less than the broadband cavity loss. But broadband cavity loss is completely compensated by the gain of the active medium in contrast to narrowband etalon loss which left uncompensated and as the result the emission spectrum of the laser is extremely sensitive even to such small loss modulation.

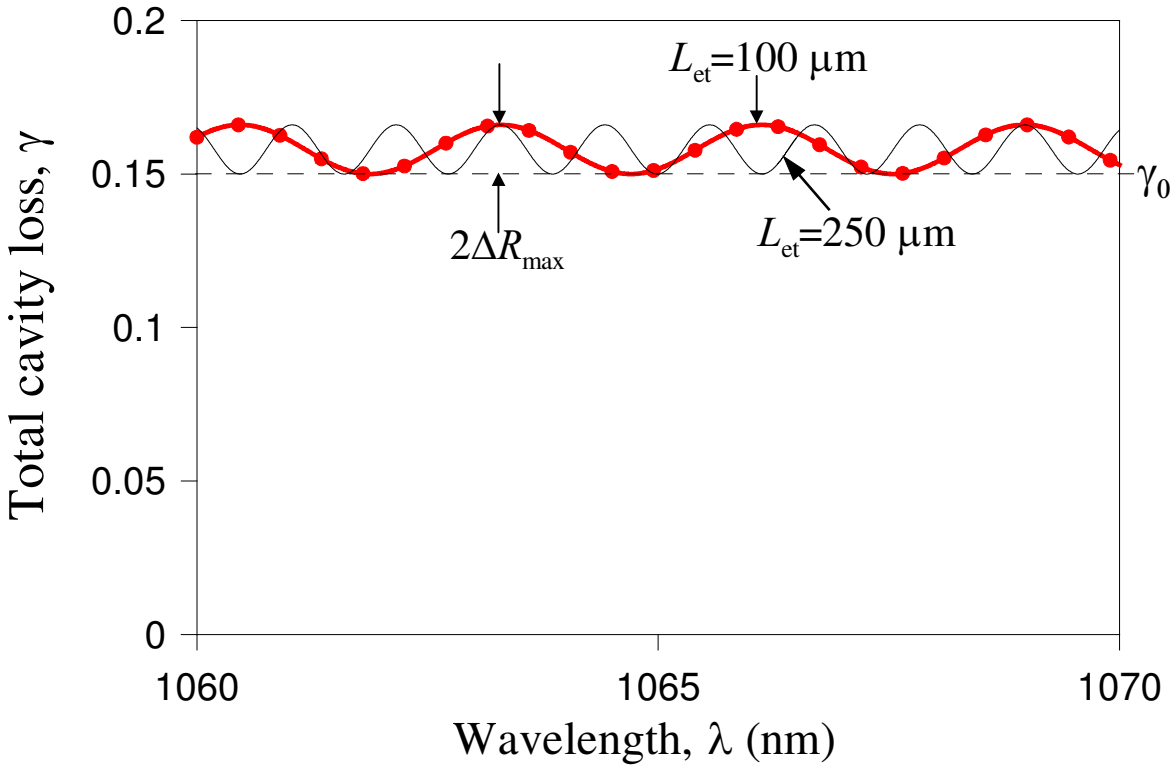

Fig. 6.8: Total cavity loss per round trip, $\gamma = \gamma_0 + 2\Delta R$, including the broadband cavity loss, $\gamma_0 \approx 0.15$, and loss modulation by the intracavity etalon, $2\Delta R$. Maximum etalon loss per round trip $2\ \Delta R_{max} \approx 0.016$ (1.6 %).

The intracavity etalon provides the additional cavity loss ΔR, which depends on the coupling efficiency of the etalon to the laser cavity α, the reflectivity of light amplitude by etalon surfaces r and the operation frequency ν of the laser:

$$\Delta R \approx 2\alpha r^2 \cos^2(4\pi\nu L_{et}) \tag{6.2}$$

From the emission spectrum of the laser one can calculate so called effective number of light trips N_{eff} through the cavity. N_{eff} and the effective absorption path length L_{eff} characterise the spectral sensitivity. Two these parameters are related as:

$$L_{eff} = N_{eff} L_{cav} \tag{6.3}$$

where L_{cav} is the length of the laser cavity.

To find out the value of N_{eff} one calculates the value of etalon loss ΔR, at which the laser output drops by factor of 2 as it is shown in Fig. 6.9. After that N_{eff} is determined from the measured line width of oscillating regions $(\Delta\nu)$ and free spectral range of the etalon $1/2L_{et}$.

According to Lambert-Beer law transmitted light intensity I_1 after one trip through the cavity equals

$$I_1(\nu) = I_{10} \exp(-\kappa(\nu) L_{cav}) \tag{6.4}$$

Laser output spectrum is described by the equation:

$$I(\nu) = I_0 \exp(-\kappa(\nu) L_{eff}) = I_0 \exp(-\Delta R(\nu) L_{eff} / L_{cav}), \tag{6.5}$$

where

$$\kappa(\nu) = \frac{\Delta R(\nu)}{L_{cav}} \tag{6.6}$$

is the absorption coefficient of ICA.

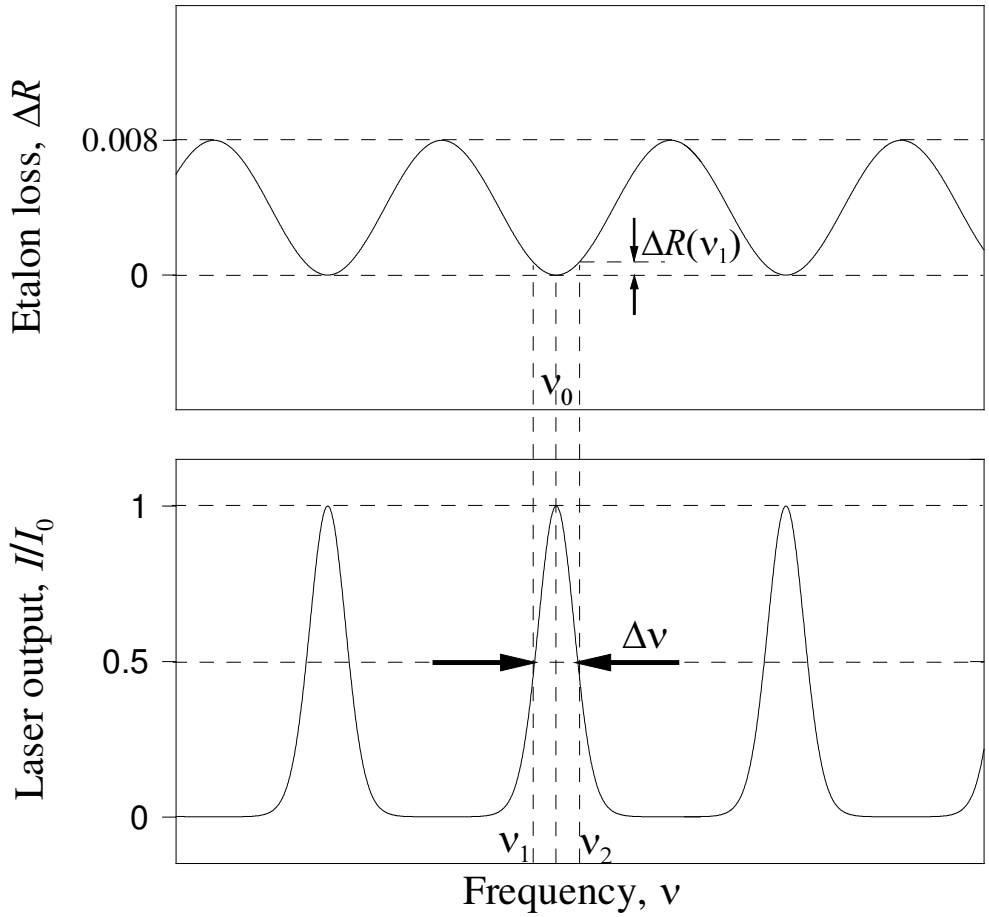

Fig. 6.9: Etalon loss (top) and corresponding laser output (bottom)

The absorption signal at which the laser output drops by factor of 2 (Fig. 6.9) equals:

$$K(\nu_1) = \ln(I_0 / I((\nu_1)) = \kappa(\nu_1) L_{\text{eff}} = \ln 2 \tag{6.7}$$

Effective absorption path length is obtained from Eqs. (6.6) and (6.7):

$$L_{\text{eff}} = \ln 2 \; L_{\text{cav}} / \Delta R(\nu_1) \tag{6.8}$$

The effective number of light trips through the cavity N_{eff} is obtained from Eqs. (6.3), (6.6) and (6.8):

$$N_{\text{eff}} = \frac{L_{\text{eff}}}{L_{\text{cav}}} = \frac{\ln 2}{\kappa(\nu_1) L_{\text{cav}}} = \frac{\ln 2}{\Delta R(\Delta\nu/2)} \tag{6.9}$$

In Fig. 6.10 one can see the influence of loss modulation, ΔR, due to intracavity etalon on the output intensity of laser radiation at different number, N, of light trips through the cavity. The increase of the number N leads to the increase of the modulation depth of the laser intensity and decrease of the linewidth $\Delta\lambda$.

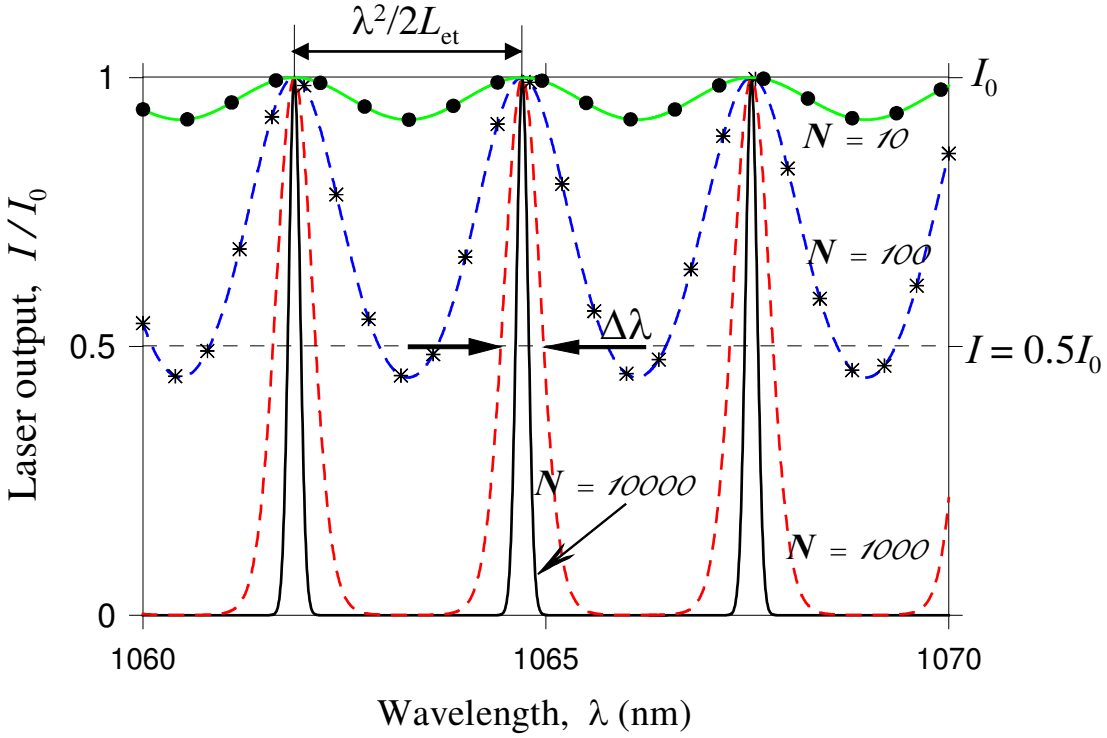

Fig. 6.10: Laser output at different number, N, of light trips through the cavity in presence of intracavity etalon, L_{et} = 100 μm.

Fig. 6.11 shows the emission spectra of a Nd-doped fiber laser at the different lengths of the intracavity etalon measured at room temperature and at the pump rate η = 3.2. Periodic structure in the emission spectra is determined by the intracavity etalon. One can see that the decrease of the etalon length leads to the broadening of the oscillating spectral regions. The important feature is that the line width of the spectral regions increases faster, than intermode spacing of the etalon at small values of the etalon length.

Fig. 6.12 demonstrates the behaviour of the linewidth of oscillating regions $\Delta\nu$ in the emission spectrum at the change of the etalon length in the cases of Nd-doped and Yb-doped fiber lasers. One can see the growth of $\Delta\nu$ at the values of etalon length smaller than 50 μm.

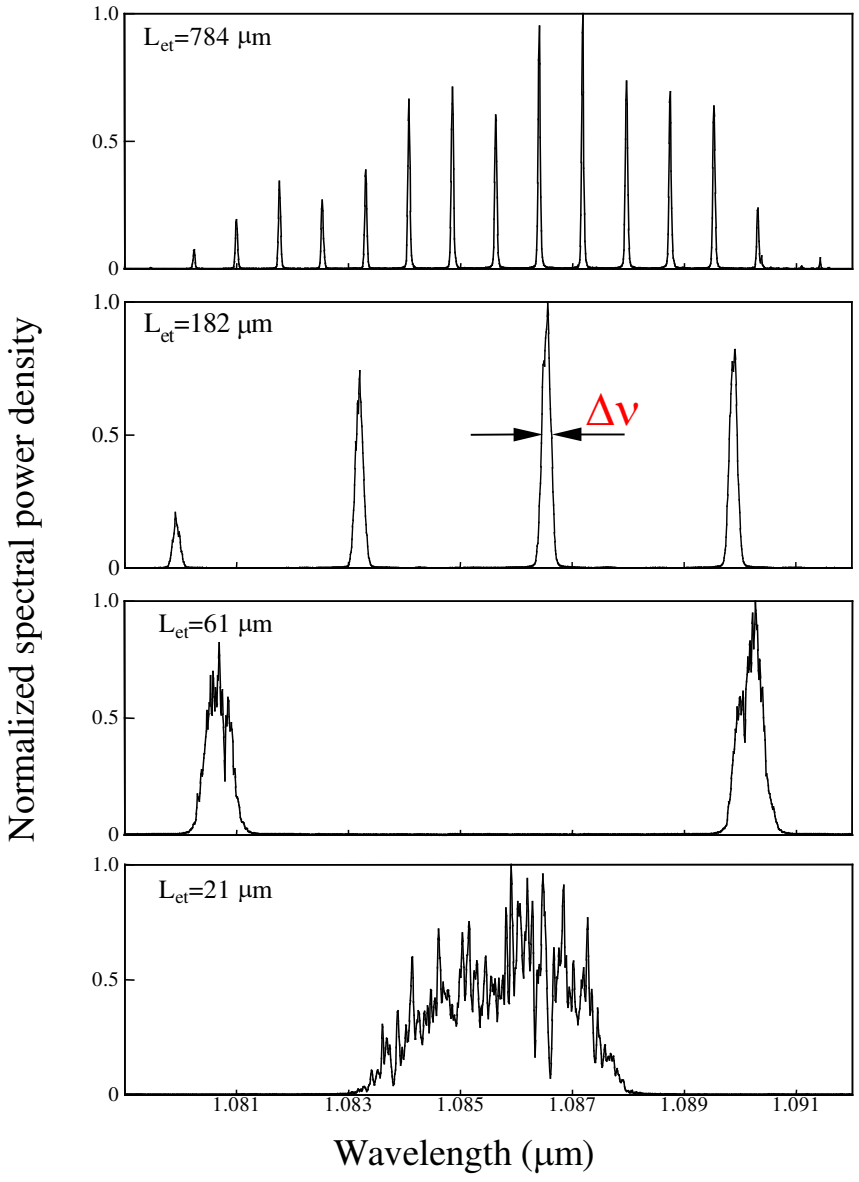

Fig. 6.11: Emission spectra of the Nd-doped fibre laser at different lengths, L_{et}, of intracavity etalon, at pump rate η = 3.2. Periodic structure in the emission spectra is determined by the etalon.

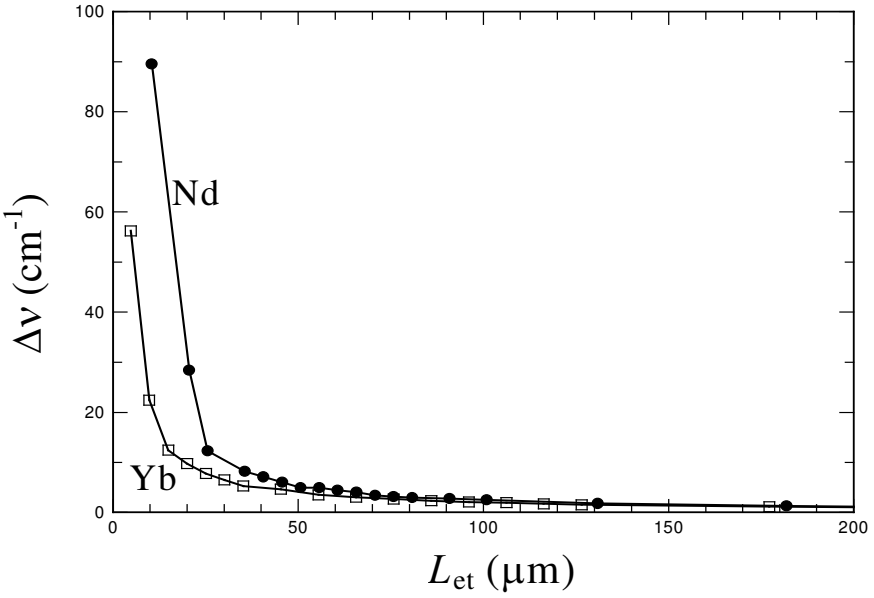

Fig. 6.12: Linewidth, $\Delta\nu$, of oscillating regions in the emission spectrum of fiber lasers vs. etalon length, L_{et}.

By substituting Eqs. (6.2) and (6.9) into Eq. (6.3) follows:

$$L_{eff} = \frac{\ln 2\, L_{cav}}{\Delta R(\Delta\nu/2)} = \frac{\ln 2\, L_{cav}}{2\alpha r^2 \cos^2(\Delta\nu / 1/2L_{et})} \tag{6.10}$$

One sees from Eq. (6.10) that the effective path length depends on the ratio of the linewidth of oscillating regions to intermode frequency spacing of the etalon. Fig. 6.13 demonstrates this ratio versus the length of the intracavity etalon.

The spectral sensitivity L_{eff} calculated from the emission spectra is shown in Fig. 6.14. One can see that with Nd-doped laser spectral sensitivity drops by several orders of magnitude if the etalon length smaller than 70 μm. In this case the linewidth of intracavity loss becomes larger than the homogeneous linewidth of the gain. With the Yb-doped laser the sensitivity reduction is also observed, but only if the etalon length is smaller than 15 μm. These results show that the Yb-doped fibre has significantly larger homogeneous linewidth of the gain than the Nd-doped fibre. Therefore with Yd-doped fibre laser the sensitivity to ICA begins to drop at significantly larger values of the line width of the intracavity loss.

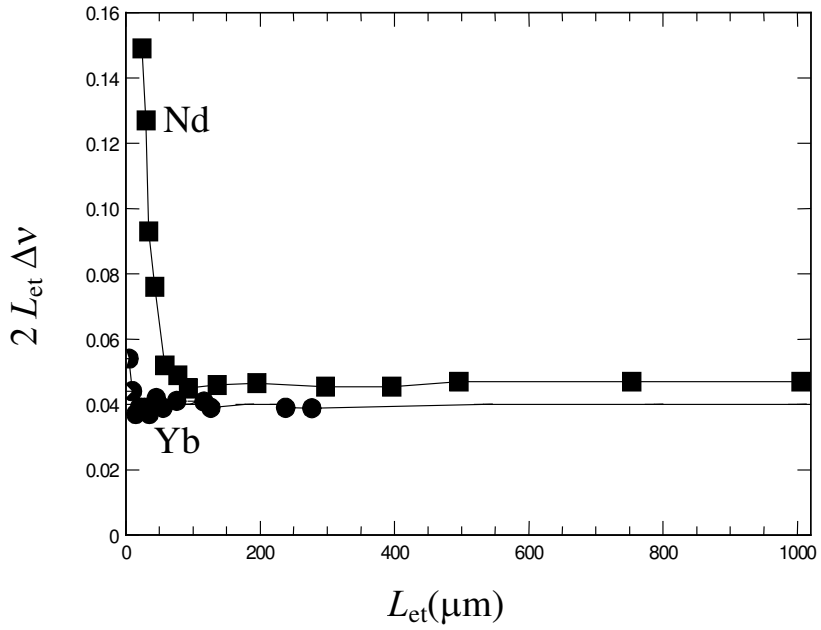

Fig. 6.13: Relative linewidth of laser emission $\Delta\nu$ in respect to the free spectral range of the etalon $(2L_{et})^{-1}$ vs. etalon length at pump rate η=4, γ=4.6·10^6 s^{-1}, L_{cav}=270 cm, L_{fib}=106 cm (Nd-laser); η=8.3, γ=2.4 ·10^7 s^{-1}, L_{cav}=210 cm, L_{fib}=73 cm (Yb-laser).

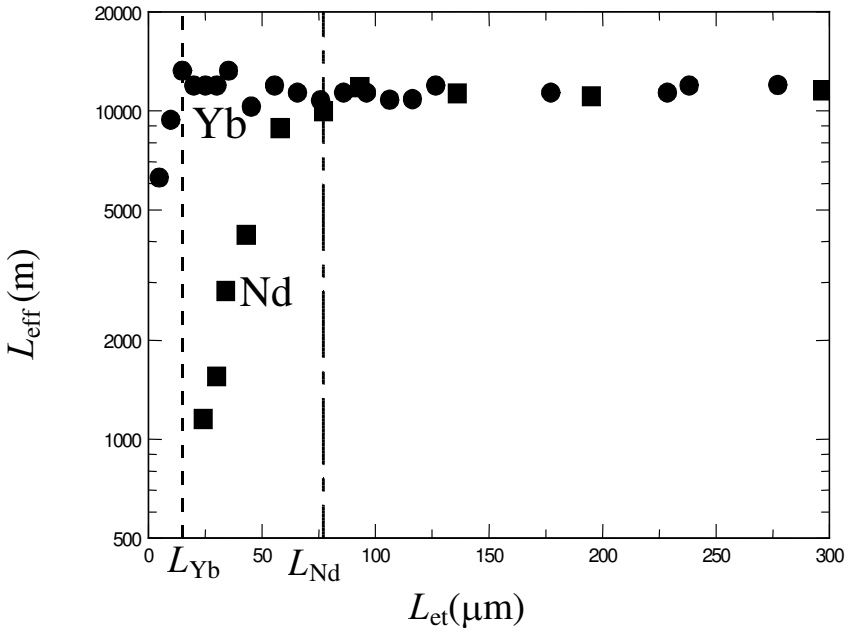

Fig. 6.14: The effective absorption pathlength, L_{eff}, measured with Nd- and Yb-doped fiber lasers. L_{Yb} and L_{Nd} show the smallest etalon lengths required for high sensitivity of intracavity absorption measurements.

In the next experiment the Nd-doped fibre was cooled down to the temperature T=77 K in the vessel with liquid nitrogen. Fig. 6.15 shows the corresponding experimental emission spectra of a Nd-doped fiber laser at the different lengths of the intracavity etalon at the pump rate η=5.5. In this case the sensitivity reduction (see Fig. 6.16) is observed already at the values of etalon length of less than 300 μm. That means that the homogeneous line width of the gain decreases and the sensitivity begins to drop at significantly smaller values of the line width of intracavity loss. The homogeneous line width of the gain of the Nd-doped fibre decreases by cooling the fibre. Significant reduction of the sensitivity was observed already at the absorption line width of ~30 cm^{-1} (corresponding to etalon length ~150 μm). The sensitivity to intracavity absorption at short wavelengths drops at much smaller absorption linewidth than in the long wavelength range (see Fig. 6.15). The reason for this phenomenon may be a different homogeneous line width of the gain in the different spectral regions.

The experimental data allow to estimate the homogeneous linewidth of the gain of the fibres. The homogeneous line width of the gain of the Nd-doped fibre is estimated to be 35 cm^{-1} at room temperature and 8 cm^{-1} at the temperature of liquid nitrogen (T=77 K). The Yb-doped fibre shows the linewidth of the gain larger than 150 cm^{-1}, which is favourable for high sensitive detection of broadband ICA. In the case of Yb-doped laser there was no essential change of the spectral sensitivity to ICA with an increase of the absorption line width up to 300 cm^{-1} (it corresponds to elation length 15 μm). Experiments with Nd-doped laser showed another behaviour. A reduction of the sensitivity was observed at the value of the absorption line width larger than 100 cm^{-1} (corresponding to etalon length 50 μm). The reason for this sensitivity reduction is that the absorption line width becomes larger than the homogeneous line width of the gain. As a result broadband cavity loss is compensated by the enhanced gain. This leads to the strong reduction of the sensitivity to ICA.

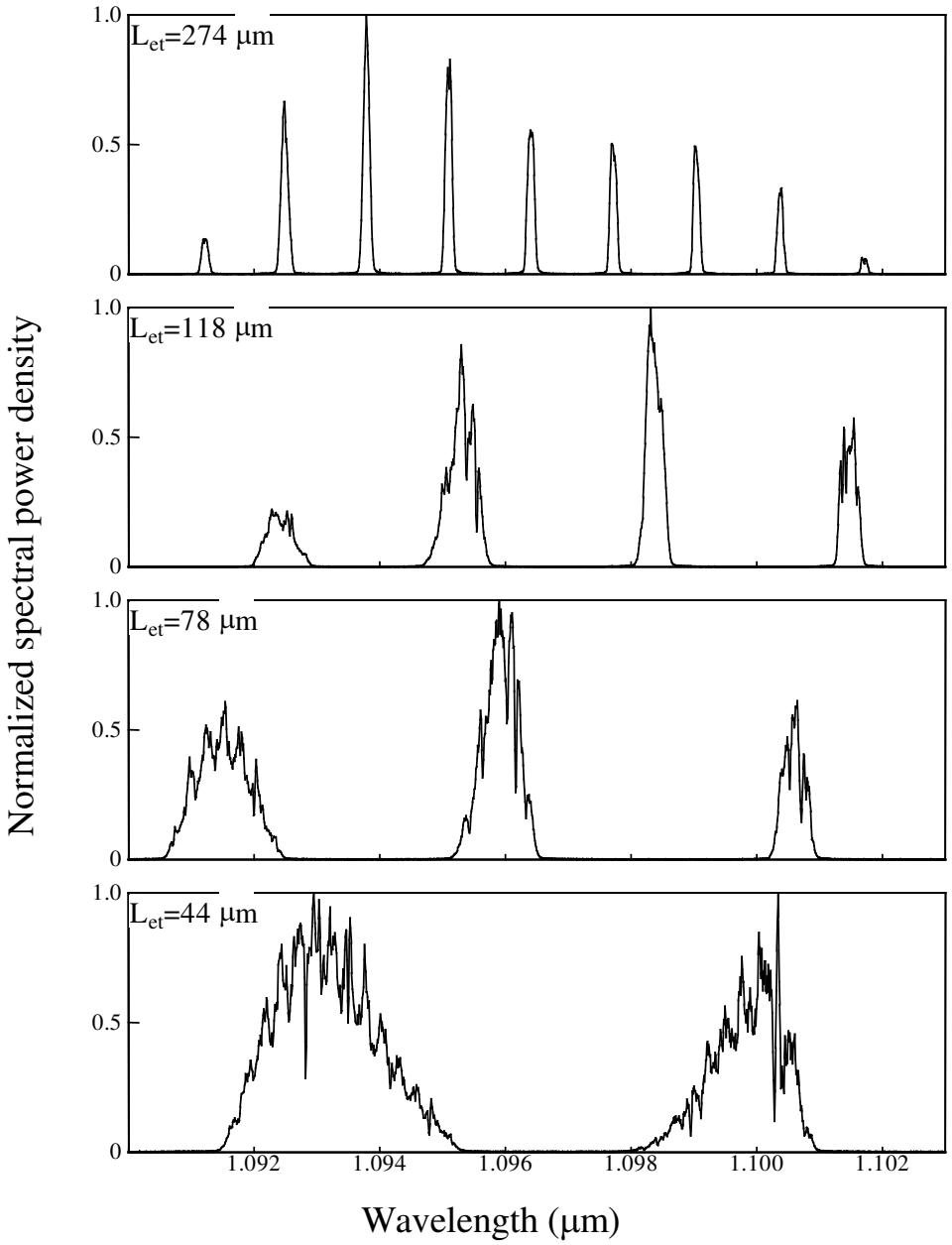

Fig. 6.15: Emission spectra of a Nd-doped fiber laser at different lengths of intracavity etalon, at temperature T=77 K and pump rate η=5.5

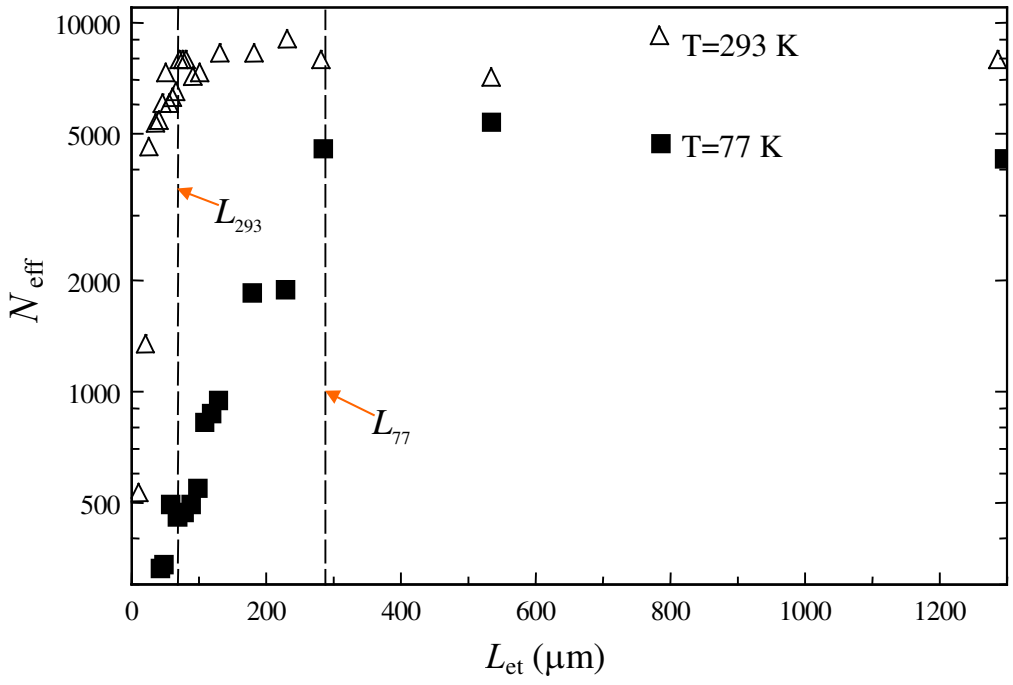

Fig. 6.16: Effective number of light trips through the cavity measured with Nd-doped fibre laser at the temperature T=77 K and T=293 K. L_{77} and L_{293} show the smallest etalon lengths required for high sensitivity of ICA measurements at two these temperatures.

7. Summary

Emission spectral dynamics of a broadband laser is very sensitive to intracavity absorption and to mode coupling in the cavity. Mode coupling in the laser causes low frequency oscillations of the power in individual laser modes and may limit the sensitivity of intracavity absorption measurements.

Present work shows that one of the most important mode coupling in solid-state lasers is spatial inhomogeneity of the saturation of the laser gain in longitudinal and azimuthal directions. Investigation of emission dynamics of various multimode lasers shows that this type of mode coupling can be significantly reduced by proper choice of laser parameters. Especially efficient way of the reduction of mode coupling and, therefore, of the enhancement of sensitivity of the laser emission spectrum to intracavity absorption is the increase of the number of oscillating laser modes, reduction of the pump rate and the selection of only one polarization mode. With an 8-meter long Nd-doped fibre laser the number of oscillating modes has been increased to 50,000 and in this way the sensitivity of ICAS has been increased to more than 100 km.

Spontaneous emission becomes the main factor limiting the spectral sensitivity of the fibre laser to intracavity absorption if the cavity loss is large and if the laser operates not far above threshold. The influence of spontaneous emission is most pronounced if the laser shows strong relaxation oscillations.

The emission spectrum of a multimode laser is very sensitive to intracavity absorption, if the absorptive linewidth does not exceed the homogeneous linewidth of the gain. This condition is fulfilled with gaseous absorbers of small molecules placed in the laser with broadband gain. When, however, the absorptive linewidth exceeds the homogeneous linewidth of the gain the sensitivity drops significantly. The transition from the narrowband to broadband intracavity spectroscopy was studied experimentally with a Nd- and an Yb-doped fibre lasers. The sensitivity of a Nd-doped fibre laser drops by several orders of magnitude, if the absorptive linewidth is larger 35 cm^{-1}. In contrast, an Yb-doped fibre laser shows sensitivity reduction only when absorptive linewidth is larger than 150 cm^{-1}. It means that the Yb-doped fibre laser has larger homogeneous broadening and is better suited for sensitive measurements of broadband intracavity absorption.

Sensitivity of ICA measurements can be enhanced by using the active media with broad spectral gain, applying smaller pump rates, reducing cavity losses, increasing the cavity length and by reducing the length of the active media.

Bibliography

[1] V.M. Baev, T.Latz, P.E. Toschek, Laser intracavity absorption spectroscopy, Applied Physics B **69**, 171-202, (1999).

[2] P.A. Khandokhin, E. A. Ovchinnikov, E.Yu. Shirokov, Optical spectrum of a solid-state diode-pumped Fabry-Perot laser, Phys.Rev.A **61**, 053807, (2000).

[3] N.B. Abraham, L.L. Garson, V. Seccareccia, P.A. Khandokhin, Ya.I. Khanin, I.V. Koryukin, V.G. Zhislina, Anomalies, symmetries and asymmetries in relaxation oscillations spectra of multimode standin-wave solid-state lasers, Phys.Rev.A **62**, 013810, (2000).

[4] B. Peters, J. Hünkemeier, Ya. Khanin, V.M. Baev, Low-frequency dynamics of a Nd:glass laser, Phys.Rev. A **64**, 023816, (2001).

[5] I.V. Koryukin, P. Mandel, Two-mode threshold of a solid-state Fabry-Perot laser, J.Opt. B: Quantum Semiclass. Opt. **4**, pp.27-29, (2002).

[6] E. Ovchinnikov, Polarization dynamics of a multimode solid-state laser with a Fabry-Perot cavity, Master's thesis, Nizhny Novgorod (1997).

[7] E. Ovchinnikov, U. Stapelfeld, V.M. Baev, P.E. Toschek, Intracavity laser spectroscopy with inhomogeneously broadened fiber laser, International Quantum Electronics ´Conference, IQEC 2002, Moscow, Russia, 22-28.06.2002, Technical Digest p.110.

[8] M. Risch, A. Stark, V.M. Baev, P.E. Toschek, Transient dynamics of intracavity absorption signals in solid state lasers, Frühjahrstagung der AG Quantenoptik der Deutschen Physikalischen Gesellschaft, Berlin, 2.4-6.4.2001; Verhandl. DPG (VI) 36, 5/224, Q31.15 (2001).

[9] D. A. Gilmore, P. Vujkovic Cvijin, G. H. Atkinson, "Intracavity absorption spectroscopy with a Titanium:sapphire laser", Opt. Commun. **77**, 385-389 (1990).

[10] J. Sierks, J. Eschner, V. M. Baev, and P. E. Toschek, "Sensitivity of intracavity absorption measurements with Ti:sapphire laser", Opt. Commun. **102**, 265-270 (1993).

[11] R. Böhm, A. Stephani, V. M. Baev, and P. E. Toschek, "Intracavity absorption spectroscopy with Nd^{3+}-doped fibre laser", Opt. Lett. **18**, 1955-1957 (1993).

[12] J. Hünkemeier, R. Böhm, V. M. Baev, and P. E. Toschek, "Spectral dynamics of Nd^{3+}- and Yb^{3+}-doped fibre lasers", Opt. Comm. 6523 (2000).

[13] S. J. Harris and A. M. Weiner "Continuous wave intracavity dye laser spectroscopy. II A parametric study", J. Chem. Phys. **74**, 3673-3679 (1981). S. J. Harris, "Power dependence of continuous-wave intracavity spectroscopy", Optics Lett. **7**, 497-499 (1982); S. J. Harris, "Intracavity laser spectroscopy: an old field with new prospects for combustion diagnostics", Appl. Opt. **23**, 1311-1318 (1984).

[14] Yu. M. Aivazyan, V. M. Baev, V. V. Ivanov, S. A. Kovalenko, and E. A. Sviridenkov, "Kinetics of emission spectra of multimode lasers and its influence on the sensitivity on intracavity absorption spectroscopy" Kvant. Elektron. **14**, 279-287 (1987) [Sov. J. Quantum Electron. **17**, 168-173 (1987)].

[15] S. Wu, A. Yariv, H. Blauvelt, N. Kwong, Appl. Phys. Lett. **59**, 1156 (1991).

[16] J. Sierks, T. Latz, V. M. Baev, and P. E. Toschek, "Spectral dynamics of multi-mode dye lasers and single-atom absorption", Proceedings of the 1996 European Quantum Electronics Conference, (EQEC'96), 8-13 September 1996, Hamburg, p.100, QWB6.

[17] J. Sierks, V. M. Baev, and P. E. Toschek, "Enhancement of the sensitivity of a multimode dye laser to intracavity absorption", Optics Comm. **96**, 81-86 (1993).

[18] Yu. M. Aivazyan, V. M. Baev, V. V. Ivanov, S. A. Kovalenko, and E. A. Sviridenkov, "Kinetics of emission spectra of multimode lasers and its influence on the sensitivity on intracavity absorption spectroscopy" Kvant. Elektron. **14**, 279-287 (1987) [Sov. J. Quantum Electron. **17**, 168-173 (1987)].

[19] Ya. Khanin, Fundamentals of laser dynamics, Moscow, Nauka, Publishing Company Fizmatlit (1999).

[20] M. Risch, Spectrale Dynamik der Emission eines Vielmodenlasers mit Absorption im Resonator, Diplomarbeit, Hamburg 2001.

(21) P. Mandel, M. Georgiou, K. Otsuka, and D. Pieroux, Opt. Commun. **106**, 341 (1993).

(22) E. Lacot and F. Stoeckel, J. Opt. Soc. Am. B **13**, 2034 (1996).

[23] J. Hünkemeier, *Dynamik und Absorptionsempfindlichkeit von vielmodigen Faser- und Glas-Lasern*, Dissertation, Hamburg (2001).

[24] V.M. Baev, T. Latz, P.E. Toschek, Laser intracavity absorption spectroscopy, Appl. Phys. B **69**, 171-202 (1999).

[25] V.M. Baev, J. Eschner, E. Paeth, R. Schüler, P.E. Toschek, Intra-cavity spectroscopy with diode lasers, Appl. Phys. B **55**, 463-477 (1992).

[26] J. Siekers, J. Eschner, V.M. Baev, P.E. Toschek, Sensitivity of intracavity absorption measurements with Ti:sapphire laser, Opt. Commun. **102**, 265-270 (1993).

[27] Ya. Khanin, Principles of laser dynamics, North-Holland/Elsevier, Amsterdam, 1995.

[28] T.P. Belikova, E.A. Sviridenkov, L.V. Titova, Method of measuring the homogeneous broadening of the gain in Nd^{3+}- doped glass, Kratk. Soobshch. Fiz. No.**5**, 48-51 (1972).

[29] T.P. Belikova, B.K. Dorofeev, E.A. Sviridenkov, A.F. Suchkov, Measurements of the absolute absorption coefficient by intraresonator laser spectroscopy, Kvant. Elektron. 2 (1975) 1325-1328, [Sov. J. Quantum Electron. **5**, 722-724 (1975).

[30] D. Romanini, A. Kachanov, E. Lacot, F. Stoeckel, Loss of spectral memory in the relaxation oscillations of a multimode solid-state laser, Phys. Rev. A **54**, 920-927 (1996).

[31] C. L. Tang, H. Statz, and de Mars, J. Appl. Phys. **34**, 2289 (1963)]

[32] B. Peters, J. Hünkemeier, V. Baev, Ya. I. Khanin, Low-frequency dynamics of a Nd-doped glass laser, Phys. Rev. A **64**, 023816 (2001).

(33) P. Mandel, B. A. Nguyen, and K. Otsuka, Quantum Semiclassic. Opt. **9**, 365 (1997).

[34] D. Pieroux, P. Mandel, Quantum and Semiclassical Optics, **9**, L17 (1997).

[35] P. A. Khandokhin, Ya. I. Khanin, Yu. Mamaev, N. D. Milovsky, E. Yu. Shirokov, S. Bielawski, D. Derozier, P. Glorieux, "Low-frequency dinamics of class *B* laser with two elliptically- polarized modes", Kvan. Electron **25**, Moscow, N.6, 502-506, (1998).

[36] K. Wiessenfeld, C. Bracikowski, G. James, and R. Roy, Phys. Rev. Let. **65**, 1749 (1990).

[37] P. Khandokhin, Ya. Khanin, J.-C. Celet, D. Dangoisse, and P. Glorieux, Opt. Commun. **123**, 372 (1996).

[38] L. Stamatescu and M.W. Hamilton, Phys. Rev. E **55**, 2115 (1997).

[39] N. B. Abraham, L. Sekaric, L. L. Carson, V. Seccareccia, P. A. Khandokhin, Ya. I. Khanin, I. V. Koryukin, and V. G. Zhislina, Phys. Rev. A **62**, 013810 (2000).

(40) P. Mandel, B. A. Nguyen, and K. Otsuka, Quantum Semiclassic. Opt. **9**, 365 (1997).

[41] E.S. Kovalenko, Izv. VUZ Radiofizika **10**, 1765-1768 (1967) [Sov. Phys. Radiophys and Quantum Electron. **10**, 989-990 (1967)].

[42] E.S. Kovalenko and L.I. Shangina, Izv. VUZ Radiofizika **12**, 846-849 (1969) [Sov. Phys. Radiophys. and Quantum Electron. **12**, 674-676 (1969)].

[43] A.A. Gusev, S.V. Kruzhalov, L.N. Pakhomov and V.Yu. Petrun'kin, Pis'ma Zh. Tekh. Fiz. **4**, 1250-1252 (1978) [Sov. Tech. Phys. Lett. **4**, 503 (1979)].

[44] V.R. Mironenko and V.I. Yudson, *Opt. Commun.* **41**, 126-130 (1982).

[45] K.N. Evtyukhov, L.N. Kaptsov, and I.V. Mitin, Zh Prik. Spektrosk. **32**, 18-23 (1980) [J. Appl. Spectroscopy **32**, 10-14 (1980)].

[46] E.A. Viktorov, V.A. Sokolov, E.V. Tkachenko and V.I. Ustyugov, Opt. Spektrosk. **68**, 920-923 (1990) [Opt. Spectrosc. **68**, 537-538 (1990)].

[47] O. Evdokimova and L. Kaptsov, Kvant. Elektron. **16**, 1557-1564 (1989) [Sov. J. Quantum Electron. **19**, 1001-1006 (1989)].

[48] L. Stamatescu and M.W. Hamilton, Phys. Rev. E **55**, 2115 (1997).

[49] N. B. Abraham, L. Sekaric, L. L. Carson, V. Seccareccia, P. A. Khandokhin, Ya. I. Khanin, I. V. Koryukin, and V. G. Zhislina, Phys. Rev. A **62**, 013810 (2000).

[50] E. A. Ovchinnikov, P.A. Khandokhin E.Yu. Shirokov, Emission spectrum of a solid-state laser with an nonuniform pump distribution along a Fabry-Perot cavity, Quantum Electronics **30 (1)**, 23-29 (2000).

[51] D. Pieroux, P. Mandel, Quantum and Semiclassical Optics, **9**, L17 (1997)).

[52] P. A. Khandokhin, Ya. I. Khanin, Yu. Mamaev, N. D. Milovsky, E. Yu. Shirokov, S. Bielawski, D. Derozier, P. Glorieux, Low-frequency dinamics of class *B* laser with two elliptically- polarized modes, Kvan. Electron. **25**, N.6, Moscow, 502-506, (1998).

[53] R. Leners, P. L. Francois, G. Stephan, Simultaneous effects of gain and loss anisotropies on the thresholds of a bipolarizations fiber laser, Opt. Lett., **19**, p. 275-277 (1994).

[54] P.A. Khandokhin, Ya.I. Khanin, N.D. Milovsky, E.Yu. Shirokov, S. Bielawski, D. Derozier, P. Glorieux, Polarization dynamics of a fiber Fabry-Perot laser with feedback, *Quantum and Semiclassical Optics, JEOS* part B, v.**10**, 97 (1998).

[55] K.C. Reyzer, L.W. Casperson, Polarization characteristics of dye-laser amplifiers I. Unidirectional molecular distributions, *J.Appl.Phys.* **51**, N12, pp6075-6082 (1980).

[56] K.C. Reyzer, L.W. Casperson, Polarization characteristics of dye-laser amplifiers II. Isotropic molecular distributions, *J.Appl.Phys.* **51**, N12, pp6083-6090 (1980).

[57] P. Khandokhin, N. Milovsky, Yu. Mamaev, E. Ovchinnikov, E. Shirokov, Polarization dynamics of Nd:YAG laser with weakly anisotropic Fabry-Perot cavity, SPIE, v. **3682**, 53-62 (1998).

[58] M. Sargent III, M.O. Scully, W.E. Lamb, Jr., Laser physics, Addison-Wesley Publishing Company, London (1974).

[59] O. Svelto, Principles of Lasers, Plenum Publishing Corp. (1998).

[60] C. O. Weiss, R. Vilaseca, Dynamics of Lasers, VCH Verlagsgesellschaft mbH, Weinheim (1991).

Acknowledgements

I am very grateful to Prof. Dr. **Peter. E. Toschek** and Priv.-Doz. Dr. **Valery. M. Baev** for offering me the possibility to obtain a scholarship and to work in their research team in the wonderful scientific atmosphere of the Institute of Laser Physics in Hamburg. I would like to thank my supervisor Dr. **Valery M. Baev** for his kind guidance, for support of my work, goodwill and patience. I really appreciate his help in understanding various problems and in carefully correcting my mistakes. His extraordinary knowledge and authority were the most important impulses for me to perform my investigations.

I am extremely thankful to Prof. Dr. **Yakov I. Khanin** (unfortunately, deceased this year), Dr. **Pavel. A. Khandokhin** and Dr. **Nikolay D. Milovsky** for providing me with the opportunity to work at the Department of Nonlinear Dynamics and Optics in the Institute of Applied Physics in Nizhny Novgorod and then to proceed with my research in Hamburg. I would like also to thank the whole staff of the laboratory in Nizhny Novgorod for their assistance, friendly and cooperative spirit.

Many thanks to Dr. **Jörg Hünkemeier** for his help in the beginning of my work at the Institute of Laser Physics. He has shown me how to handle fibre lasers, prepare multilayer mirrors and make data processing with computer.

Special thanks to **Arnold Stark** who helped me in many cases to find the answers to various questions concerning theoretical physics and practical work in the laboratory.

I am grateful to **Stefan Salewski** for his attention and readiness to help in various situations.

I would like to thank **Marcus Risch** and **Uwe Stapelfeld** for their contribution to my research and for useful discussions.

Thanks to Prof. Dr. **Günter Huber**, Speaker of the Graduiertenkolleg "Spectroscopie an lokalisierten atomaren Systemen – Felder und lokalisierte Atome – Atome und lokalisierte Felder", and Prof. Dr. **Klaus Sengstock**, Director of the Institut of Laser Physics, for their interest and support of my research work.

This work was supported by the Deutsche Forschungsgesellschaft and by the Graduiertenkolleg "Spectroscopie an lokalisierten atomaren Systemen – Felder und lokalisierte Atome – Atome und lokalisierte Felder".